2024-05-01

Microstructural Characterization and Oxidation Behavior of Al-Cu-Ni-Mn and Al-Cu-Ni-Mn-Si Non-Body Centered Cubic High Entropy Alloys

Mckenna Mae Lin Hitter
University of Texas at El Paso

MICROSTRUCTURAL CHARACTERIZATION AND OXIDATION BEHAVIOR

OF Al-Cu-Ni-Mn AND Al-Cu-Ni-Mn-Si

NON-BODY CENTERED CUBIC

HIGH ENTROPY ALLOYS

MCKENNA MAE LIN HITTER

Doctoral Program in Material Science and Engineering

APPROVED:

Shailendra K. Varma, Ph.D., Chair

Arturo Bronson, Ph.D.

Stella Quinones, Ph.D.

David Roberson, Ph.D.

Stephen L. Crites, Jr., Ph.D.
Dean of the Graduate School

Dedication

I would like to dedicate this work to my parents, brother, and my grandparents. I would not be the person I am today if I was not surrounded by their love. The amount of support, encouragement, wisdom, and guidance that they have poured into my life is the reason I am the person I am today. This is for my angels in heaven who have looked over me every step of the way, Grandma Alice, Papa Ed, and Grandma. I know you all are watching above and glistening down sunshine so that I can still feel your warmth. This is for my grandpa, who continues to always be on the sideline cheering me on. Between your jokes, stories, high fives, and constantly asking how I am doing, these moments have always been a meaningful touch throughout my life. This is for my mom and dad who have shown me nothing but unconditional love. From watching me stress out learning how to write my name in kindergarten to watching me write my dissertation, and every moment in between, whether it was big or small, you both have been the strength behind every step that I have taken thus far. This is for my younger brother, Jordan. Experiencing college with you has been tremendously special. Having you beside me these past couple years is everything I needed and more, and I would not want to cross the finish line with anyone else but you. This dissertation can be seen as a piece of work that I have shaped over a few years, while I am a person who has been shaped by my family my entire life. For that, this dissertation is dedicated to them because this would not have even existed if it were not for my family. There is no me without them. I love you all with all my heart.

MICROSTRUCTURAL CHARACTERIZATION AND OXIDATION BEHAVIOR OF AL-CU-NI-MN AND AL-CU-NI-MN-SI NON-BODY CENTERED CUBIC HIGH ENTROPY ALLOYS

by

MCKENNA MAE LIN HITTER

B.S. in Metallurgical and Materials Science and Engineering

DISSERTATION

Presented to the Faculty of the Graduate School of

The University of Texas at El Paso

in Partial Fulfillment

of the Requirements

for the Degree of

DOCTOR OF PHILOSOPHY

Materials Science and Engineering

THE UNIVERSITY OF TEXAS AT EL PASO

May 2024

Acknowledgements

I would like to thank everyone who has walked along side of me during my academic journey. I would not be writing this dissertation if it was not for Dr. Varma. Dr. Varma, thank you so much for seeing potential in me when others did not see potential in me, and thank you for always having confidence in me even when I did not have confidence in myself. You have been one of the greatest role models, and I absolutely loved being your student, teaching assistant, and graduate research assistant. Every lecture, lesson, and moment that I had with you, I will truly cherish forever and hold near and dear to my heart. Thank you to Dr. Bradley for your welcoming nature and always lending a helping hand and knowledge when needed. I always appreciated your cheerful encouragement along the way. Thank you to Dr. Roberson for your genuine care and for showing me a new love for scanning electron microscopy. I always enjoyed our conversations and your stories over the years, they were always refreshing and greatly needed during stressful times. Thank you, Dr. Quinones, Dr. Joddar, Dr. Smith, Dr. Stafford, Darren, and Dr. Misra, you all helped establish a foundation that I was able to continuously build from. Overall, this journey was not easy and there were many obstacles that discouraged me. I am so grateful for every individual that I encountered that made this adventure difficult. Every challenge along the way only made me want to reach the end goal more. At times this was extremely hard, but I would not have wanted it any other way. Thank you, God, for giving me the strength and courage to continue down this road. The path You guided me down was better than the one I could have ever envisioned for myself. Thank you to all my extended family and friends. Knowing that I was able to turn to you all for support or even give me a quick break from school to ease the heavy workload, it truly was the extra push I needed at times. Thank you to my metallurgy family, our moments in the lounge will never be forgotten. Our early mornings

always turned to long nights, and they were filled with laughs, snacks, stress, lunches, and most importantly a shared bond that I know we can never replace. I will miss walking to our cars together at the end of the day ranting about the insane amount of work we still need to get done, and somehow still managing to squeeze in a joke about who knows what, only to wake up and repeat this again the next day together. Some of my favorite memories are at our table in the lounge, and I am going to miss sitting there with you all. Please keep mine and Jordan's seat warm for us. Thank you to Victoria, from ballet class to graduate school, you have always brought the biggest smile to my face. With one shared glance, you have always brought me an overflowing amount of happiness and comfort. I am so lucky to be able to call you my best friend, and I am glad little three year old us met and never looked back. A special thank you to my mom, Linda, and dad, Gerald. You both have been my rock my entire life. I would not be the person I am today if it wasn't for your love. Mom, you have always been the first person to protect me and stand up for me. Dad, you have always been the first person to put a smile on my face and make me laugh and give me a big hug. You all have made me feel like the luckiest daughter in the world. I look up to both of you so much, and I am extremely grateful that I get to call you, Mom and Dad. I love you both. Lastly, thank you to my little brother. Jordan you are my best friend, and I could not imagine doing life without you. I am so blessed for all the memories we have created over the years together at UTEP. From carpooling, to being classmates, to lab partners, to being teaching assistants, to coauthors, to defending our thesis and dissertation the exact same day, and now we get to walk across the stage together. You have always been a shining light in my life that motivates me to continue to move forward. Thank you for being you. I love you so much.

This piece of work is not just mine, but OURS. Thank you to everyone from the bottom of my heart.

"I wanna be defined by the things that I love,

Not the things I hate, Not the things I'm afraid of…

I just think that

You are what you love"

-Taylor Alison Swift

Abstract

High entropy alloys (HEA) differ from traditional alloying systems because five elements are mixed in equi-atomic proportions, as opposed to having one main principal element. As a result of exploring this new method of alloying, it was found that high entropy alloys demonstrate exceptional mechanical properties, an example being oxidation resistance, and are capable of enduring elevated temperatures. Seeing the potential that this new area of interest contains, studies involving a combination of elements to form various HEA have been performed. Most refractory metals are body-centered cubic and possess extremely high melting temperatures, so they are regularly considered when designing high entropy alloys. However, the main goal of this investigation is to characterize and study the oxidation behavior of a high entropy alloying system that is comprised of only non-body centered cubic elements. The two alloys of interest are Al-Cu-Ni-Mn (Non Si Alloy) and Al-Cu-Ni-Mn-Si (Si Alloy). Each element that was selected for the HEA did not occupy a body centered cubic crystal structure and did possess a relatively high melting temperature. During this investigation the main objective was to microstructurally characterize each alloy in the as received condition and subject each alloy to different oxidation experiments. Exposing each HEA toelevated temperatures, 600ºC and 1000ºC, led to the study of their static and cyclic oxidation behavior. For static oxidation experiments, each alloy was held for a time duration of 24 hours, 48 hours, and 72 hours at 600ºC and 1000ºC. For cyclic oxidation experiments, each alloy was exposed to heating for a 24 hour time period and then remained cooled for 24 hours, and this process was repeated until the heating time equaled 1 full week. After experimentation the next objective was to identify microstructural features, characterize the oxide layer, and analyze the interface between the bulk microstructure and the oxidation layer. This characterization was done by using transmission

electron microscopy (TEM), x-ray diffraction (XRD), scanning electron microscopy (SEM), and energy dispersive spectroscopy (EDS) to identify microstructural characteristics in the as received and oxidized condition.

Table of Contents

List of Tables

List of Figures

Chapter 1: The Development of High Entropy Alloys

1.1 Traditional Alloying Systems

Metallurgy and material science has been relevant for many years. The study of materials has always been an evolving science. From the bronze age, to steel production, to copper refinement, to the creation of super alloys, manufacturing and producing materials that are useful and beneficial for society has always been a priority for the engineering field [1], [2]. Many different alloys and alloying systems have been studied, and there is a general understanding of their construct. In conventional methods, one main element is used in a large proportion and alloying elements are added to the mix in smaller amounts. The mixture of the main element and the alloying elements utilized are based on the application and the desired properties that the new material system is needed for. Stainless steel is a good representation of this standard practice. Viewing this from a chemical compositional level, iron is the main element present while chromium and additional alloying elements are mixed into the composition to add certain properties for service application, which in this case would be for corrosion resistance [3]. This recipe of alloy design can be viewed as a traditional version, and as metallurgical processes have been improving, new alloys have been developed that defy this approach. A very common example is brass. Brass is composed of large amounts of copper and zinc, making this alloy have more than one main element [4]. Seeing how altering the elemental composition has a direct impact on the final properties can be explained through basic physical metallurgy principles. The spine of physical metallurgy revolves around the relationship between structure, processing, properties, and performance of materials (Figure 1.1).

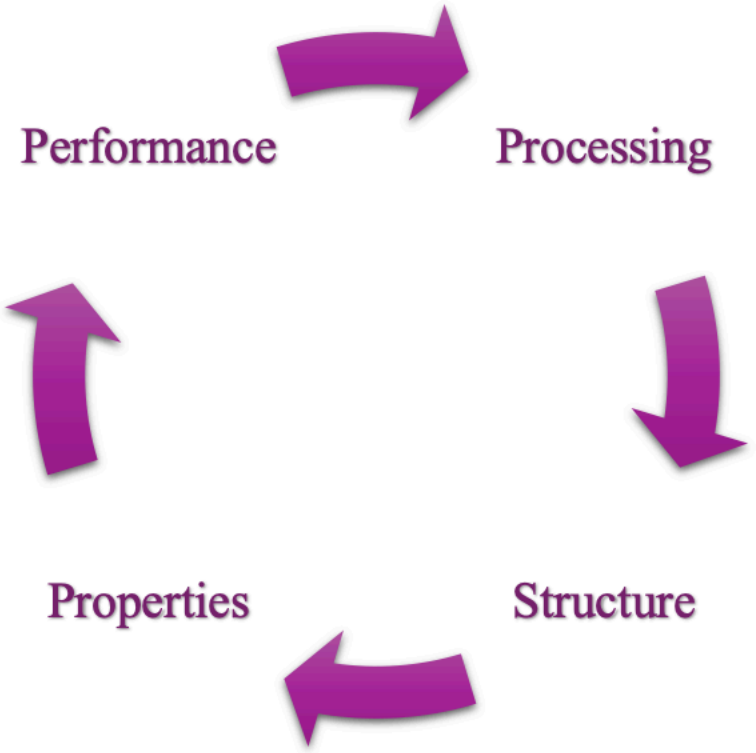

Figure 1.1 Structure, processing, properties, and performance materials paradigm

These four pillars demonstrate how each one is interconnected with one another and how if one is affected, the following three are also impacted. For instance, the chemical makeup of a material and the method as to which it is processed, will directly impact the microstructure of the material, which will then affect the properties that the final product will possess in service. These pillars can be described as a domino effect and are the backbone of alloy design to this day.

Understanding these primary physical metallurgical concepts allows room for growth and exploration among alloy development. By adapting these techniques, new doors have been opened that stray away from the traditional alloying method.

1.2 The Beginning of High Entropy Alloys

One recent development in this field is the study of high entropy alloys. HEA were first investigated by Cantor and Yeh, and originally, they began their exploration by combining nearly twenty elements at a time. Through this trial-and-error process, they discovered that a certain alloy with five elements, all with equal compositions, portrayed promising characteristics compared to the alloy with twenty elements which appeared to be extremely brittle. This alloy was composed of chromium, manganese, iron, cobalt, and nickel (CrMnFeCoNi), and this alloy became coined as the Cantor alloy. Through experimentation it was found that this alloy was able to produce a single-phase solid solution, had increased its configurational entropy, and showed an enhancement in mechanical properties [1], [2], [4]. This discovery was novel due to the fact that not many expected an alloy with five different elements to be capable of producing a single-phase solid solution, rather than an intermetallic.

Based on these findings, Cantor and Yeh decided to establish a basis for this new field of multi-component principal alloys. The two main concepts that held a high importance included the elemental composition and configurational entropy [2]. The relationship that these two factors share is proportional within this scenario, as the number of compositional elements increases within a system then the entropy is directly affected, and the configurational entropy will increase as well. This thermodynamic relationship can best be expressed by the follow equations [5].

$$\Delta G = \Delta H - T\Delta S \tag{1}$$

$$\Delta G_{mix} = \Delta H_{mix} - T\,\Delta S_{mix} \tag{2}$$

The terms are defined as follows:

G: Gibbs Free Energy

H: Enthalpy (measure of energy change under constant pressure)

T: Temperature

S: Entropy (measure of randomness and/or disorder in a system at an atomic level)

Knowing that five separate elements are being mixed in equi-atomic proportions, this will result in an increase in ΔS_{mix}, otherwise can be explained as an increase in disorder amongst the different atoms within the system. By increasing the value of ΔS_{mix} will lead to an increase in ΔG_{mix}, or Gibbs free energy, as the outcome. Understanding this basis led to building an overall definition of the term "high entropy alloys," due to the increasing configurational entropy. However, in order for a material system to be classified as a "high entropy alloy," the alloy must be comprised of at least five principal elements and should be added in equal atomic concentrations. Using the Boltzmann hypothesis for equi-atomic alloys, the configurational entropy of mixing for a given number of constituents can be calculated using the following equation.

$$\Delta S_{mix} = \mathrm{R} \ln(n) \tag{3}$$

Where, R is the ideal gas constant and n is the total number of constituent elements present. By using the previous equation and being able to determine the value of the configurational entropy of equi-atomic alloys, there were three categories that were developed to differentiate between

the level of entropy within a material system. The categories included high entropy, medium entropy, and low entropy alloys.

Low entropy alloys were first defined as:

$$\Delta S_{conf} \leq 0.69\ R \tag{4}$$

Medium entropy alloys were first defined as:

$$1.61\ R\ \geq \Delta S_{conf} \geq 0.69\ R \tag{5}$$

High entropy alloys were first defined as:

$$\Delta S_{conf} \geq 1.61\ R \tag{6}$$

If an alloy contains a configurational entropy lower than 0.69R, R being defined as the ideal gas constant, then it is identified as a low-entropy alloy (LEA), if an alloy's configurational entropy falls between 0.69R and 1.61R then is it considered to be a medium-entropy alloy (MEA), and lastly, if an alloy has a configurational entropy greater than 1.61R then it can be acknowledged as a high entropy alloy [5], [6], [7].

Equations 4-6 were established under the assumption that the alloy contained five elements in exactly equi-atomic proportions. Yet, some believe that if there are five elements present and their chemical composition falls in the range between 5% - 35% then it still meets the criteria to be classified as a high entropy alloy. To calculate the configurational entropy of a

material system that was not made in equ-atomic proportions the following equation was established.

$$\Delta S_{conf} = -R \sum_{i=1}^{n} X_i \ln X_i \tag{7}$$

The term X_i can be defined as the mole fraction of the ith constituent.

Also, creating these levels of entropy as shown in equations 4-6, appeared to not work for all scenarios and did exclude certain material systems that possibly contained less or more than five elements. Due to this inconsistency a more general statement, shown in equations 8-10, was developed that allowed more multiple component alloys and systems to be accepted into this new classification of material systems [8].

Low Entropy Alloys:

$$\Delta S_{conf} \leq 1\ R \tag{8}$$

Medium Entropy Alloys:

$$1.5R \geq \Delta S_{conf} \geq 1R \tag{9}$$

High Entropy Alloys:

$$\Delta S_{conf} \geq 1.5\ R \tag{10}$$

1.2.1 Core Effects of High Entropy Alloys

By recognizing the main definition of a high entropy alloy, a foundation was built surrounding the characteristics that make a high entropy alloy different than traditional alloys. These characteristics that high entropy alloys possess can be viewed as "core effects." HEA have four core effects that distinguish this new material system from varying material systems, and these four core effects include having high entropy, lattice distortion, sluggish diffusion, and cocktail effect [6], [9].

1.2.2 High Entropy

As previously discussed, configurational entropy is a key factor within high entropy alloys because there are approximately five principal elements in equal atomic concentrations. Therefore, from a thermodynamic perspective, since there are large amounts of different elements mixed, this results in a high degree of disorder within the system. By intentionally creating a system that occupies a high amount of disarray at an atomic level, this can help promote the formation single solid solutions. Thermodynamically, there is a constant battle between the formation of intermetallics and single solid solutions within a material. Depending on the magnitude of configurational entropy of mixing, this can overpower the formation of intermetallic compounds. Single solid solutions are favored due to the simplicity of the microstructures they form, while intermetallic compounds tend to be complex and are brittle in nature [6], [10], [11], [12].

1.2.3 Lattice Distortion

Next, because there are five different elements added to the system it is important to recognize that each principal element will contain a different atomic radius. Introducing varying atomic sizes to the lattice will create a heavy distortion within the unit cell because the atoms will have to be arranged in a way that is accommodating for the various sized atoms to fit.

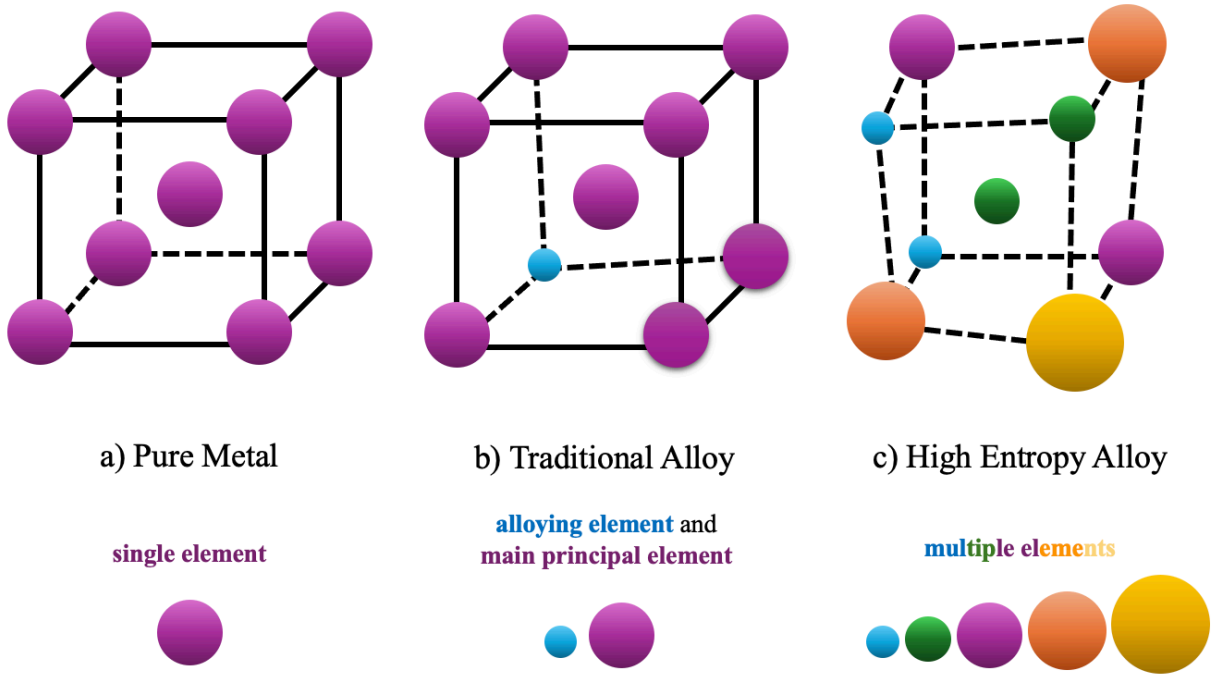

Figure 1.2 Schematic of lattice distortion within high entropy alloys: a) Pure metal unit cell b) Traditional alloy unit cell c) High entropy alloy unit cell

In Figure 1.2, it can be seen that within a pure metal unit cell since all of the atoms are the same element, the lattice remains unaltered since the atoms have the same dimensions. Within a traditional alloy, the majority of space that is occupied within a unit cell is taken up by the main element. The other atom(s) present are alloying elements and are added in very small amounts. They are arranged in a way that does not result in an excessive amount of distortion. Normally, these alloying elements can also fill interstitial sites within the lattice as well, which does not result in major distortion either. As shown above, the depiction of the high entropy alloy

portrays how all the atomic sizes are diverse and results in the unit cell being distorted. The atoms must arrange themselves in an unconventional way to accommodate for the great range of atomic sizes [6] [13].

1.2.4 Sluggish Diffusion

By understanding the distortion that is present within the lattice, this can be directly related to sluggish diffusion. In more conventional alloying systems, when enough energy is added to a system, atoms are able to move in an easier fashion because the main principal atoms are the same size, and normally, alloying atoms are smaller in size so they do not create a significant amount of resistance during diffusion. For example, in Figure 1.3 the alloying element, or solute atom, will not have that much difficulty moving through the unit cells due to it being smaller in size and requiring less energy to diffuse. However, within the HEA system, shown in, the movement of all the principal atoms are slowed due to the wide variation in sizes, this prohibits diffusion to occur at a rapid pace. Diffusion is also difficult to occur because each atom is going to require a different activation energy needed to initiate the movement of the atom. Having so many variables makes it a hard process for the atoms to migrate amongst one another [6], [13].

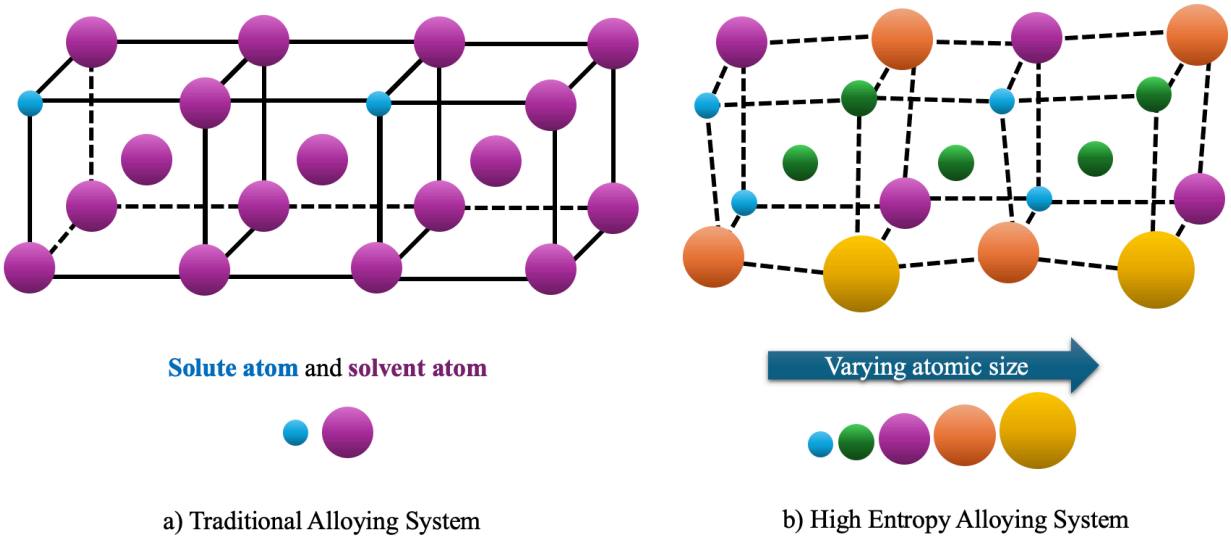

Figure 1.3 Schematic of sluggish diffusion within a distorted high entropy lattice: a) Traditional alloying system with solute atoms and solvent atoms b) High entropy alloying system with varying atomic size

1.2.5 Cocktail Effect

The last core effect is the cocktail effect. This effect can be explained when many elements are combined together and as a result, surprisingly, leads to a beneficial outcome and consequently possess unique properties [6], [7], [9], [14].

1.3 Mechanical Properties and Applications of High Entropy Alloys

Currently, superalloys are a common material system that have been successful for applications relating to aerospace, structural, and extreme environmental conditions. These products have proven to be reliable due to their high creep resistance, high fatigue resistance, and high corrosion resistance. With high entropy alloys opening a new door for exploration, previous research has studied various combinations of refractory metals and transition metals that could potentially have the same outstanding properties or even better [15], [16].

1.4 Elevated Temperature Oxidation

With high entropy alloys showing promising mechanical properties, especially oxidation resistance, their oxidation behavior when exposed to extreme environments such as elevated temperatures can be further explored. When a metal is subjected to high temperature oxidation in air, oxygen molecules come into contact with the surface of the metal or substrate. The initial stage of oxidation is through the process of adsorption. The oxygen molecules are able to adsorb to the metal and an exchange between the oxygen molecules and the metal atoms occurs. With oxygen being an interstitial atom, the oxygen atoms are small enough in size to diffuse into the metal and this becomes the catalyst for oxidation to propagate. The metal and the oxygen atoms will interact and begin to form an oxide on the surface of the substrate. The oxide will begin to grow into a thin film and expand over the surface of the substrate creating a barrier between the environment and the metal. Depending on the oxide film that is created, this can lead to information regarding the oxidation rate [17], [18]. A generalized visual representation is schematically shown in Figure 1.4.

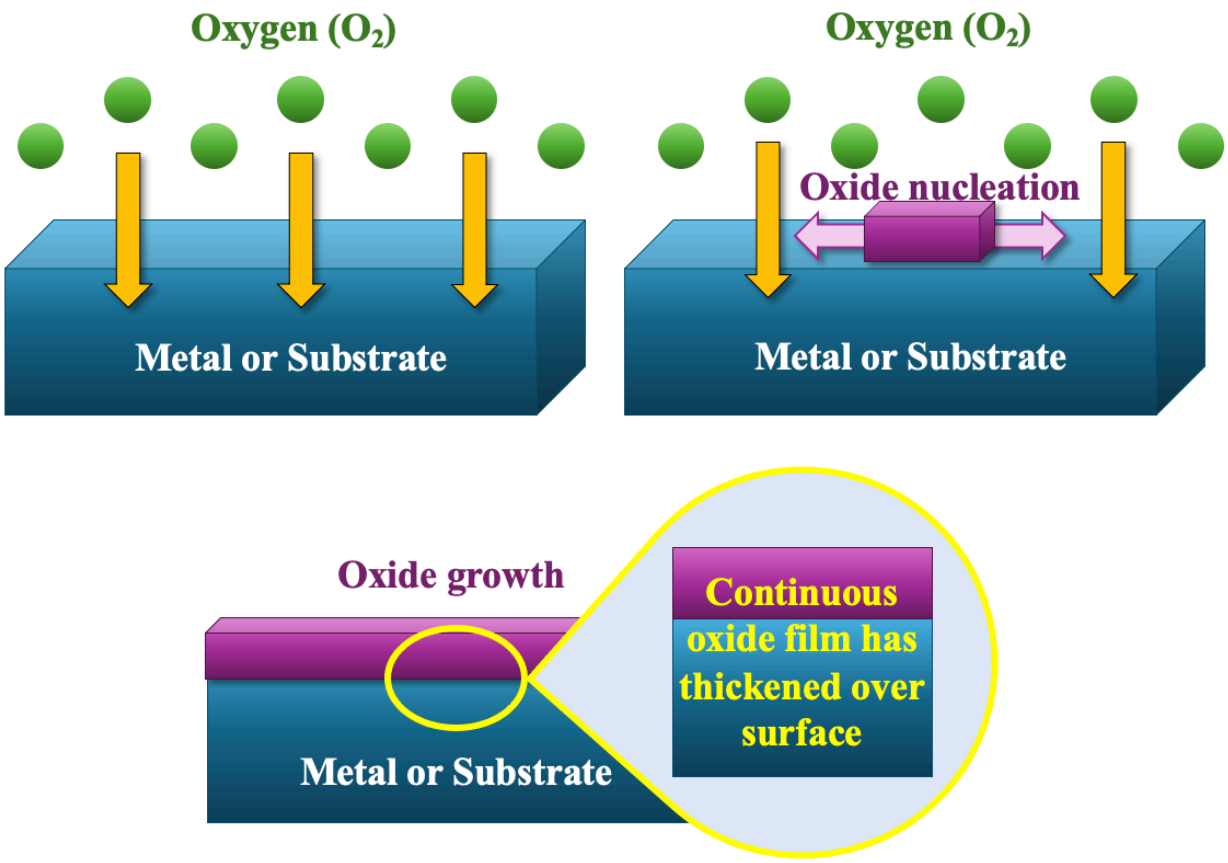

Figure 1.4 Elevated temperature oxide film growth and nucleation on metal substrate

Understanding that the combination of elevated temperatures and a metal can promote oxidation, predicting which oxides are likely to initially form and which oxides are more stable is important. Relating this back to equation 1, the change of Gibbs free energy can allow insight on which oxides have a higher stability. Thermodynamically, the lower the change in Gibbs free energy means that the reaction between oxygen and the metal is more likely to occur because it has a higher spontaneity. A useful diagram that displays this relationship is known as the Ellingham diagram. This diagram plots the relationship between the change in Gibbs free energy, ΔG, and temperature. Displayed below is an example of an Ellingham diagram. Various oxide reactions are plotted by a straight line on the diagram, and this shows the thermodynamic

stability of each oxide. The farther down the line is located on the diagram indicates a more negative free energy and more stability [17], [18], [19].

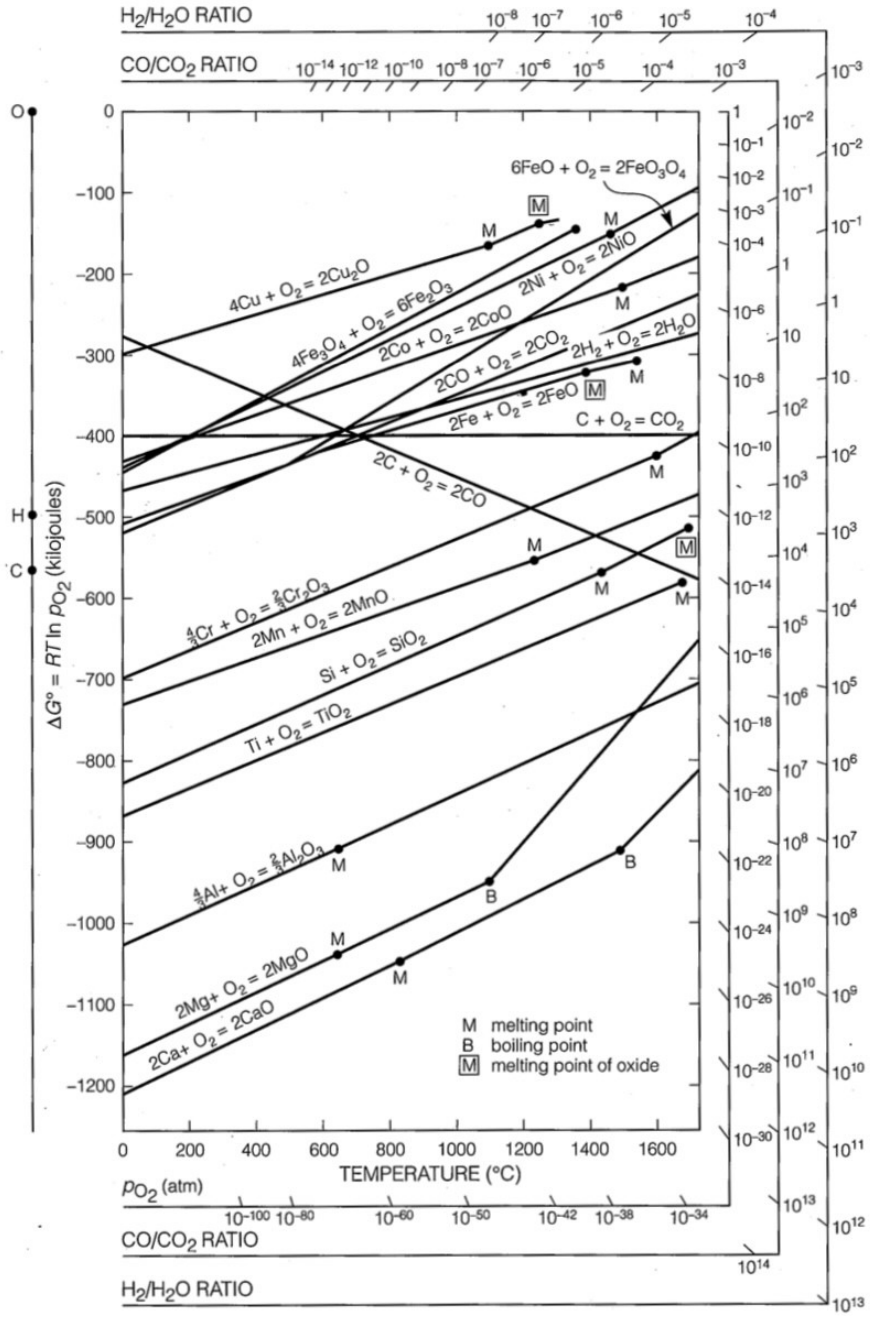

Figure 1.5 Ellingham diagram utilized to predict oxide stability based on the relationship between the change of Gibbs free energy and temperature [18]

1.5 Hume Rothery Rules

Knowing that alloy design involves the mixing of different elements, there has been a set of rules that have been established that assist with the prediction if two elements can truly mix and result in a solid solution. This criterion has been followed for years and they are generally recognized as the Hume Rothery rules. The Hume Rothery rules mainly are utilized when analyzing binary systems. There are four rules that must be followed in order for a solid solution to form and they are as followed:

1. Must have similar crystal structure
2. Must have an atomic radii difference $\leq$ then 15%
3. Must have a similar electronegativity
4. Must have similar valence

During alloy design the Hume Rothery rules are extremely beneficial, especially when forming a solid solution is the primary goal. In high entropy alloys, solid solutions are normally favored over intermetallic compounds. Applying these concepts can be a useful guide when aiming to form a HEA with solid solution formation [20].

Table 1.1 Hume Rothery rules: Crystal structure, atomic radius, electronegativity, and valence of each element and binary combinations

Element	Crystal Structure	Atomic Radius	Electronegativity	Valence
Aluminum (Al)	Face Centered Cubic	1.432	1.61	3
Copper (Cu)	Face Centered Cubic	1.278	1.90	2
Nickel (Ni)	Face Centered Cubic	1.243	1.91	2
Manganese (Mn)	Cubic	1.12	1.55	2, 4, 7
Silicon (Si)	Diamond Cubic	1.176	1.90	4
Al-Cu	Same	12% ✓	15%	Similar
Al-Ni	Same	15% ✓	16%	Similar
Al-Mn	Different	28% ✗	4%	Varies
Al-Si	Different	22% ✗	15%	Similar
Cu-Ni	Same	3% ✓	.5%	Similar
Cu-Mn	Different	14% ✓	18%	Varies
Cu-Si	Different	9% ✓	0%	Similar
Ni-Mn	Different	11% ✓	19%	Varies
Ni-Si	Different	6% ✓	.5%	Similar
Mn-Si	Different	5% ✓	18%	Varies

Based on the four basic concepts of the Hume Rothery rules, the elements being used for this investigation were compared to each other in a binary state. Their crystal structure, atomic radius, electronegativity, and valence relationship between two elements are shown above. Manganese and silicon do not share a face centered cubic crystal structure like aluminum, copper, and nickel. Overall, most of the atomic radii difference between two elements does abide by the ≤15% Hume Rothery rule. The only two combinations that have an atomic radii difference greater than 15% includes Al-Mn and Al-Si. The difference between each of the element's

electronegativity mainly ranges from a 15% - 19% difference. However, there are four elemental combinations that have less than a 5% difference, and those element pairs include Al-Mn, Cu-Ni, Cu-Si, and Ni-Si. Lastly, the valence of each the elements was compared. All of the elements share a similar valence, but manganese has the potential to have a valence of either 2, 4, or 7. When manganese obtains a valence of 2 or 4 then it remains similar to the other elements, although when manganese contains a valence of 7 then it does have a greater difference.

Chapter 2: Significance of Investigation

2.1 Introduction of Study

The research behind high entropy alloys has increased in magnitude over recent years. A key difference that makes high entropy alloys independent from their counter parts is their chemical composition. Most material systems contain one principal element, however, by definition, HEA are composed of five or more principal elements, and they are developed in equi-atomic proportions. Through earlier studies it was found that high entropy alloys result in excellent mechanical properties, specifically oxidation resistance. However, recent work within the realm of high entropy alloy experimentation has mainly dealt with a combination of refractory metals. The crystal structure in which most refractory metals possess is body centered cubic (BCC). The majority of transition metals and refractory metals contain a high melting temperature, and that is a prime reason as to why they are desirable for high entropy alloying systems.

For the purpose of this study, the main objective is to investigate two high entropy alloys that contain a mixture of elements that are non-body centered cubic. The two alloying systems of interest include: a) Al-Cu-Ni-Mn and b) Al-Cu-Ni-Mn-Si. Each element was selected with the basis that its crystal structure was not body centered cubic, and it contained a relative high melting temperature. With a new combination of elements, both non-body centered cubic high entropy alloy's oxidation behavior will be evaluated. These types of alloys are known for portraying exceptional oxidation resistance in elevated temperature environments. For this reason, characterization and oxidation experiments will be performed both in a static and cyclic nature. The main goal is to understand their oxidation behavior through a range of elevated temperatures, and to characterize each alloy.

2.2 Purpose of Investigation

This investigation aims to provide insight on the microstructural characterization and oxidation behavior of non-body centered cubic HEA. It has been proven that there are numerous combinations of elements that can be integrated to form a HEA system. The importance of this work is to focus primarily on elements that are not BCC in nature. The purpose for this selection is to see if this blend of elements can potentially be used for low to medium elevated temperature applications. Naturally, refractory and BCC high entropy alloys due possess an extremely high melting temperature compared to FCC materials. The scope of this work will demonstrate if the new alloying system has potential to be used for medium temperature applications since they do not possess as high as melting temperatures as refractory metals. Another important aspect of this work is to consider the conservation of metals. For example, brass is mainly composed of copper and zinc in large amounts. The difference in this work is that since more elements are being added to the alloying systems, their compositions are lowered, and they are not being used in high proportions as they would be in other alloying systems. Very common metals that are used in large amounts include aluminum, copper, and nickel. All three of these metals are being utilized in the HEA, and the metals were conserved compared to their normal applications.

Key factors to consider when designing a new high entropy alloy for this specific study include the following:

- Elements selected must not have a body-centered cubic crystal structure
- Elements should possess a relatively high melting temperature
- Conservation of metals
- Availability of elements and cost effectiveness

Based on this criteria, elements were selected and the two alloys that will be studied throughout this investigation include Al-Cu-Ni-Mn and Al-Cu-Ni-Mn-Si. This research will involve elevated temperature oxidation in air, both in a static and cyclic pattern. Through previous studies it has been seen that HEA have exceptional mechanical properties and have a high oxidation resistance. A key characteristic of these alloys is that they are microstructurally stable at elevated temperatures [21], [22]. By performing oxidation experiments it will be important to characterize the microstructure and oxidation layer. Gaining an understanding of how the selected elements interact on a microstructure level will be significant in order to determine which elements primarily oxidize when exposed to higher temperatures.

2.3 Research Objectives

The main objectives of this investigation includes the following:

- Design two non-body centered cubic high entropy alloying systems
- Perform as-received characterization on Non Si alloy and Si alloy and identify microconstituents present within each microstructure
- Subject Non Si alloy and Si alloy to elevated temperatures, 600^{o}C and 1000^{o}C, for static and cyclic oxidation in air and understand oxidation behavior of each HEA
- Characterize oxide layer present and identify oxides present after static and cyclic oxidation
- Characterize bulk microstructure after oxidation after static and cyclic oxidation
- Characterize interface between oxide layer and bulk metal after static and cyclic oxidation
- Obtain oxidation plots for static oxidation and oxidation curves for cyclic oxidation

Chapter 3: Experimental Procedure

The following experimental procedure will be followed for this investigation:

1. Alloy Design

The criteria that was established and used as a basis for alloy design included:

- Elements must have a relatively high melting temperature
- The crystal structure must not be body-centered cubic

Based on these conditions the following elements were selected for the HEA:

Table 3.1 Selected non-body centered cubic elements and their properties for high entropy alloy design

	Aluminum	**Copper**	**Nickel**	**Manganese**	**Silicon**
Crystal Structure	FCC	FCC	FCC	Cubic	Diamond Cubic
Melting Temperature (Celsius)	660.4	1084.9	1453	1244	1410
Atomic Radius (Angstroms)	1.432	1.278	1.243	1.12	1.176
Lattice Parameter (Angstroms)	4.049	3.6151	3.5167	8.931	5.43

All the elements possess a high melting temperature well above 1000 ^{o}C, besides aluminum. The reason for still selecting aluminum is because it is commonly used and readily available. The majority of the elements are face centered cubic, however manganese and silicon are cubic and diamond cubic, respectively. The driving factor as to why these specific elements were chosen, besides the initial criteria, is because the conservation of metals was considered, as previously mentioned. In addition, it is important to examine the cost and availability aspect during alloy design. Besides manganese, all of the other elements are commonly used and easily

accessible for processing. Once narrowing the selection to these five elements, it was decided that two HEA will be developed. The first HEA being composed of Al-Cu-Ni-Mn, is referred to as the Non Si alloy, and the second HEA being composed of Al-Cu-Ni-Mn-Si, is referred to as the Si alloy. The only difference being the addition of silicon. This will allow for a comparison of microstructural characterization and oxidation behavior between the two HEA.

The Non Si and the Si alloys were developed by Plasmaterials located in Livermore, California. The alloys were manufactured by vacuum arc melting, and they were requested to be made in equiatomic proportions as shown below in Table 3.2. Electric discharge machining was used to machine 5x5x5 millimeter cubes for each alloy.

Table 3.2 Requested equi-atomic composition for Non Si and Si alloy from manufacturer

Non Si Alloy		**Si Alloy**	
Element	**Atomic %**	**Element**	**Atomic %**
Aluminum	25	Aluminum	20
Copper	25	Copper	20
Nickel	25	Nickel	20
Manganese	25	Manganese	20
Silicon	-	Silicon	20

2. As Received Characterization

The first step for as received characterization was to perform metallography on each alloy, and they were grinded to approximately 800-1200 grit paper to reveal the microstructure for the alloys. A Hitachi 3500 Scanning Electron Microscope was used to analyze to the alloy's microstructure. X-ray color mapping and point ID energy dispersive spectroscopy (EDS) methods were used to identify microconstituents that were present. Next, using a Bruker D8 Discover Diffractometer, XRD was utilized to detect phases present. Using and comparing the results from both methods, the as received condition was able to be characterized.

3. Transmission Electron Microscopy

Transmission Electron Microscopy samples of both alloys in the as received condition were prepared at The University of Texas at Austin by the Texas Material Institute Laboratory. The samples were made utilizing the in-situ lift out method within a focus ion beam scanning electron microscope. Upon receiving the samples, TEM images were taken in the as received condition.

4. Static Oxidation

Each alloy was subjected to static oxidation in air for a duration of 24, 48 and 72 hours. The temperatures at which the alloys were exposed to included 600^{o}C and 1000^{o}C. Before beginning the oxidation experiments a Non Si and Si alloy were taken and each face of the cube was grinded down using 300 grit paper in order to remove the exterior surface. The exterior surface was removed so any residuals and/or contamination from manufacturing would not be present during oxidation, and the bulk material will predominantly be exposed to the elevated temperatures. With the samples being 5x5x5 millimeter cubes, each face of the cube was slightly grinded down after using the grit paper. Using calipers, measurements were taken in the X, Y, and Z directions, so the new dimensions of the sample could be obtained.

Next, the sample and the crucible that was going to be used during oxidation were weighed multiple times and an average was taken. The sample was placed into the crucible and then left in the furnace for a given time duration and temperature. The furnace was set to increase and decrease in temperature by a rate of 10^{o}C per minute. After oxidation and cooling, the crucible with the sample in it was removed from the furnace and weighed multiple times with an average taken. This information led to finding the mass gain or mass loss of the sample as a result of

oxidation, and oxidation plots were obtained. This process was repeated each time a static oxidation experiment occurred, this includes each temperature and duration.

5. Cyclic Oxidation

Both alloys were exposed to cyclic oxidation in air. One cycle resulted in the sample being heated for 24 hours and then cooled to room temperature. A total of seven cycles were repeated to achieve a week's worth of elevated heat exposure. The temperatures at which the cyclic oxidation occurred included 600^{o}C and 1000^{o}C. The same sample preparation and measurements that were conducted during the static oxidation experimentation were continued during cyclic experiments. However, after each cycle the crucible with the sample was weighed multiple times and an average was documented. This was to find the mass gain or loss per surface area after each cycle. Oxidation curves were obtained, and this procedure reoccurred for each cyclic oxidation experiment.

6. Oxide Layer Characterization

Post static and cyclic oxidation, each alloy's oxide layer was characterized using a Hitachi 3500 SEM. The same methods that were used during as received characterization were applied during this step. EDS techniques were used to identify oxides present on the exterior oxide layer. XRD was also used again as another way to characterize the oxide layer. This process was repeated on each sample after being exposed to oxidation in both static and cyclic patterns.

7. Interface and Bulk Characterization

Metallography was performed on one face of the samples. By doing so, this revealed the bulk microstructure after oxidation. From a side profile the interface of the oxide layer and the bulk material was able to be seen. Both these areas of interest were characterized with the same techniques used above.

Chapter 4: As Received Characterization Results

4.1 As Received Microstructural Characterization of Non Si and Si Alloy

After the metallographic process, the microstructure of the Non Si alloy is revealed in Figure 4.1. Through EDS elemental mapping, it can be found that three major microconstituents were identified. The three microconstituents present include a gray region, white, region, and black region. The average elemental composition of each microconstituent can be seen in Table 4.1 The white microconstituent appears to be rich in nickel and the black microconstituent is rich in manganese. The gray region can be recognized to be a matrix of nickel, copper, aluminum, and manganese. The overall structure does depict a dendritic appearance, which is normally seen in cast products [23].

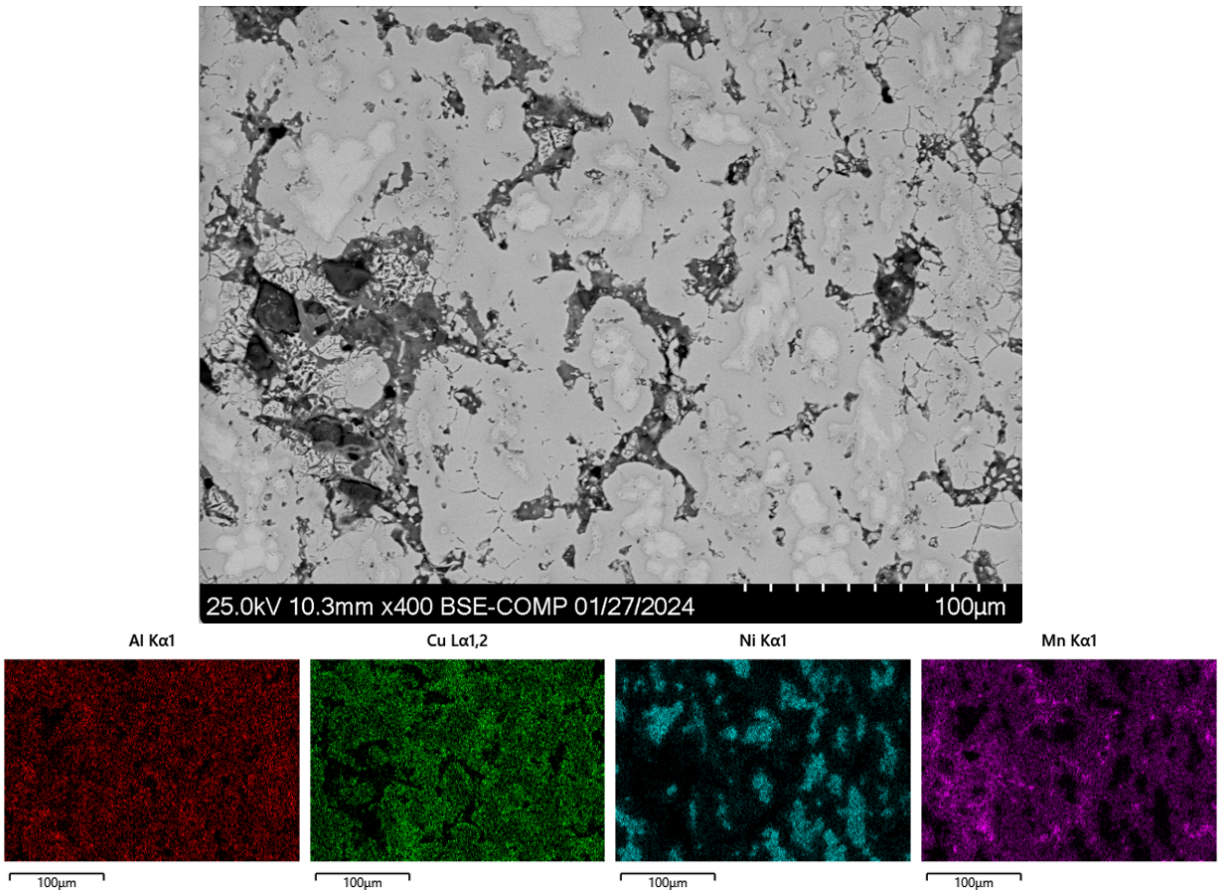

Figure 4.1 As received microstructure of Non Si alloy and energy dispersive spectroscopy elemental mapping

Table 4.1 Average elemental composition of as received microstructure of Non Si alloy

Elemental Composition	
Element	**Average At %**
Aluminum	26.5
Copper	25.9
Nickel	23.5
Manganese	24.0

The as received microstructure for the Si alloy is portrayed in Figure 4.2 along with EDS mapping. There were similarities between the microconstituents in the Non Si alloy and the Si alloy, and the average elemental composition can be found in Table 4.2. The microconstituents present included a white region, black region, and a gray matrix. The white microconstituent was nickel rich. The black microconstituent was rich in manganese and occupies a different shape compared to the black microconstituent in the Non Si alloy. Silicon appears to be present in the same regions where manganese is rich. The matrix was a combination of the elements but primarily rich in copper, aluminum, and nickel. It can be noted that even though this alloy contains the addition of silicon, there was no microconstituent that was primarily rich in silicon [23].

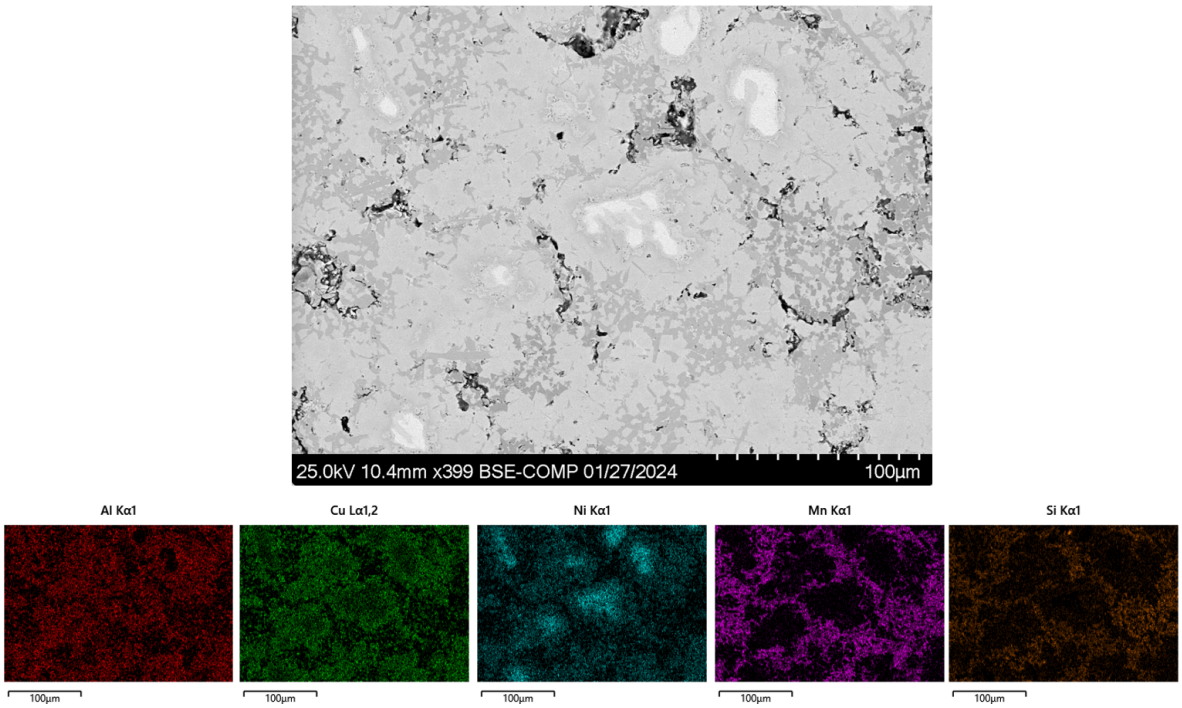

Figure 4.2 As received microstructure of Si alloy and energy dispersive spectroscopy elemental mapping

Table 4.2 Average elemental composition of as received microstructure of Si alloy

Elemental Composition	
Element	**Average At %**
Aluminum	24.3
Copper	14.3
Nickel	19.3
Manganese	15.5
Silicon	26.6

Chapter 5: Static Oxidation Results

5.1 Static Oxidation for 24 Hours at 600°C and 1000°C for Non Si and Si Alloy

Once being exposed to 24 hour oxidation for 600°C the oxide layer of the Non Si alloy can be viewed below (Figure 5.1). The oxide layer appears to be rich in manganese and aluminum. There is cracking that surround some of the oxides present. There are smaller regions where nickel and copper are rich and can be seen in the blue and green elemental maps.

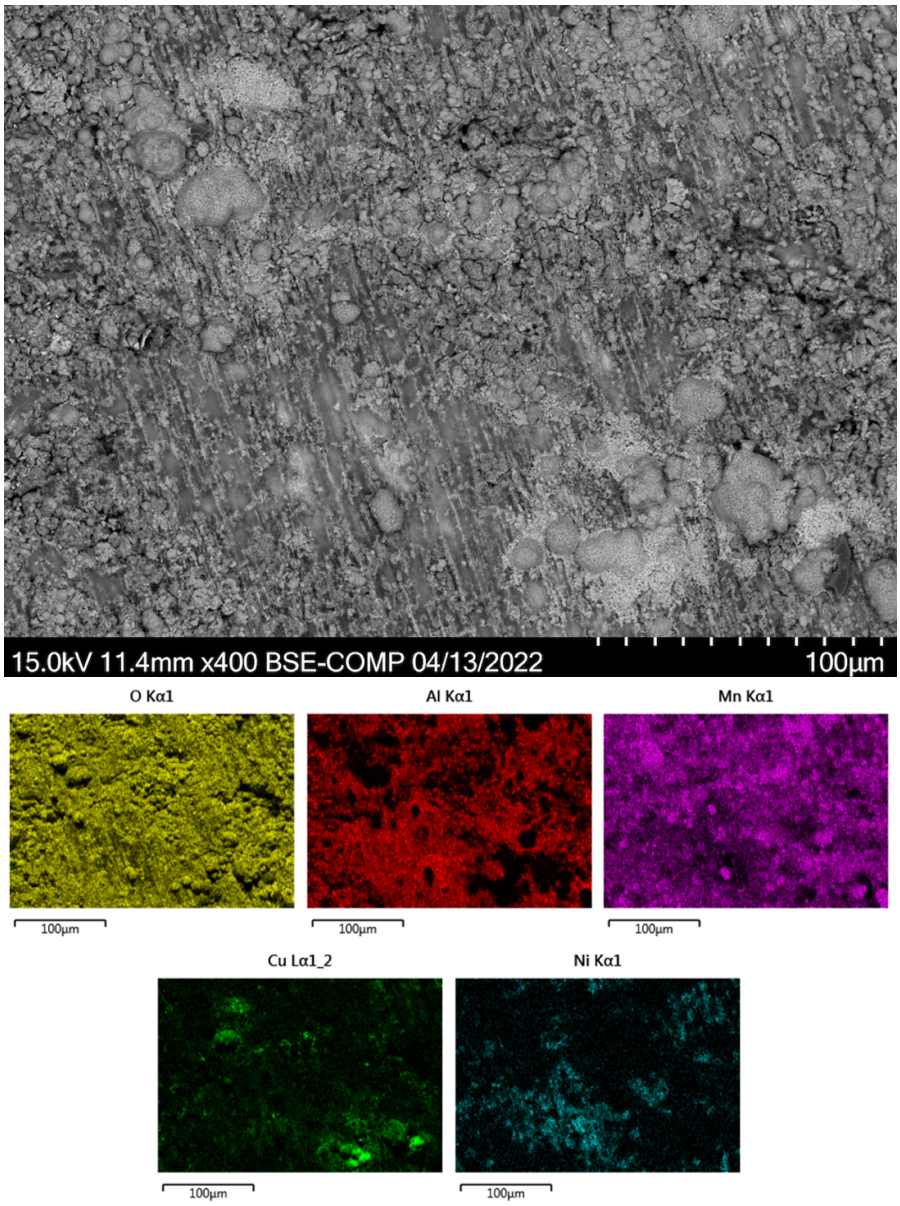

Figure 5.1 Oxide layer of Non Si alloy after 24 hour static oxidation at 600°C and energy dispersive spectroscopy elemental mapping

Once being subjected to oxidation in air for 24 hours at 600°C, the microstructure of the Non Si alloy can be viewed in Figure 5.2. The dark regions are rich in oxygen and manganese with some aluminum. The white nickel rich region is still present and can be viewed in the blue elemental map. The gray matrix does appear to be rich in copper, aluminum, and nickel. With the structure being dendritic, it appears that manganese and aluminum oxides are located in the interdendritic regions.

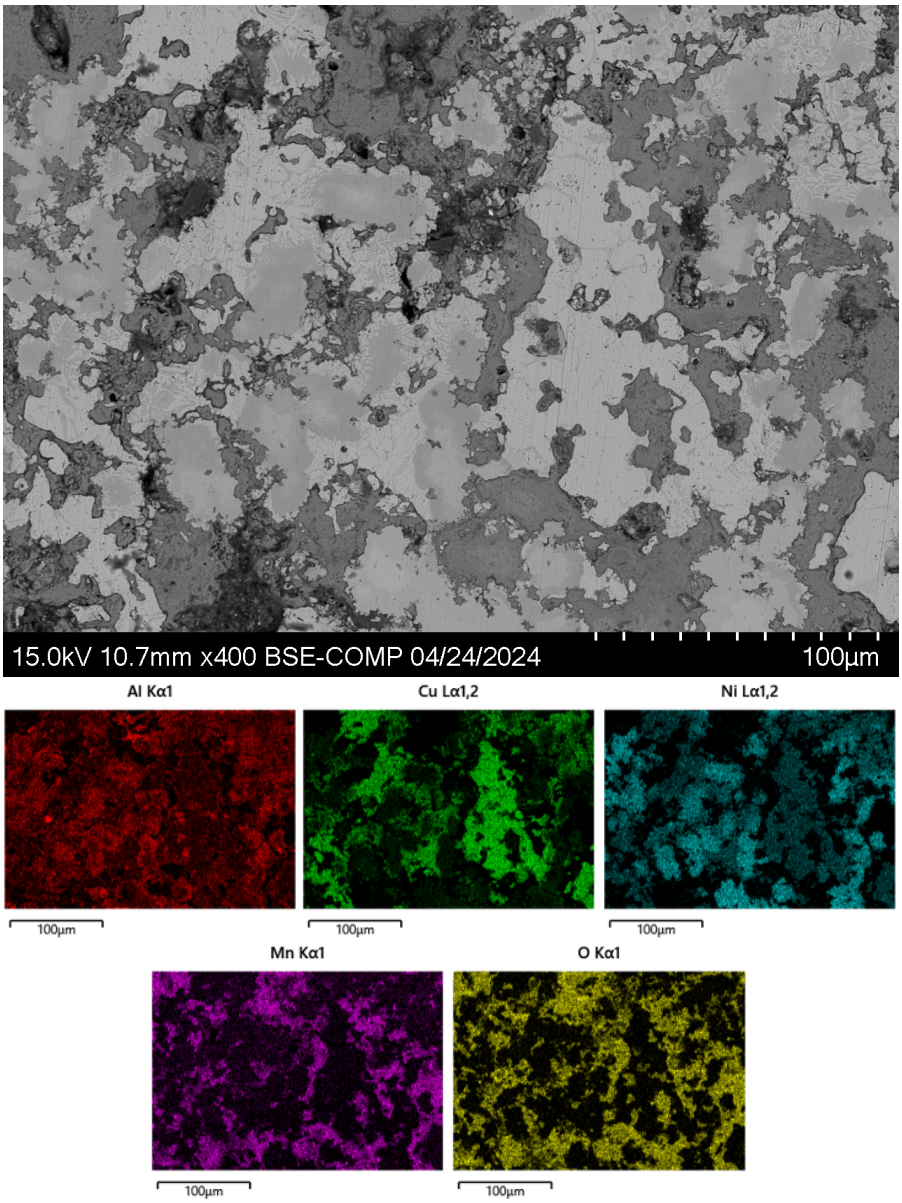

Figure 5.2 Microstructure of Non Si alloy after 24 hour static oxidation at 600°C and energy dispersive spectroscopy elemental mapping

The interface between the bulk of the Non Si alloy and the oxide layer can be viewed below. It can be noted that this sample was hot mounted. The mount was not conductive, and this is the primary reason for electron charging in the image. When looking at the elemental maps, there is a layer of aluminum, manganese, and oxygen that is located at the interface. Copper and nickel remain rich only within the bulk of the material.

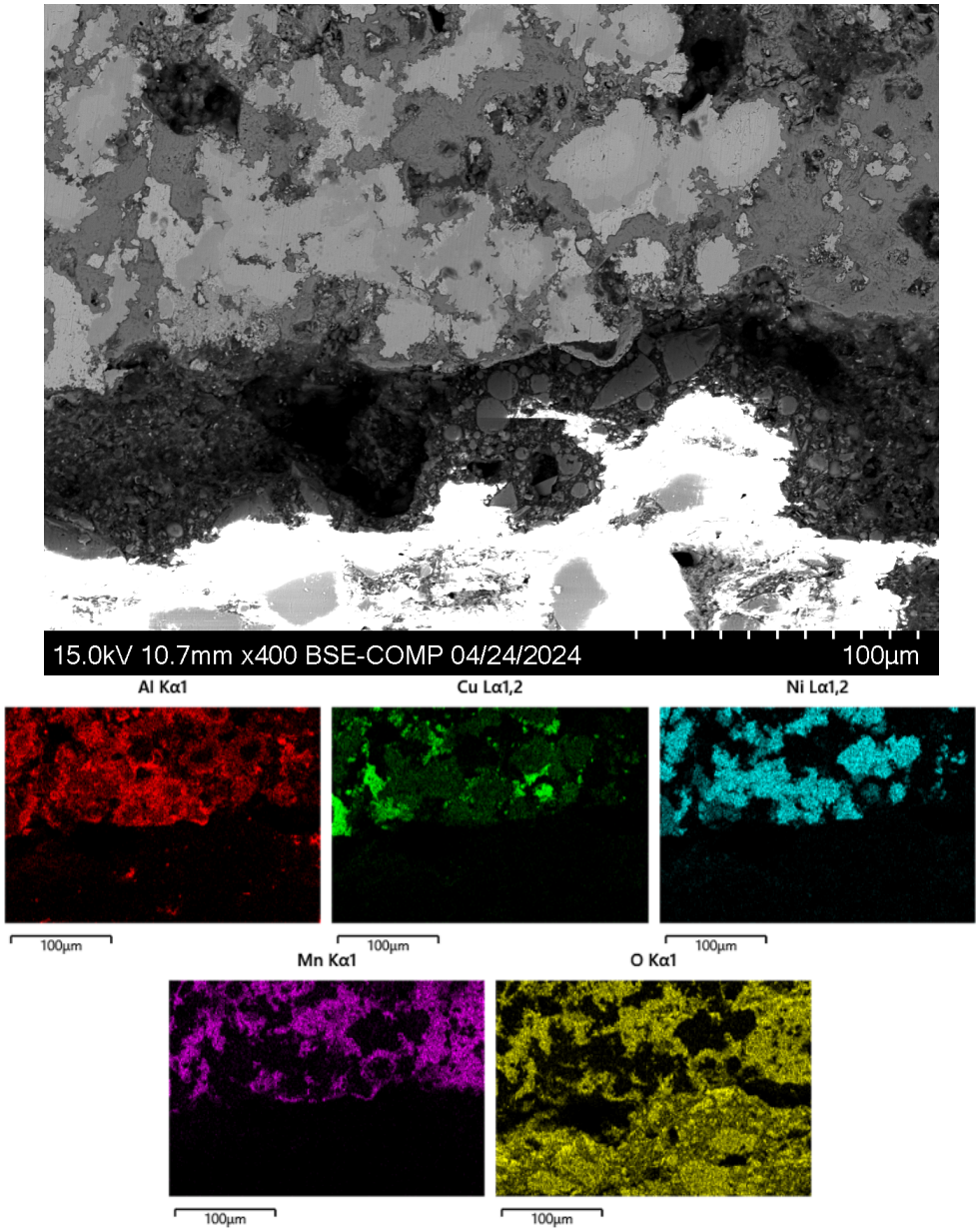

Figure 5.3 Oxide and bulk interface of Non Si Alloy after 24 hour static oxidation at 600°C and energy dispersive spectroscopy elemental mapping

The Si alloy was subjected to 24 hour oxidation and was heated to 600°C. The oxide layer that formed can be shown in Figure 5.4. Manganese is rich throughout the surface and there are regions where aluminum, copper, and nickel appear to share similar areas where they are present. Silicon does not have a great presence within the oxide layer. There is cracking that runs along the oxide formation.

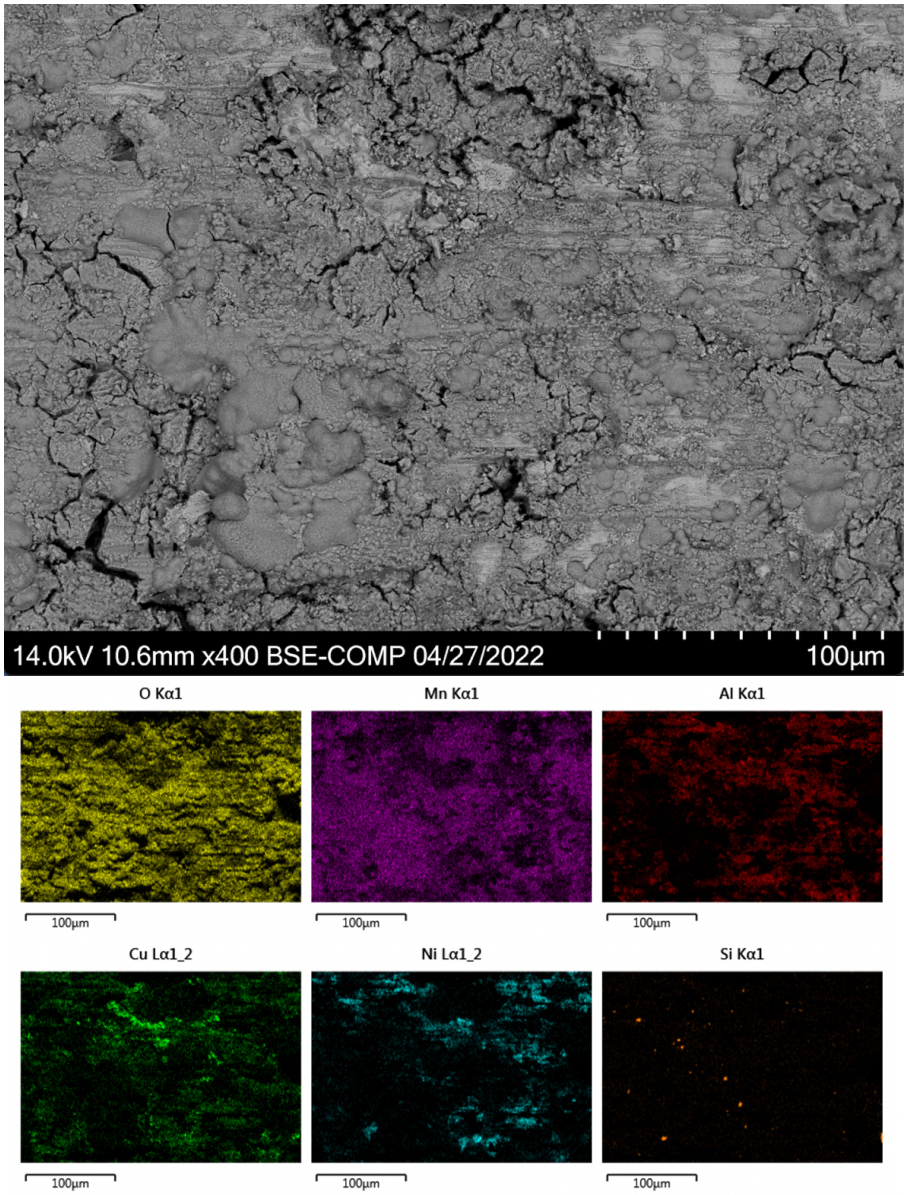

Figure 5.4 Oxide layer of Si alloy after 24 hour static oxidation at 600°C and energy dispersive spectroscopy elemental mapping

In the SEM image below, the microstructure of the Si alloy after a 24 hour oxidation period at 600°C can be seen. The microstructure does remain consistent with the as received condition and remains in its dendritic form. The dark regions are rich in manganese with silicon present. The gray matrix is rich with copper, nickel, and aluminum. Nickel continues to have a white region where it is rich in composition.

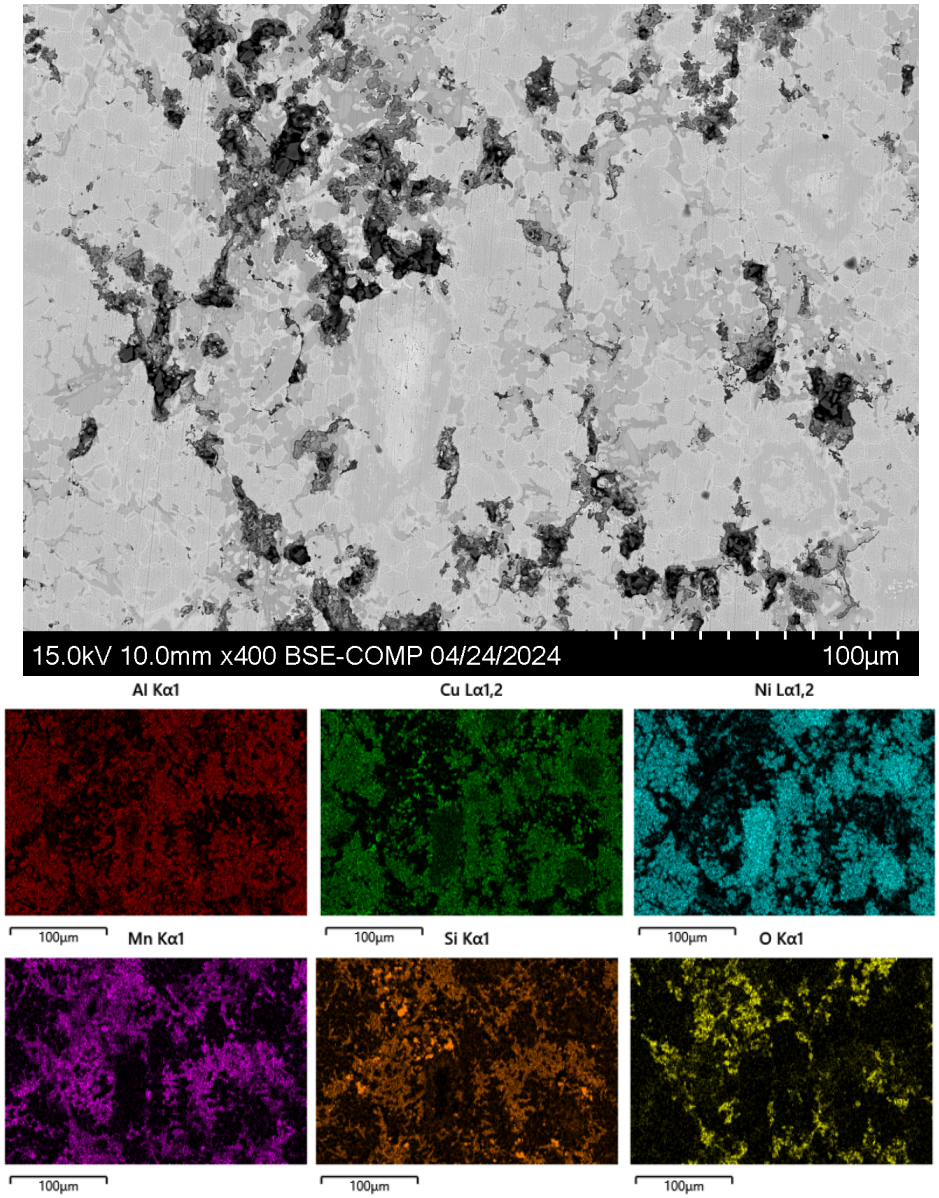

Figure 5.5 Microstructure of Si alloy after 24 hour static oxidation at 600°C and energy dispersive spectroscopy elemental mapping

The interface of the Si alloy after being exposed to 600°C for 24 hours is represent below (Figure 5.6). There is a very distinct oxide layer present on the edge of the bulk sample. When comparing the elemental maps, aluminum, manganese and oxygen are the three main elements that can be found within this oxide layer. Also, it should be noted that this sample was also mounted the same way that the Non Si alloy was mounted above. Therefore, due to the mount, this led to an increase of charging, and this is also why there is silicon present on the outside portion of the sample shown in the orange elemental map and it is not included within the oxide layer.

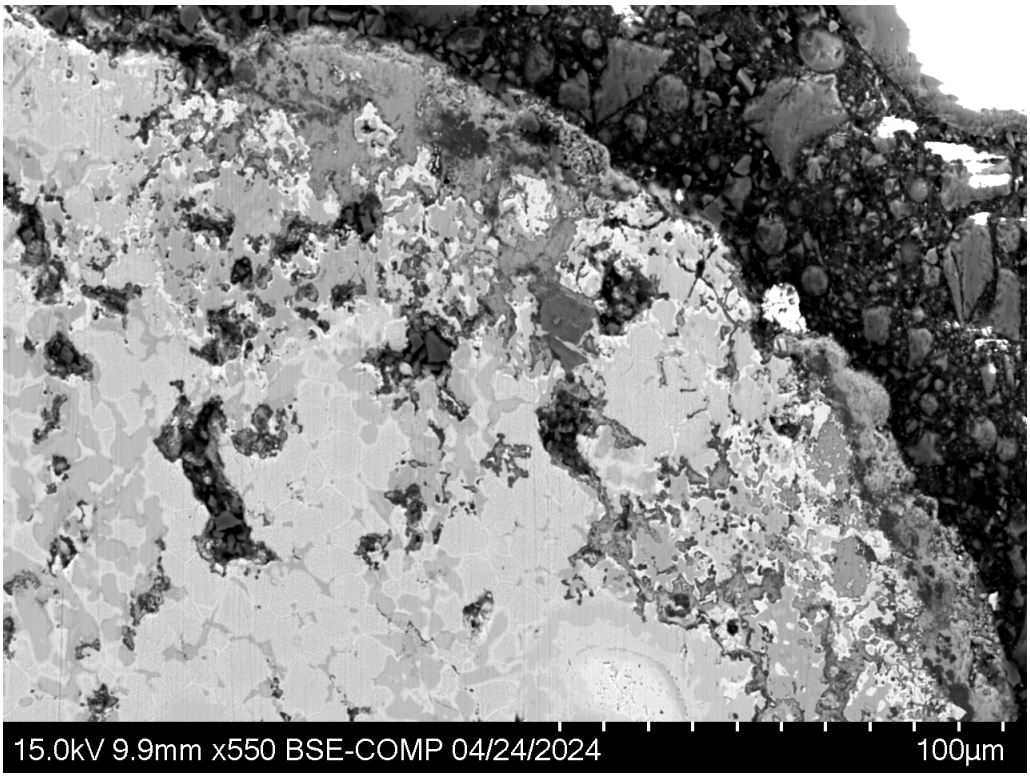

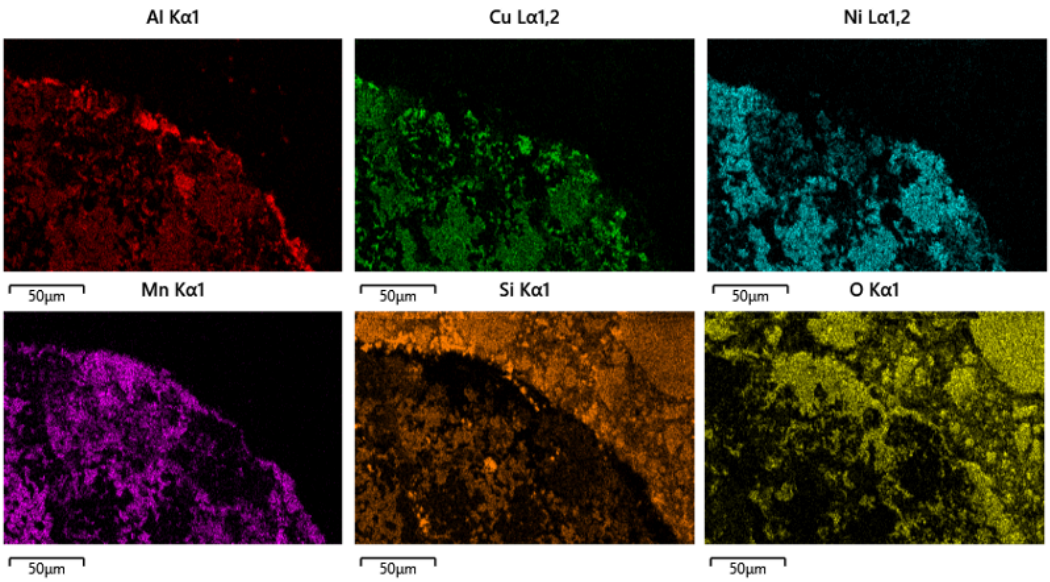

Figure 5.6 Oxide and bulk interface of Si Alloy after 24 hour static oxidation at 600°C and energy dispersive spectroscopy elemental mapping

Figure 5.7 displays the XRD spectra that was gathered from the oxide layers from both the Non Si and Si alloy after 24 hour oxidation at 600°C. Seeing how manganese is rich within the oxide layer through EDS, it can be noted that the oxides relating to this have been identified as Mn_2O_3.

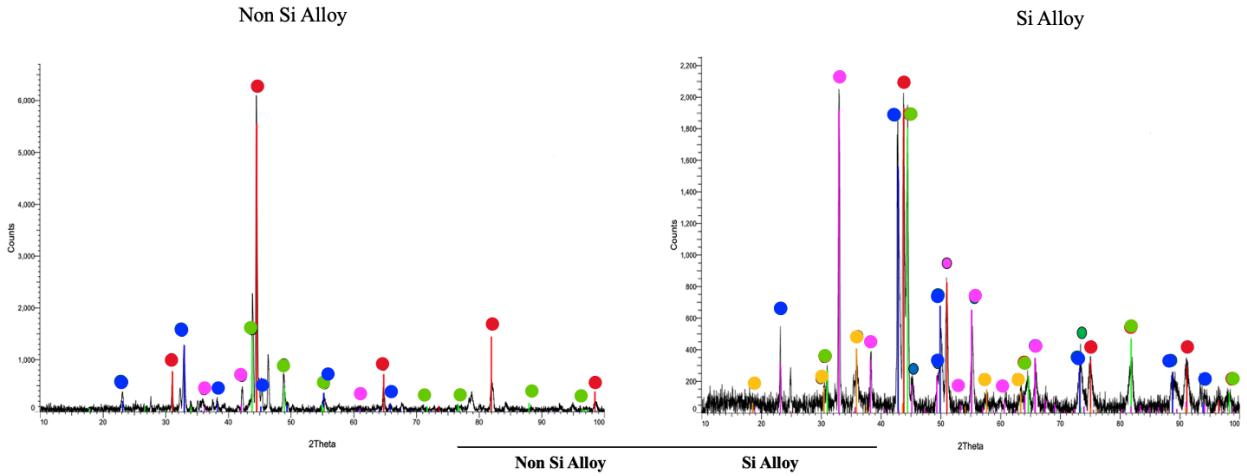

Non Si Alloy	Si Alloy
Mn_2O_3	Mn_2O_3
$Al_{0.9}Ni_{1.1}$	$(Al_{0.4}Cu_{0.6})Ni_3$
Al_3Ni_5	$(Al_{15}Cu_{85})_{0.04}$
$(NiO)_{0.5}(MnO)_{0.5}$	$Al_{0.96}Ni_{1.04}$
	$Cu(Cu_{0.5}Mn_{1.5})O_4$

Figure 5.7 X-ray diffraction of oxide layer of Non Si and Si alloy after 24 hour static oxidation at 600°C

Next, the Non Si alloy was held for the same oxidation time, but the temperature was increase to 1000°C. The oxide layer post heating is shown in the SEM image below. It is evident that the oxide size has increased with temperature. The main oxide covering the surface had a high presence of manganese shown in the elemental map. The manganese rich oxide is faceted and there are "twin-like" features that are present within the crystals. The green and blue elemental maps help show that the "twin-like" features are rich in copper and nickel. Aluminum appears to be rich in the region where there are smaller crystals are present, and visually it almost appears as if the aluminum oxide sits underneath the manganese oxide.

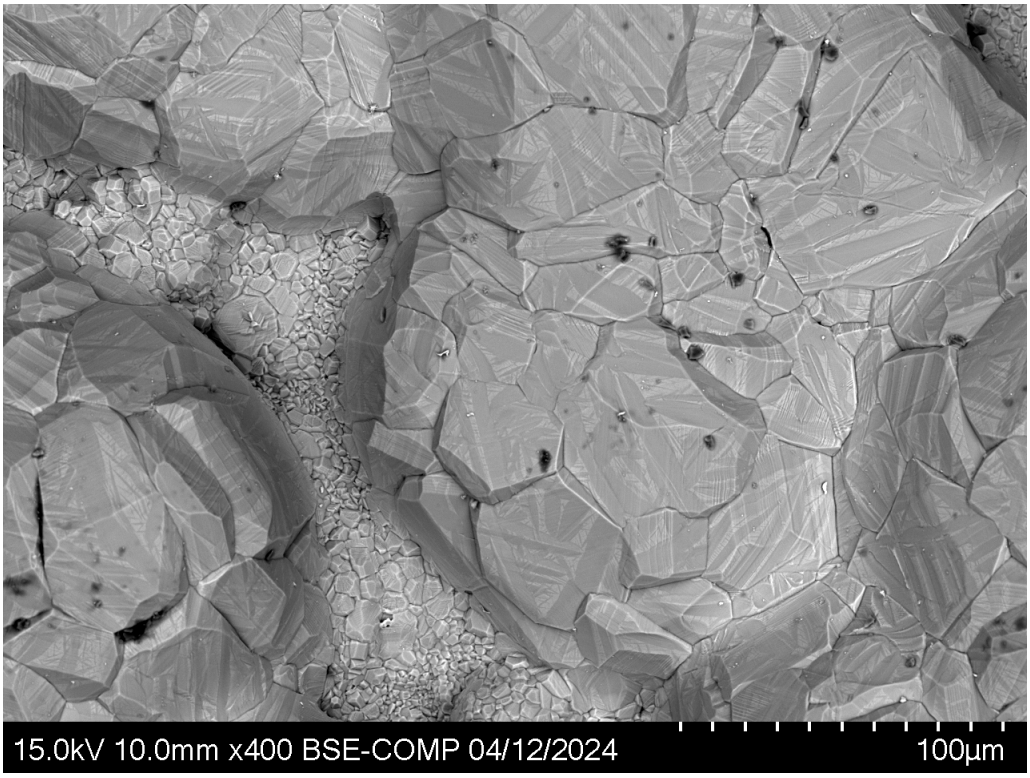

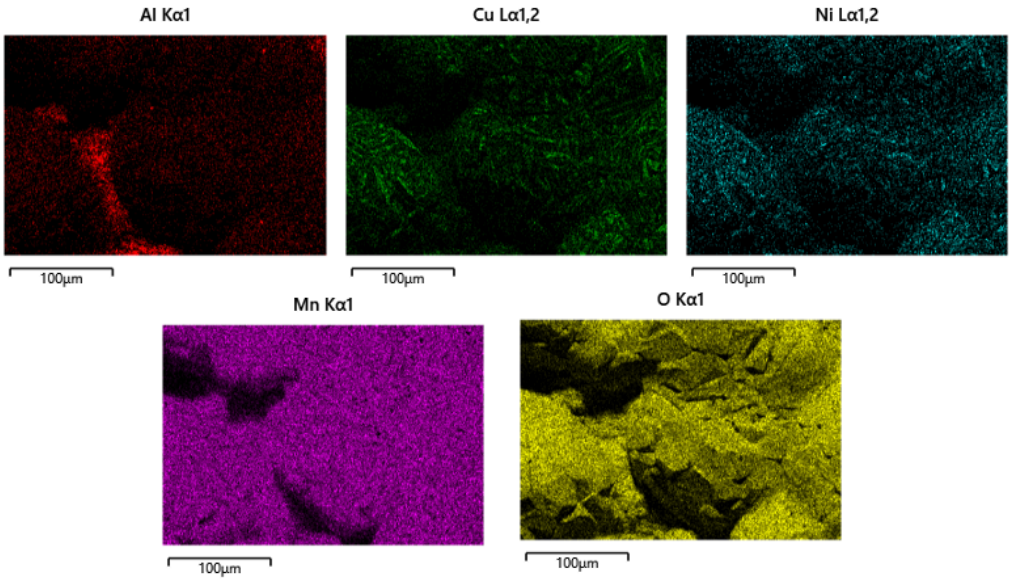

Figure 5.8 Oxide layer of Non Si alloy after 24 hour static oxidation at 1000°C and energy dispersive spectroscopy elemental mapping

The bulk microstructure of the Non Si alloy after being exposed to 1000°C for 24 hours is shown in Figure 5.9. The SEM image shows that the aluminum oxide is present within the bulk material and can be related to the dark regions. The gray matrix is rich in copper, nickel, and manganese.

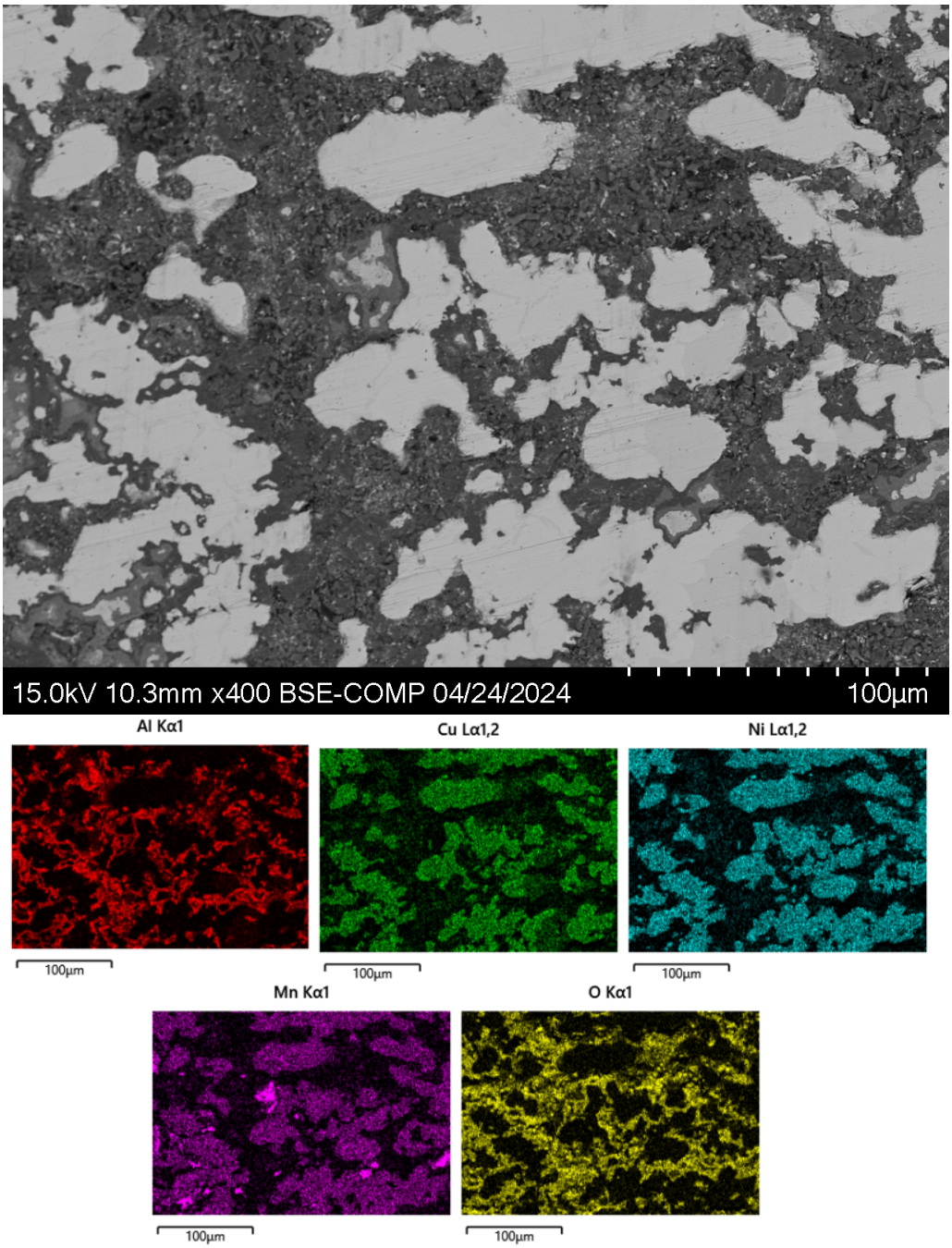

Figure 5.9 Microstructure of Non Si alloy after 24 hour static oxidation at 1000°C and energy dispersive spectroscopy elemental mapping

The interface between the oxide layer that was formed at 1000°C for 24 hours for the Non Si alloy is displayed in Figure 5.10. The aluminum oxide is present within the bulk material and there is a thin layer on the interface. This can be seen in the red elemental map below that represents

the location of aluminum present. On the exterior of the oxide layer, and covering the thin aluminum oxide, there are manganese oxides that fill most of the surface. From this angle, the morphology of the manganese oxides is very clear.

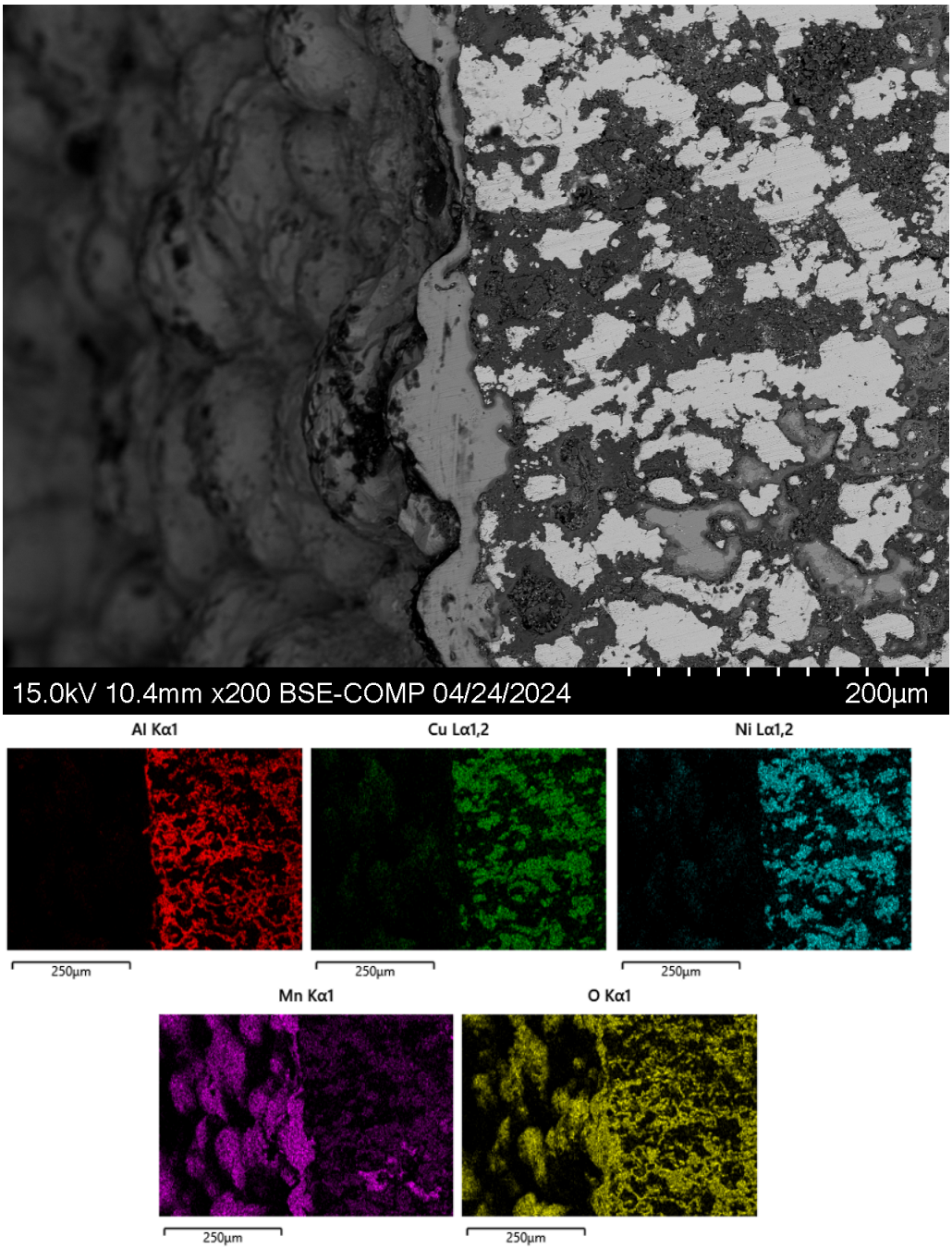

Figure 5.10 Oxide and bulk interface of Non Si Alloy after 24 hour static oxidation at 1000°C and energy dispersive spectroscopy elemental mapping

The results for the Si alloy at 1000°C held for a 24 hour time period can be viewed in the image below. Based off the elemental maps, the oxide layer is rich in aluminum and oxygen. There is a white region that is rich in manganese and has a different morphology than the aluminum oxide areas.

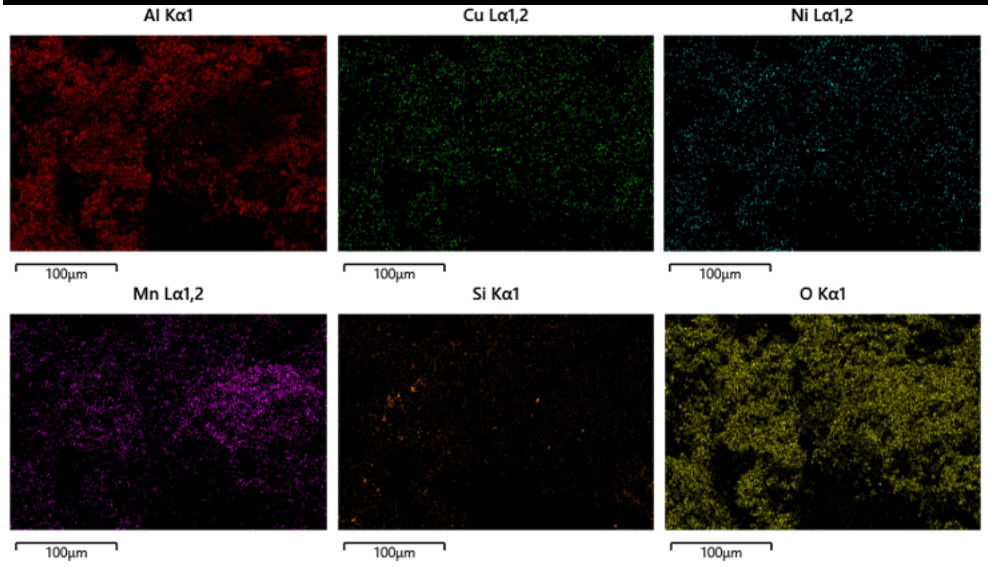

Figure 5.11 Oxide layer of Si alloy after 24 hour static oxidation at 1000°C and energy dispersive spectroscopy elemental mapping

Metallography was not able to be performed on the Si alloy after being exposed to 1000°C. The sample was oxidized, and scaling was present. The Si alloy was not structurally stable and would fragment once touched (Figure 5.12). Due to this, the bulk microstructure and the interface was not able to be analyzed.

Figure 5.12 Si alloy after 24 hour static oxidation at 1000°C

X-ray diffraction data was collected from the oxide layer from both alloys. Through EDS it was evident that aluminum and manganese were rich with the oxide layer, therefore it was important to identify any oxide peaks relating to these two elements. Figure 5.13 shows that these oxides are present in the form of Mn_3O_4 and Al_2O_3.

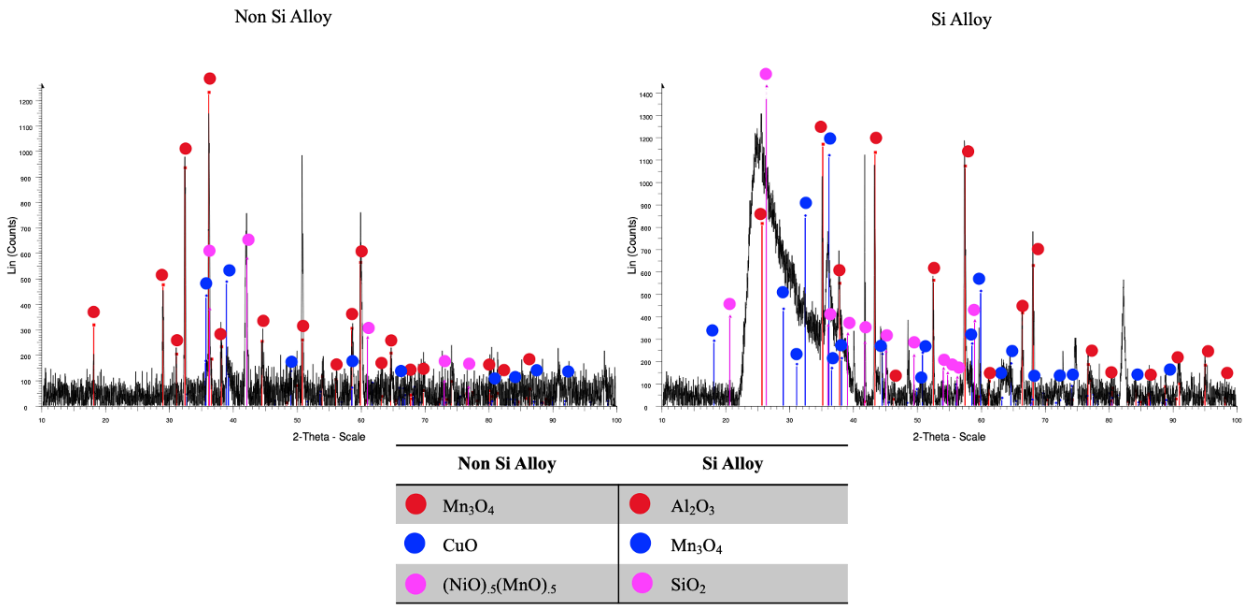

Figure 5.13 X-ray diffraction data of oxide layer of Non Si and Si Alloy after 24 hour static oxidation at 1000°C

The average atomic percentage of each element is shown in Table 5.1. In the Non Si alloy, at both 600°C and 1000°C, the oxide layer shows a high composition of manganese. The oxide layer from the Si alloy at 600°C shows an increase in aluminum and a decrease in manganese, compared to the Non Si alloy at the same temperature. However, when the temperature increases to 1000°C the manganese composition decreases and leaves the oxide layer primarily rich in aluminum.

Table 5.1 Average elemental composition of oxide layer, bulk microstructure, and interface of Non Si and Si alloy after 24 hour oxidation at 600°C and 1000°C

24 Hour Oxidation at 600 C							
Non Si Alloy				Si Alloy			
	Oxide Layer	Bulk	Interface		Oxide Layer	Bulk	Interface
Element	Avg At%	Avg At%	Avg At%	Element	Avg At%	Avg At%	Avg At%
Al	7.97	17.03	13.17	Al	15.00	15.73	8.70
Cu	6.47	21.50	14.37	Cu	5.33	18.10	8.87
Ni	4.50	14.70	10.43	Ni	2.23	17.10	9.30
Mn	31.80	13.90	11.27	Mn	25.07	18.00	8.93
Si				Si	0.60	18.60	27.50
O	48.67	32.87	50.77	O	52.37	12.47	36.73
48 Hour Oxidation at 1000 C							
Non Si Alloy				Si Alloy			
	Oxide Layer	Bulk	Interface		Oxide Layer	Bulk	Interface
Element	Avg At%	Avg At%	Avg At%	Element	Avg At%	Avg At%	Avg At%
Al	0.47	23.30	20.70	Al	30.87		
Cu	5.63	13.30	10.60	Cu	2.27		
Ni	0.17	15.47	8.30	Ni	0.40		
Mn	42.30	13.13	18.20	Mn	10.23		
Si				Si	0.27		
O	51.40	34.80	42.37	O	55.97		

5.2 Static Oxidation for 48 Hours at 600°C and 1000°C for Non Si and Si Alloy

After being exposed to oxidation in air for 48 hours at 600°C the oxide layer of the Non Si alloy can be seen in Figure 5.14 below. The oxide layer does look very similar to the oxide layer that formed after 24 hours at the same temperature. The morphology seems to be consistent and based on the EDS mapping, manganese and oxygen are dominant throughout the surface. However, there are very specific small regions where copper and nickel share the same area of richness. Aluminum is rich in different areas compared to the copper and nickel. There also is cracking present generally located near the oxides.

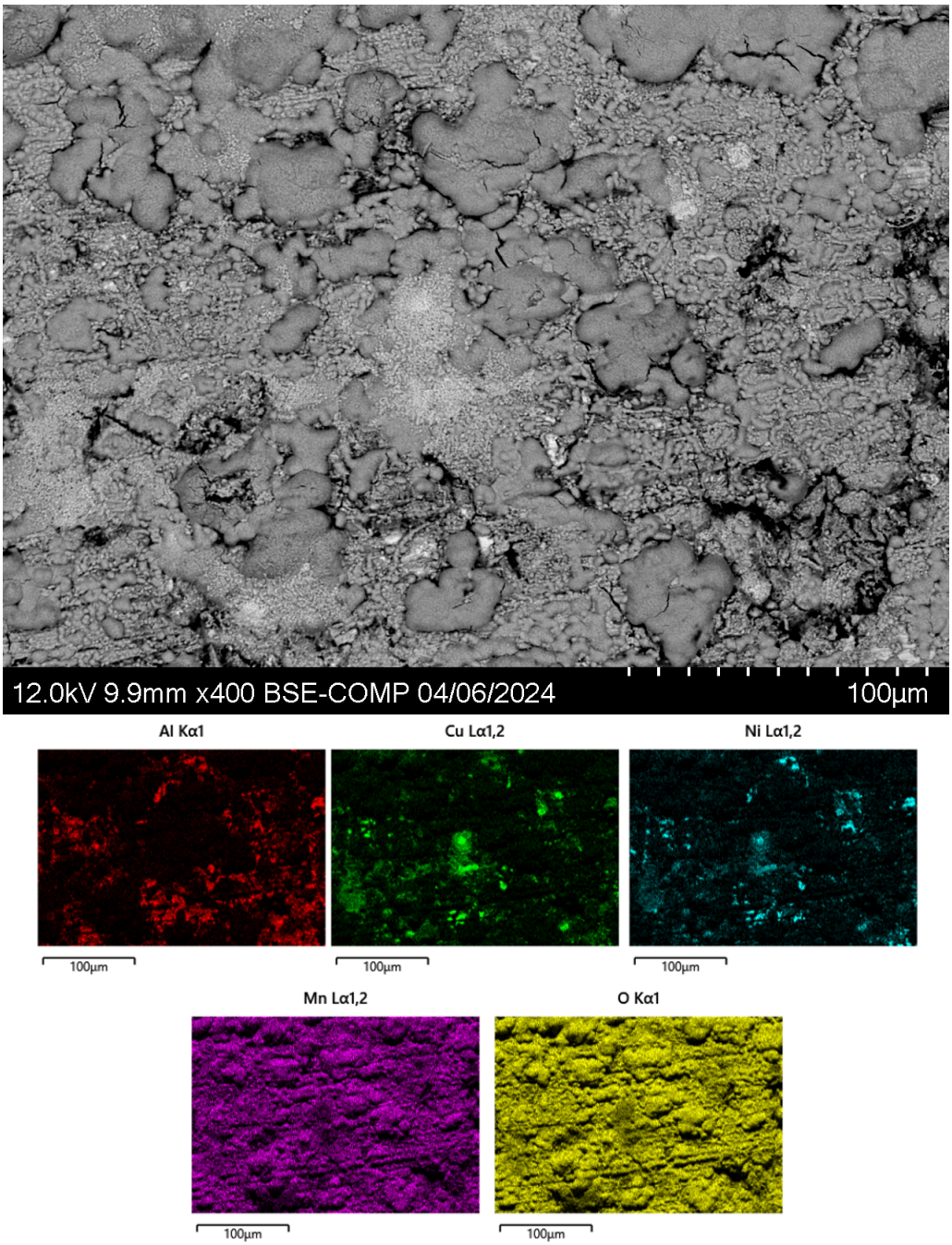

Figure 5.14 Oxide layer of Non Si alloy after 48 hour static oxidation at 600°C and energy dispersive spectroscopy elemental mapping

Figure 5.15 shows the microstructure after 48 hours of oxidation at 600°C of the Non Si alloy. There are still dark areas with aluminum and manganese oxides present. The white

microconstituent can still be viewed and remains rich in nickel. The gray matrix does consist of all the elements still, however there are thin, narrow areas where copper is rich.

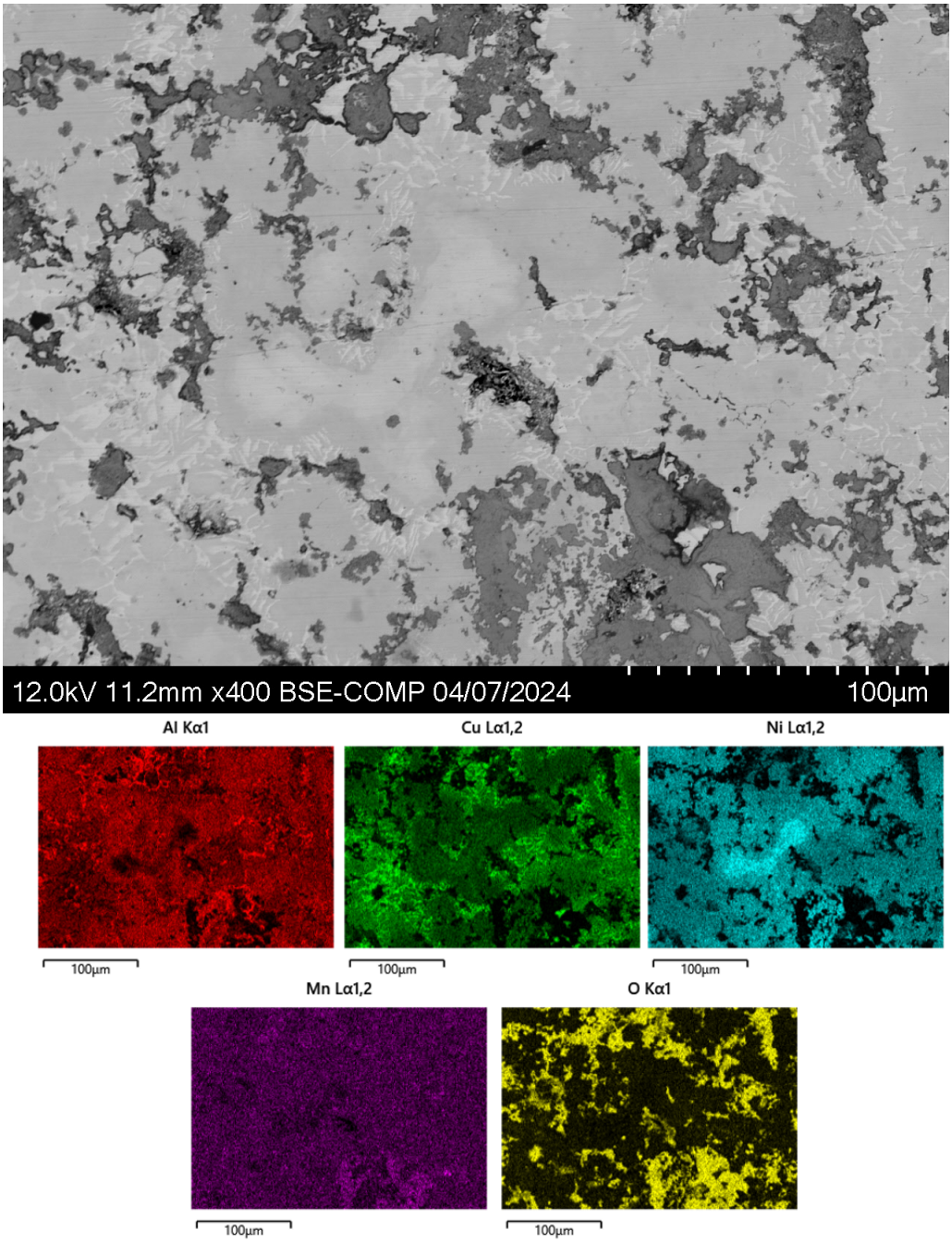

Figure 5.15 Microstructure of Non Si alloy after 48 hour static oxidation at 600°C and energy dispersive spectroscopy elemental mapping

The interface between the bulk material and the oxide layer of the Non Si alloy after 48 hours of oxidation at 600^{o}C can be seen below in Figure 5.16. Manganese oxides are predominantly present on the exterior of the oxide layer with some still within the bulk material. There is a presence of aluminum located at the interface. The copper and nickel elemental maps show that they share the same regions where they appear rich, however they are not located within the interface.

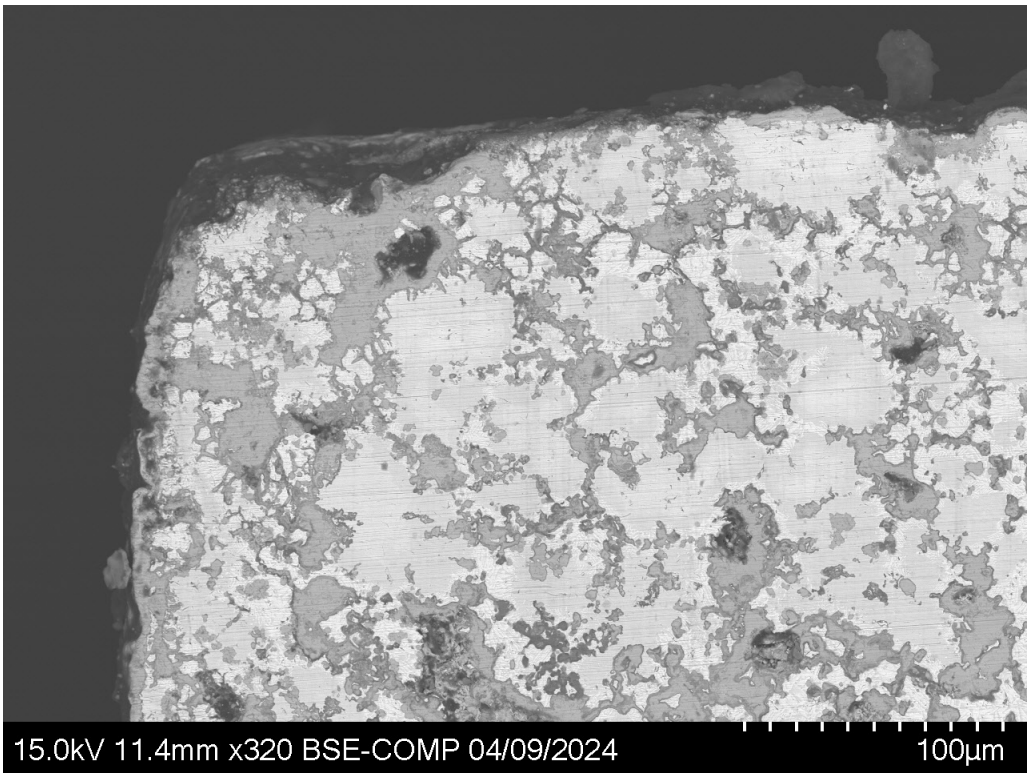

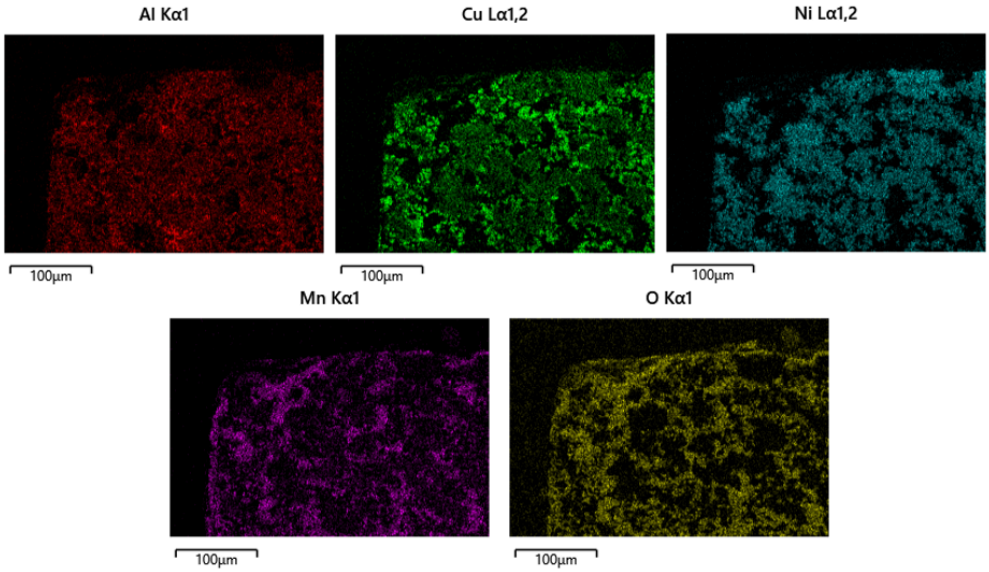

Figure 5.16 Oxide and bulk interface of Non Si Alloy after 48 hour static oxidation at 600°C and energy dispersive spectroscopy elemental mapping

The oxide layer of the Si alloy is seen below after being exposed to the same oxidation conditions as the Non Si alloy previously mentioned. The main difference is that a great amount of aluminum is present within the oxide layer along with manganese. Similar to the Non Si alloy, there are very small regions where copper and nickel are rich. Silicon does not appear to have a significant contribution to the oxide layer based on EDS mapping results. Another observation is that cracking is visible on the surface located near oxides.

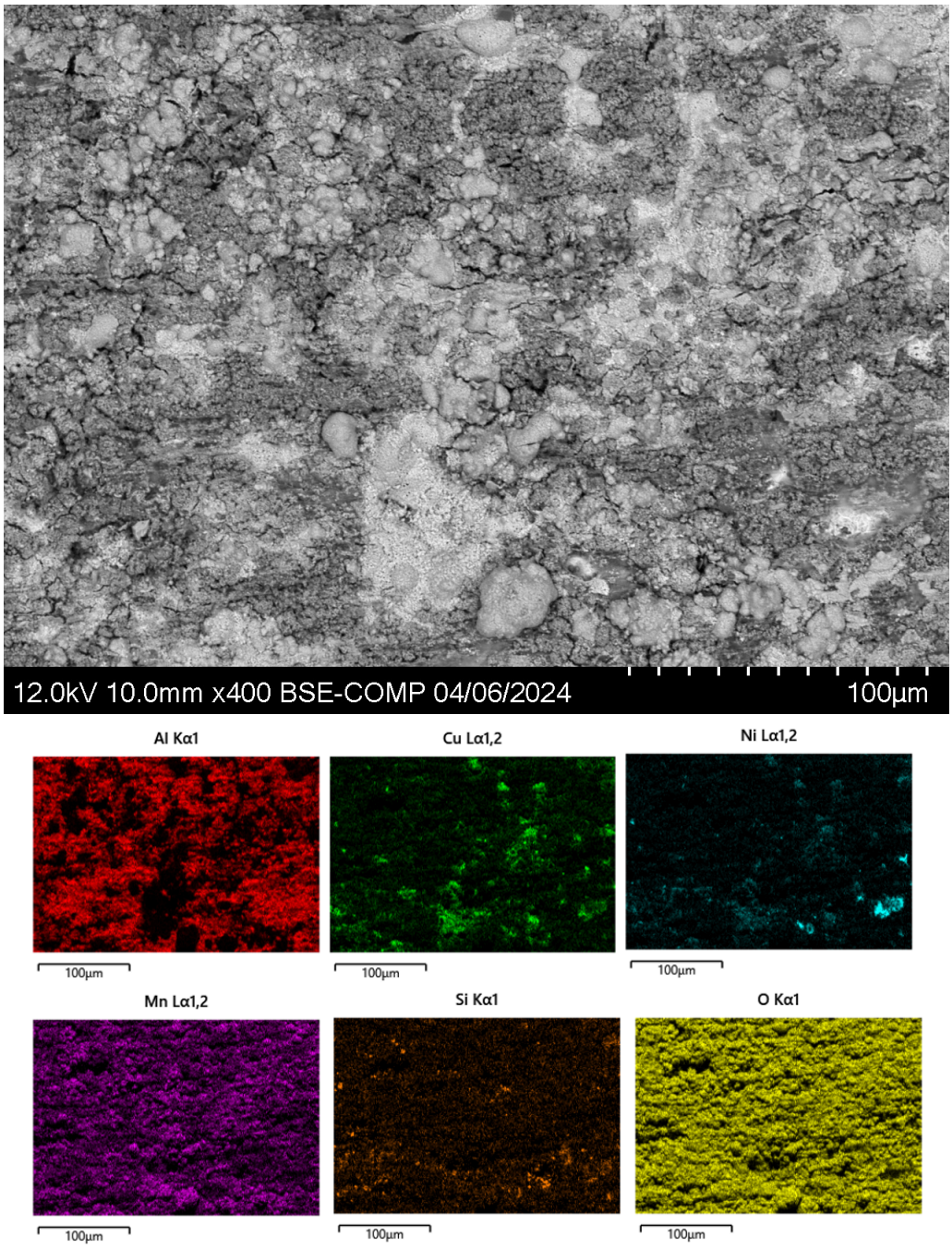

Figure 5.17 Oxide layer of Si alloy after 48 hour static oxidation at 600°C and energy dispersive spectroscopy elemental mapping

The bulk microstructure of the Si alloy can be displayed in the figure below after being exposed to 600°C for 48 hours. Overall, the microstructure does appear to be consistent with the previous Si alloy that had the same oxidation temperature but was only held for 24 hours. The

black regions are aluminum oxides present within the bulk material and are located within the interdendritic regions. The gray matrix is rich in copper, nickel, and aluminum. The manganese rich and nickel rich microconstituent is still present.

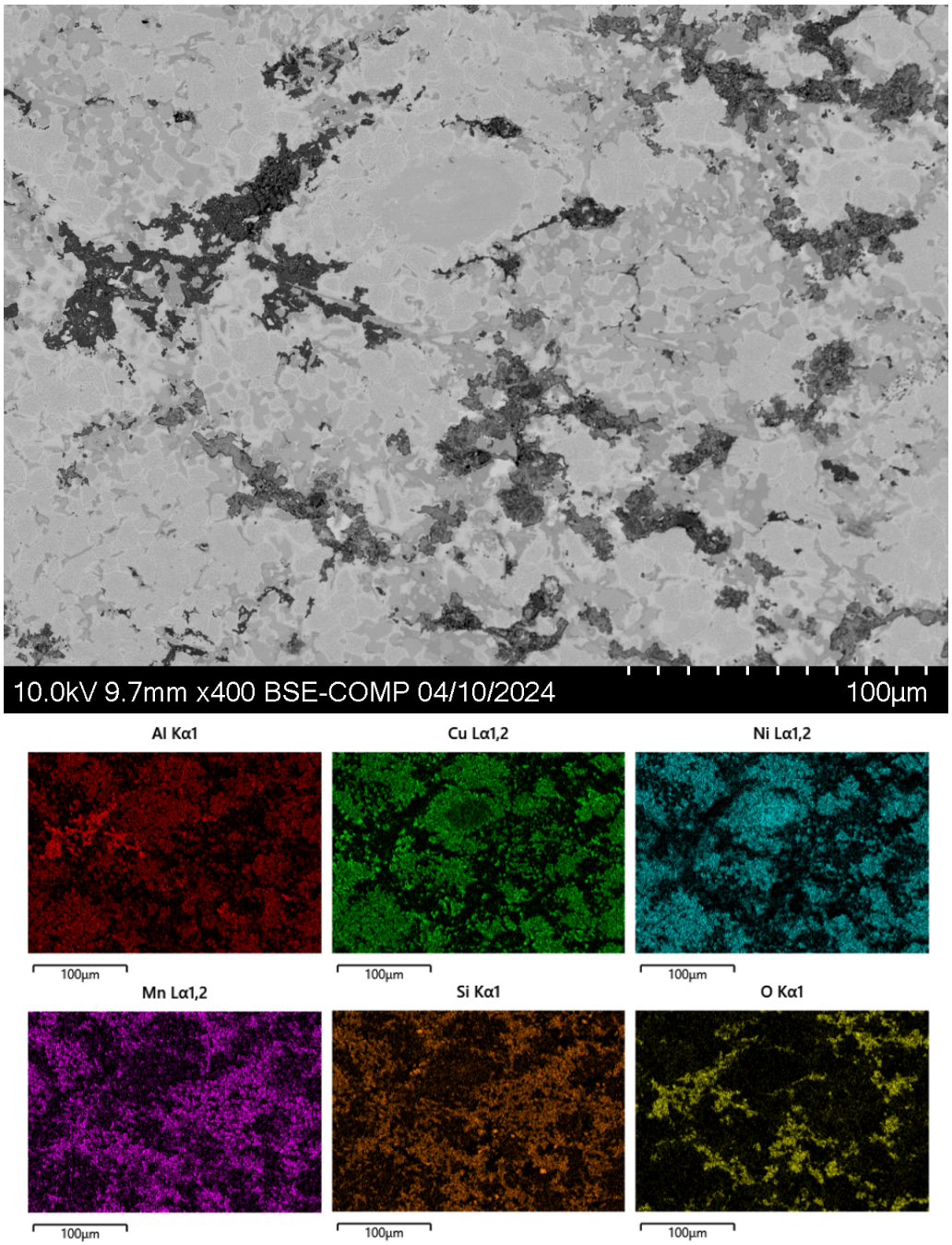

Figure 5.18 Microstructure of Si alloy after 48 hour static oxidation at 600°C and energy dispersive spectroscopy elemental mapping

The figure below represents the interface between the bulk material and the oxide layer after 48 hours of oxidation treatment at 600°C. The Si alloy's interface does show how the aluminum and manganese oxides remain present within the bulk and at the edge of the material creating the oxide layer.

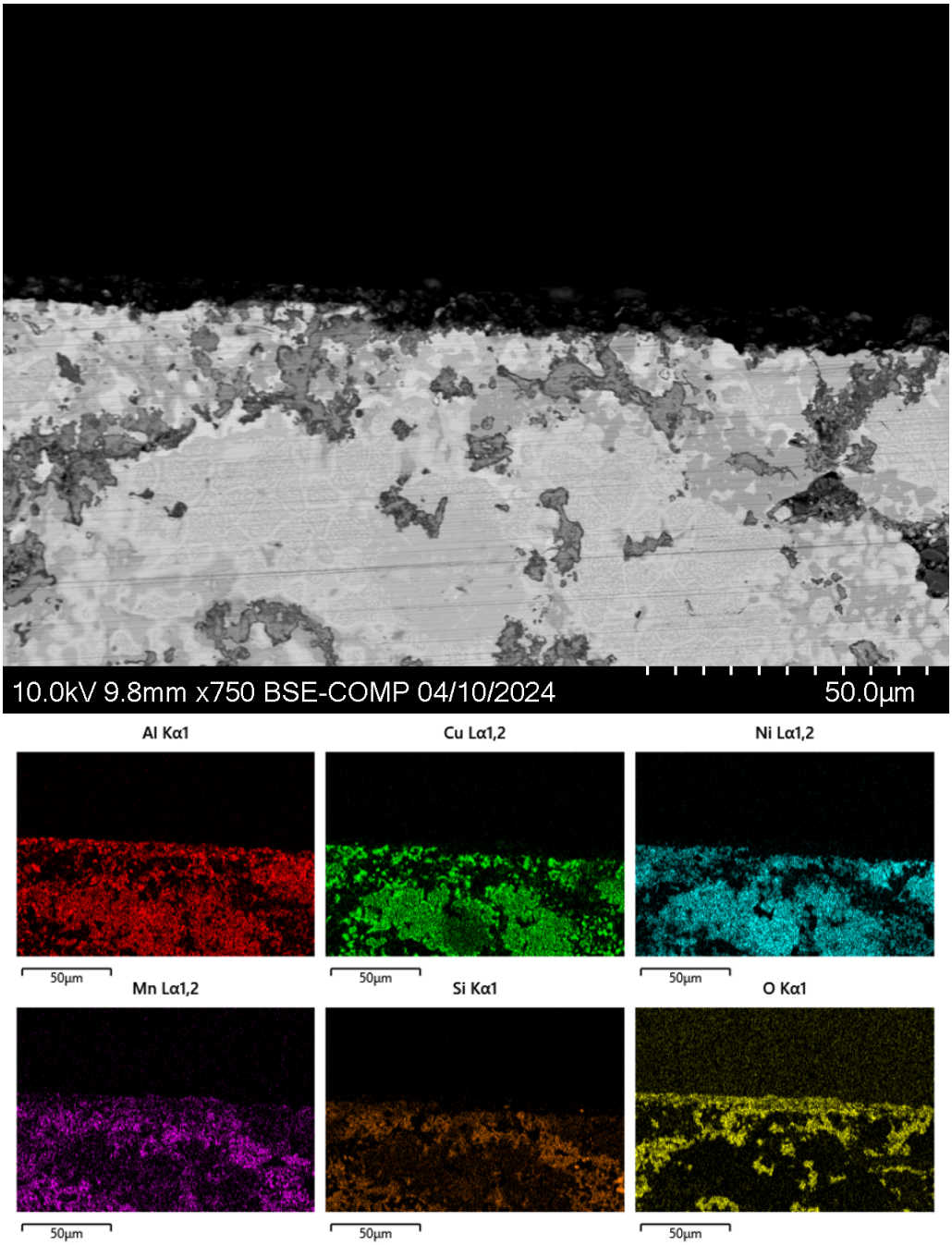

Figure 5.19 Oxide and bulk interface of Si Alloy after 48 hour static oxidation at 600°C

and energy dispersive spectroscopy elemental mapping

The XRD spectra represents the oxide layer from both alloys at 600°C (Figure 5.20). Consistent with the EDS data, aluminum and manganese are present on the oxide layer and are in the form of Al_2O_3 and Mn_2O_3.

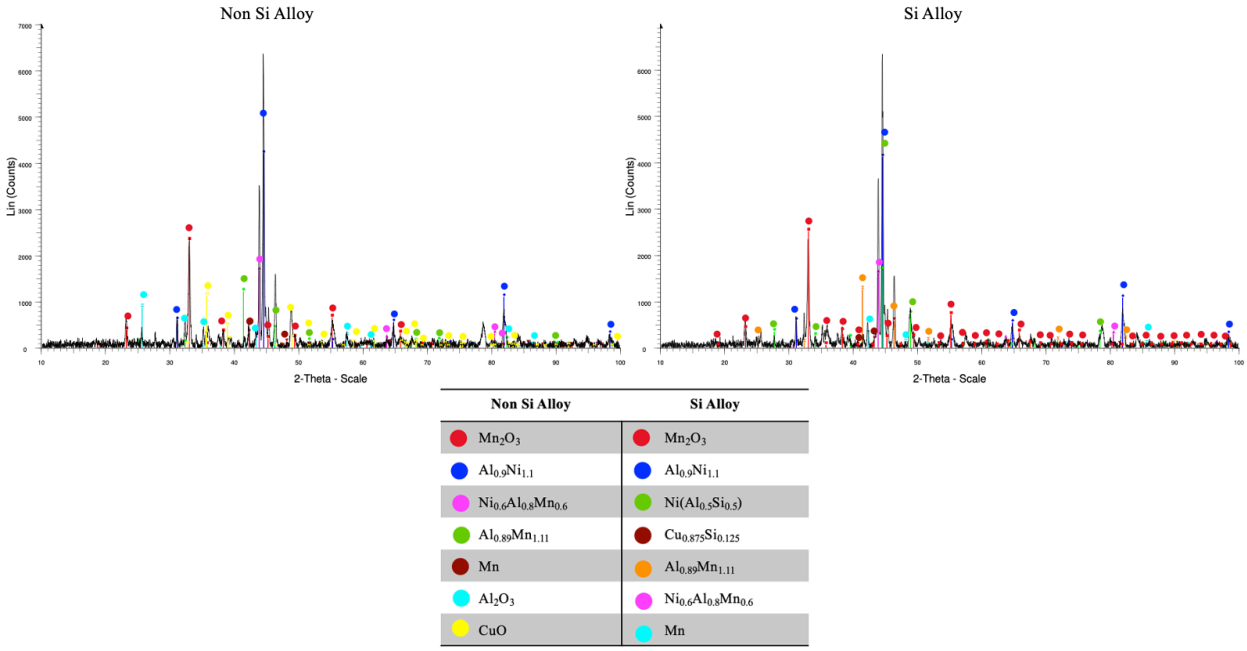

Figure 5.20 X-ray diffraction of oxide layer of Non Si and Si alloy after 48 hour static oxidation at 600°C

The oxide layer of the Non Si alloy after 48 hours held at 1000°C showed very similar oxides as seen at 1000°C but 24 hour oxidation time. The morphology of the oxide layer can be seen in Figure 5.21. Due to the increase of temperature the size of the oxides have increased and the majority of the surface is covered with manganese oxides. The manganese oxides have the same copper and nickel rich "twin-like" features that were seen before. There is a region extremely rich in aluminum and the crystals seem to be smaller in size than the faceted manganese oxides.

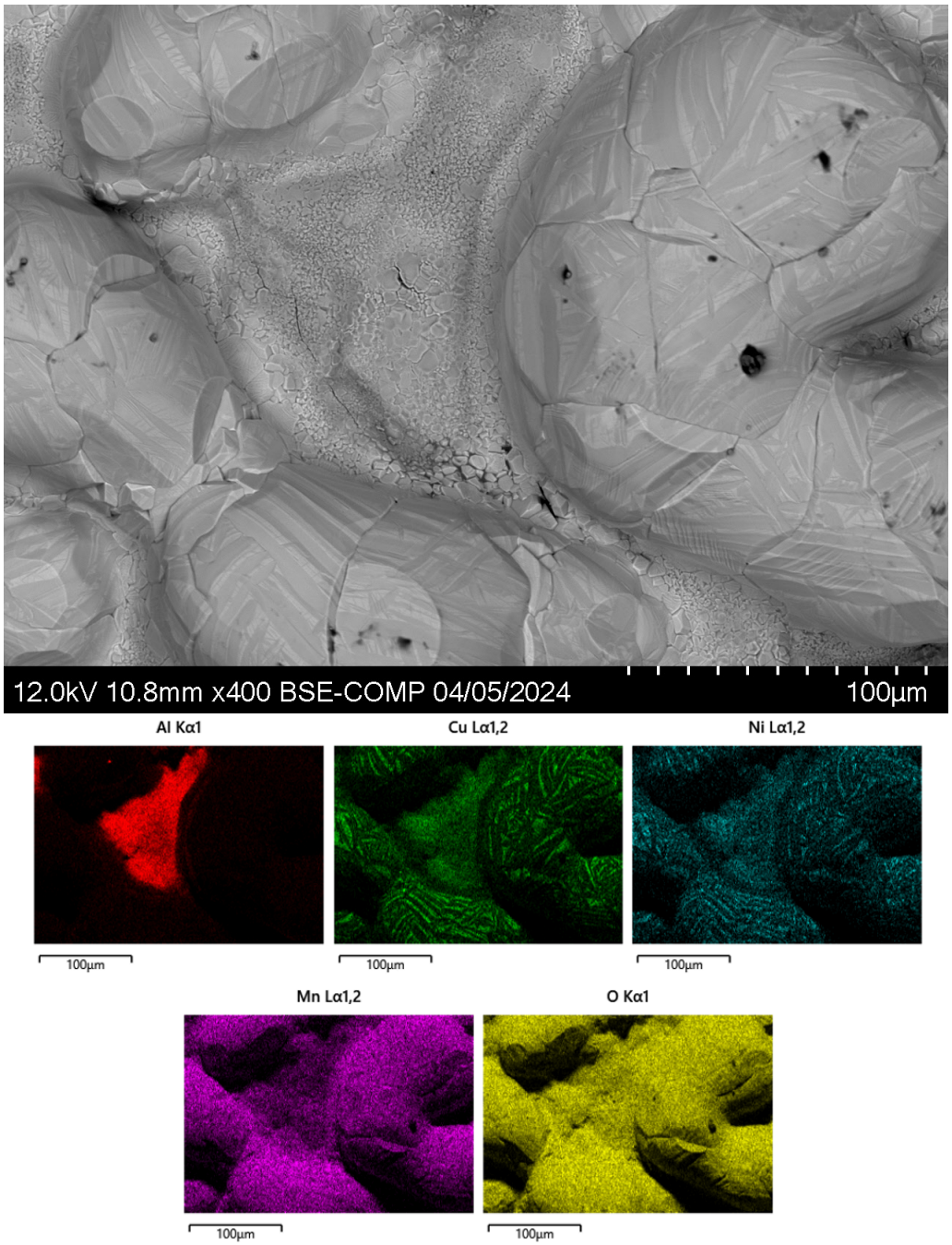

Figure 5.21 Oxide layer of Non Si alloy after 48 hour static oxidation at 1000°C and energy dispersive spectroscopy elemental mapping

The bulk microstructure of the Non Si alloy after being exposed to 1000°C for a time duration of 48 hours is shown in Figure 5.22. The black regions that are present appear to be rich in aluminum. There is a presence of manganese in these regions as well, however the aluminum

seems to have a bigger contrast within the elemental maps. The gray matrix clearly shows a richness of copper and nickel.

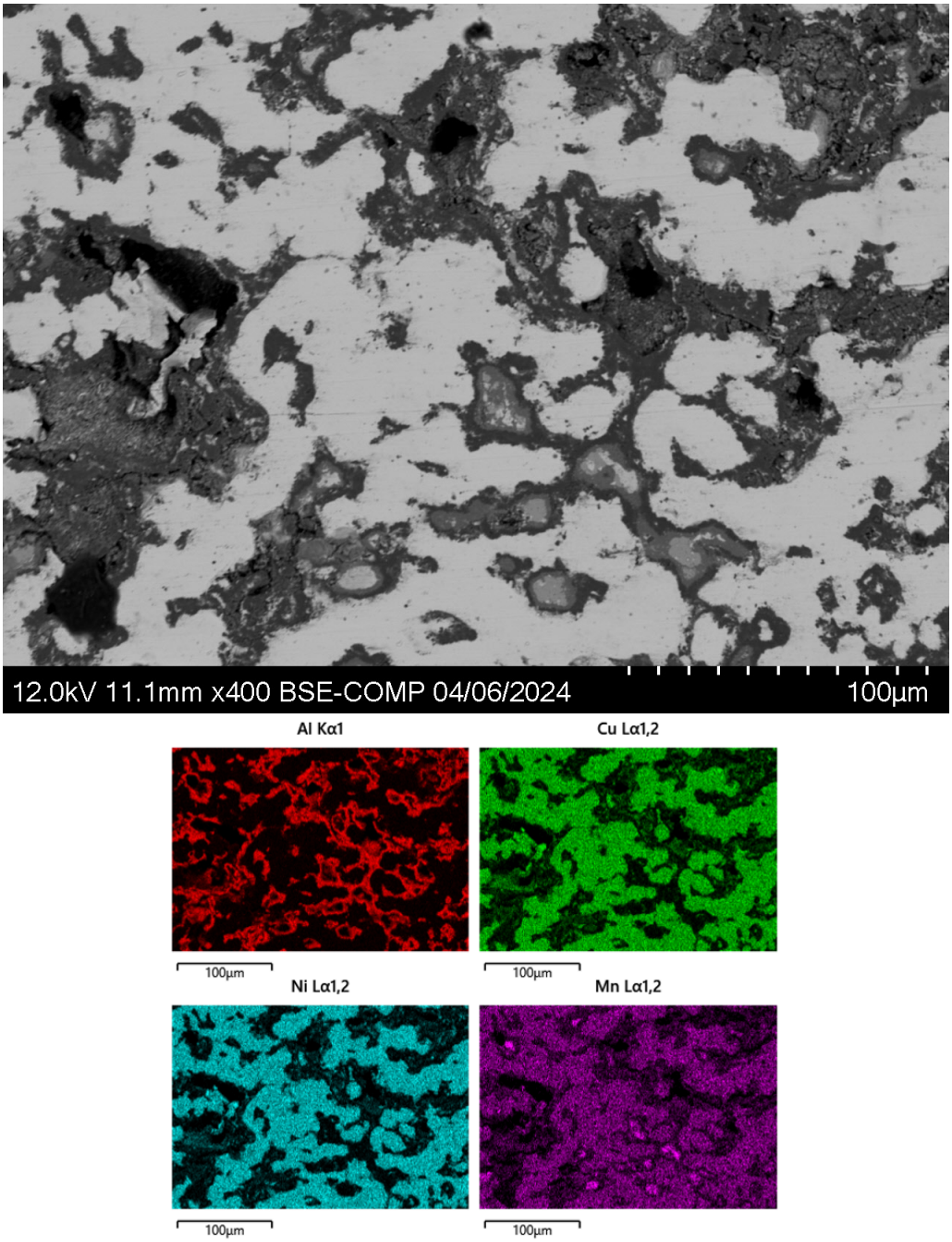

Figure 5.22 Microstructure of Non Si alloy after 48 hour static oxidation at 1000°C and energy dispersive spectroscopy elemental mapping

The images below shows a clear representation of the morphology of the oxide layer that formed after oxidation in air at 1000°C for 48 hours. In Figure 5.23 there is a distinction between the aluminum oxides and the manganese oxides. The aluminum oxides reside within the bulk material and do have a very thin layer at the interface shown in the red elemental map. The manganese oxide primarily dominates the exterior of the oxide layer shown in the purple elemental map.

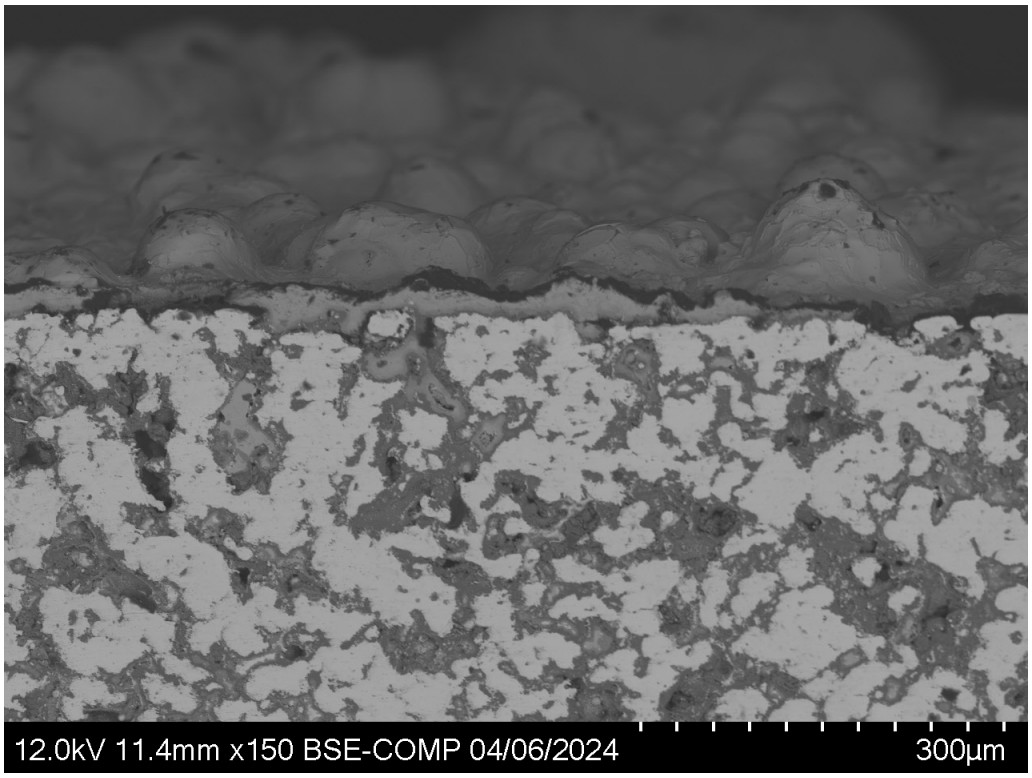

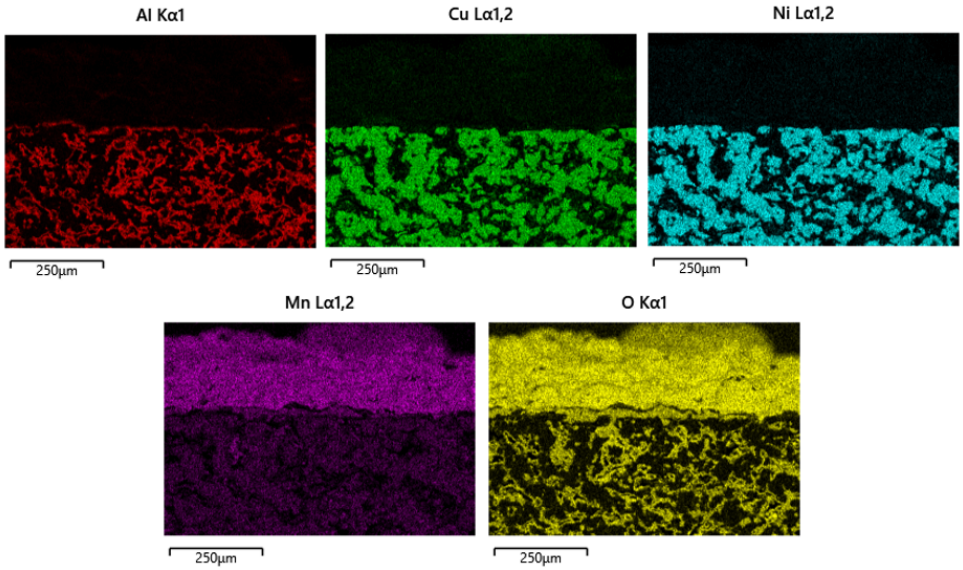

Figure 5.23 Oxide and bulk interface of Non Si Alloy after 48 hour static oxidation at 1000°C and energy dispersive spectroscopy elemental mapping

The oxide layer that developed after 48 hour oxidation at 1000°C for the Si alloy is shown in Figure 5.24. The light gray regions appear to be rich in manganese while the darker regions are rich in aluminum. Copper, nickel, and silicon do not have a strong elemental composition presence within the oxide layer based of EDS results.

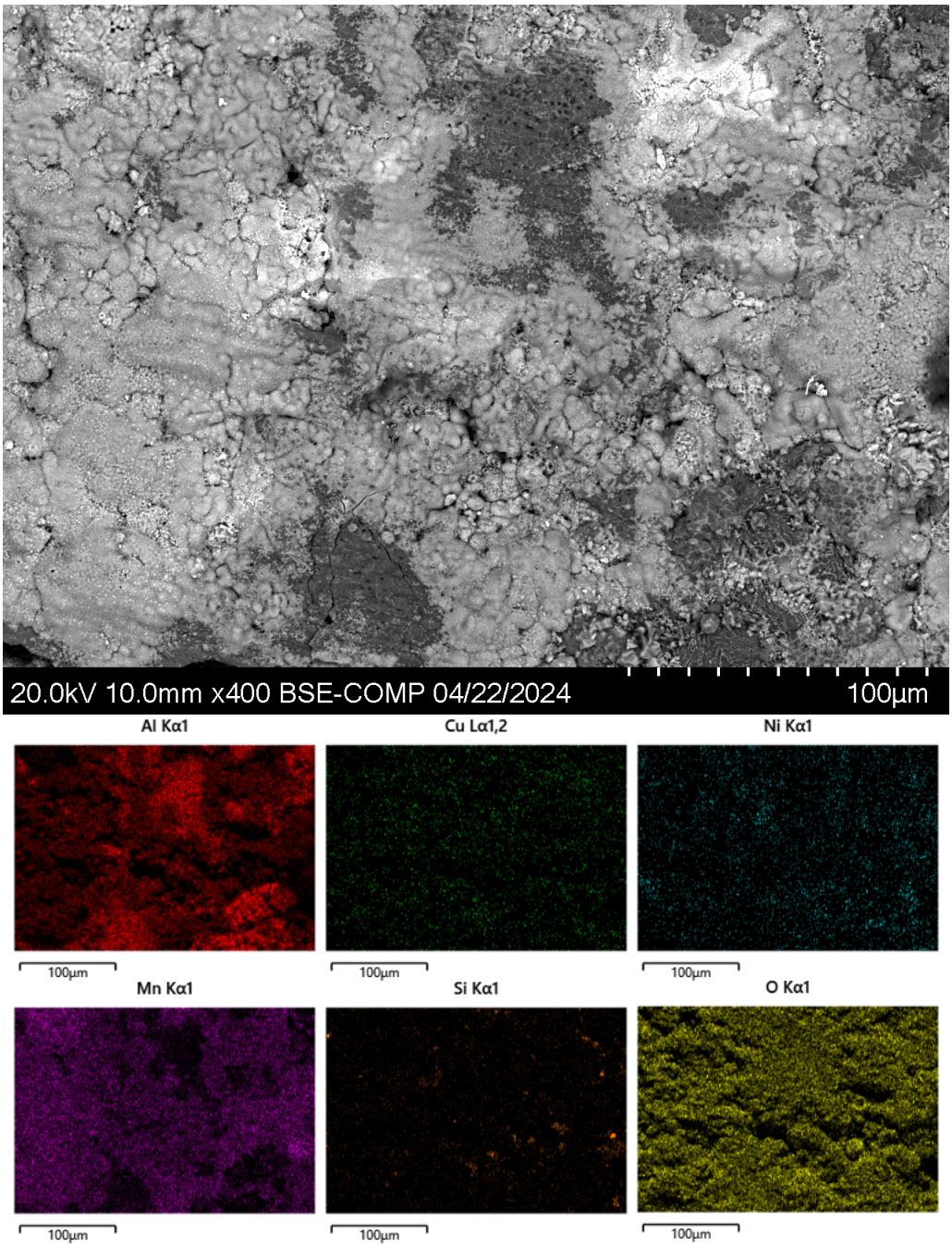

Figure 5.24 Oxide layer of Si alloy after 48 hour static oxidation at 1000°C and energy dispersive spectroscopy elemental mapping

After being exposed to 1000°C for 48 hours, the Si alloy was highly oxidized and metallography was not able to be performed on the sample. Figure 5.25 shows the appearance of

the sample after being heated and the sample did have scaling due to oxidation. Whenever handling the sample, the material would fragment and was almost “powder-like.”

Figure 5.25 Si alloy after 48 hour static oxidation at 1000°C

Through EDS the average atomic percentage was obtained for the oxide layer, bulk microstructure, and the interface. Table 5.2 displays the results. The Non Si alloy shows a higher composition of manganese at both, 600°C and 1000°C, resulting in a predominantly manganese rich oxide layer. The Si alloy shows that at 600°C, the aluminum elemental composition increases, and the manganese composition is not as high as in the Non Si alloy. This oxide layer becomes rich in both aluminum and manganese. At 1000°C, the aluminum composition increases, and the manganese composition decreases significantly.

Table 5.2 Average elemental composition of oxide layer, bulk microstructure, and interface of Non Si and Si alloy after 48 hour oxidation at 600°C and 1000°C

48 Hour Oxidation at 600 C							
Non Si Alloy				Si Alloy			
	Oxide Layer	Bulk	Interface		Oxide Layer	Bulk	Interface
Element	Avg At%	Avg At%	Avg At%	Element	Avg At%	Avg At%	Avg At%
Al	2.7	19.6	18.83	Al	19.97	15.83	14.87
Cu	4.93	18.83	15.4	Cu	2.87	18.07	15.9
Ni	1.1	19.43	19.83	Ni	1.07	19.5	15.77
Mn	39.1	16.57	13.43	Mn	24.33	18.1	15.83
Si				Si	0.4	16.1	14.4
O	52.13	25.53	32.5	O	51.37	12.47	23.2

48 Hour Oxidation at 1000 C							
Non Si Alloy				Si Alloy			
	Oxide Layer	Bulk	Interface		Oxide Layer	Bulk	Interface
Element	Avg At%	Avg At%	Avg At%	Element	Avg At%	Avg At%	Avg At%
Al	3.87	38.8	20.83	Al	31.87		
Cu	5.3	24.97	13.03	Cu	0.5		
Ni	0.2	21.43	11.7	Ni	0.53		
Mn	38.83	14.83	13.37	Mn	9.03		
Si				Si	0.42		
O	51.83		41.03	O	57.6		

Figure 5.26 displays the XRD spectra relating to the Non Si and Si alloy oxide layer after 1000°C oxidation for 48 hours. Aluminum and manganese are oxidized are they have been identified as Mn_3O_4 and Al_2O_3.

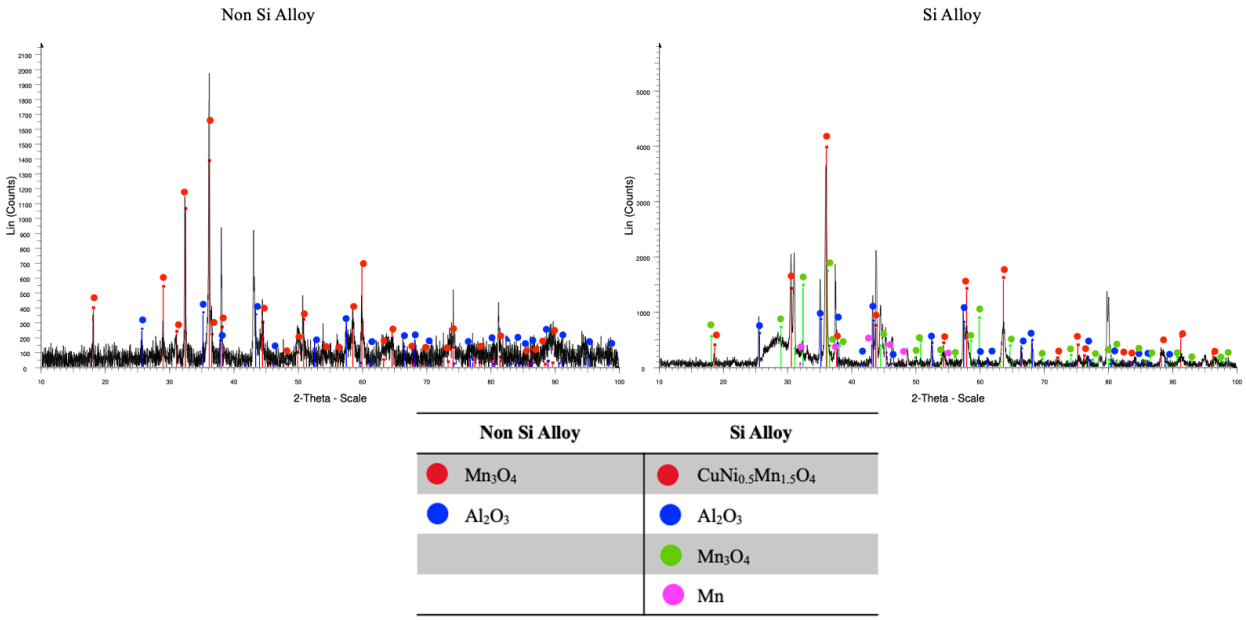

Figure 5.26 X-ray diffraction of oxide layer of Non Si and Si alloy after 48 hour static oxidation at 1000°C

5.3 Static Oxidation for 72 Hours at 600°C and 1000°C for Non Si and Si Alloy

After being subjected to oxidation for 72 hours at 600°C, the Non Si alloy's oxide layer is very consistent with the other samples that were held at the same temperature but for 24 and 48 hours. According to the elemental mapping, aluminum, manganese, and oxygen are the major elements that are rich within the oxide layer. The cracking, that was also present at 48 hours at 600°C, is also evident. This can be seen in the Figure 5.27.

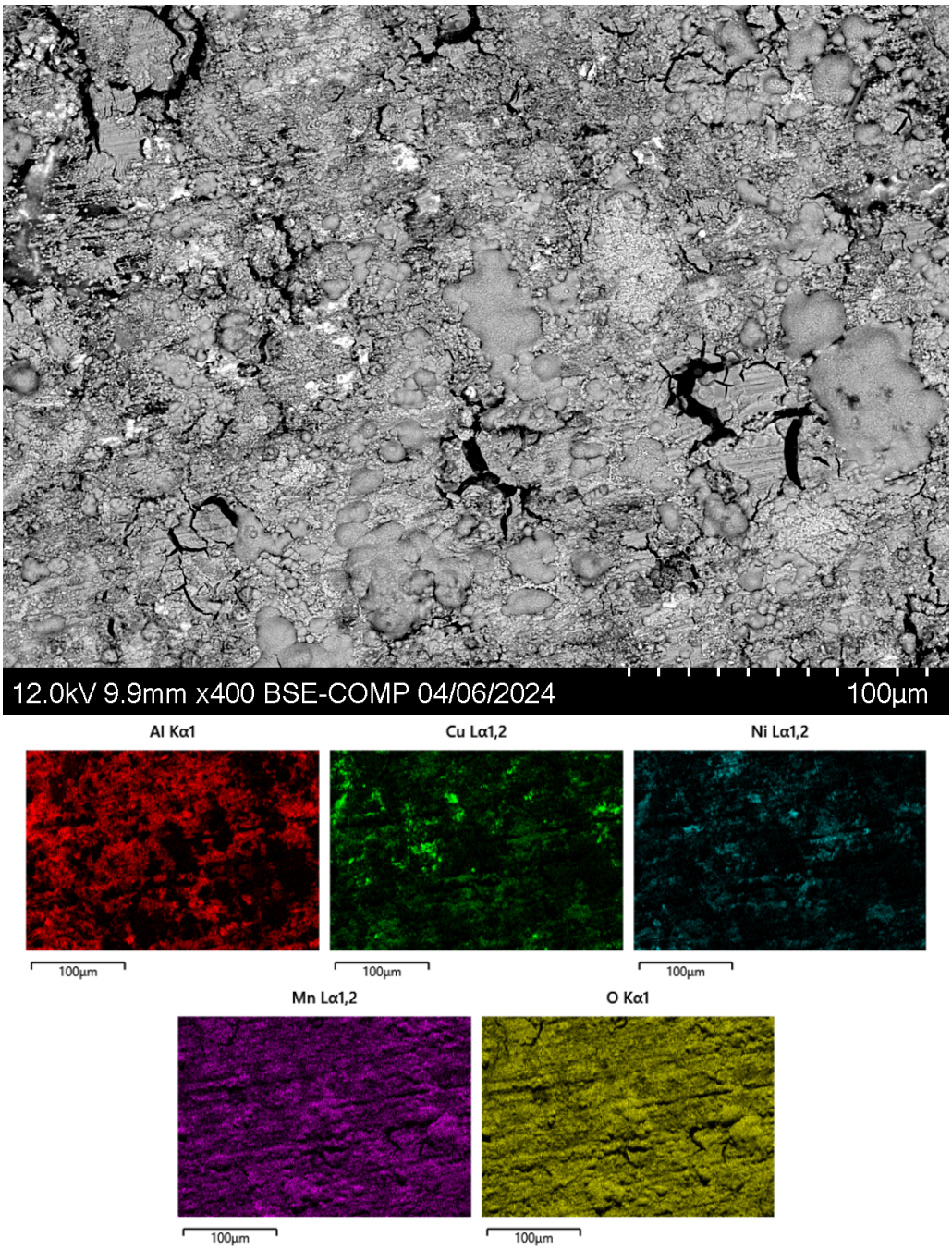

Figure 5.27 Oxide layer of Non Si alloy after 72 hour static oxidation at 600°C and energy dispersive spectroscopy elemental mapping

The bulk microstructure of the Non Si alloy post 72 hour oxidation at 600°C can be seen in Figure 5.28. The material still obtains a dendritic structure. Copper and nickel remain consistent with being not associated with oxygen rich areas present. These elements are mainly

found within the gray matrix of the microstructure, and aluminum is dispersed throughout. Manganese and oxygen are rich within the dark regions within the microstructure. The white microconstituent that is rich in nickel is still present. Also, consistent with the Non Si alloy that was exposed to oxidation at the same temperature but for 48 hours, there are small thin regions of copper rich portions.

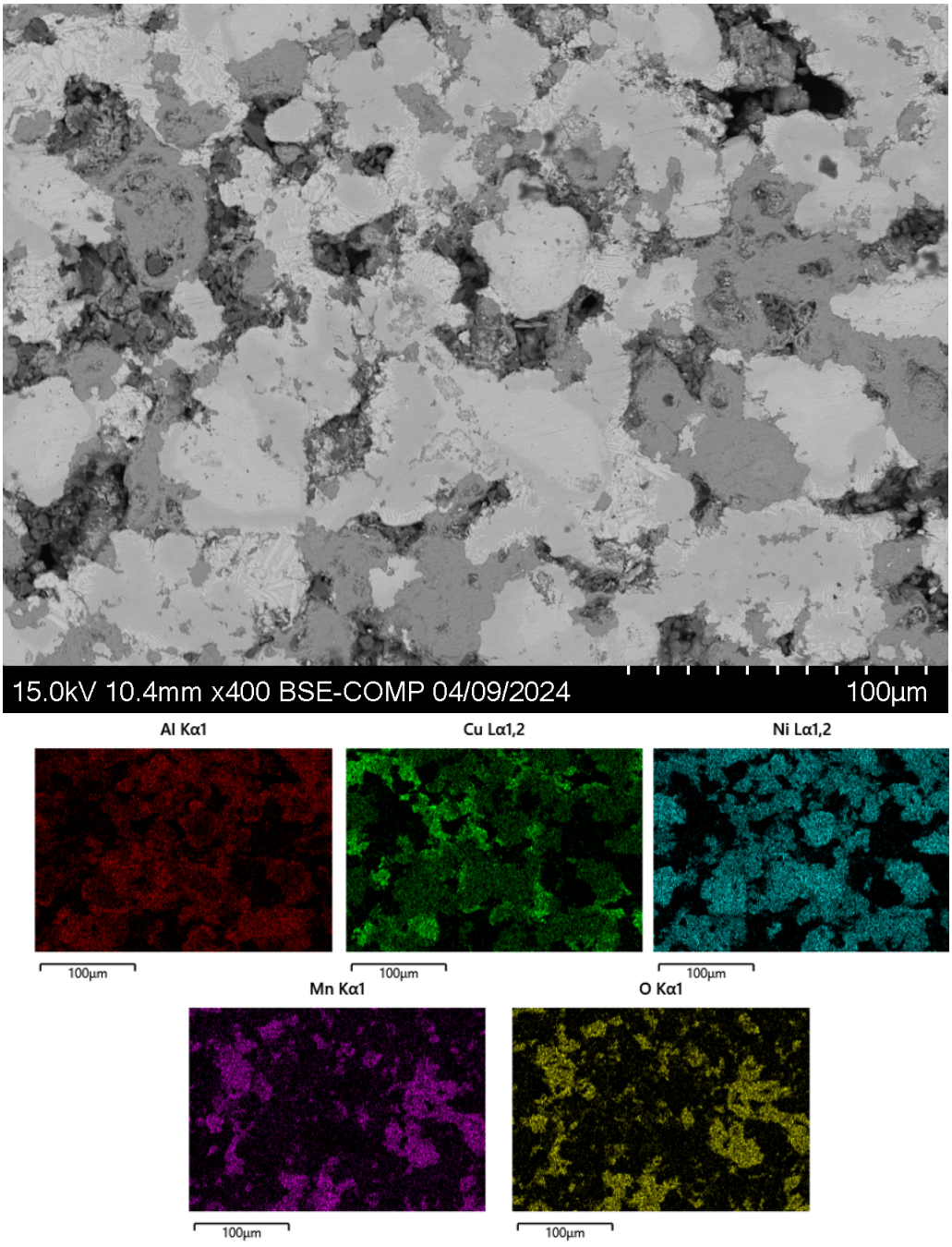

Figure 5.28 Microstructure of Non Si alloy after 72 hour static oxidation at 600°C and energy dispersive spectroscopy elemental mapping

The interface between the oxide layer and the microstructure can be viewed below in Figure 5.29 for the Non Si alloy. Based on the elemental color mapping there is a presence of aluminum and manganese within the interface. Manganese appears to be rich in the bulk region and continues into the interface.

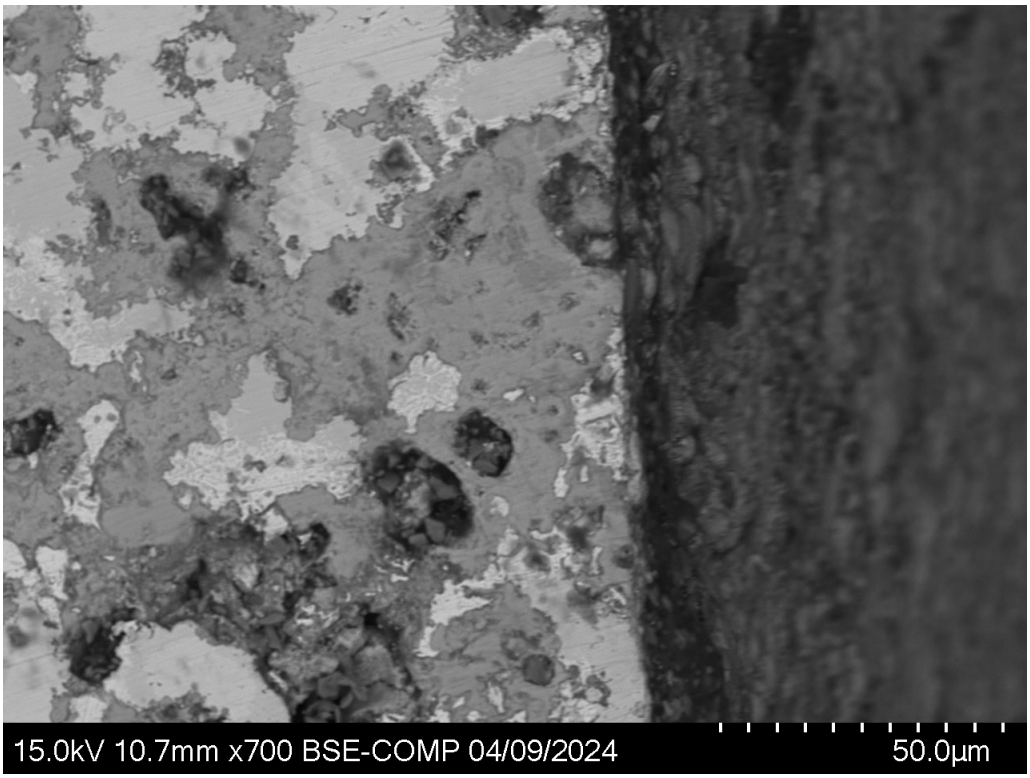

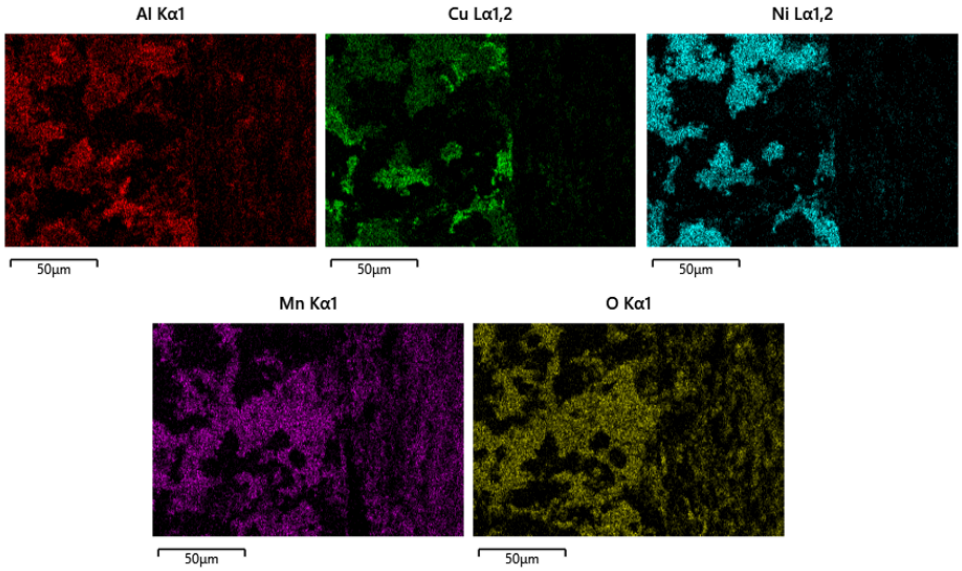

Figure 5.29 Oxide and bulk interface of Non Si Alloy after 72 hour static oxidation at 600°C and energy dispersive spectroscopy elemental mapping and Elemental Mapping

The oxide layer of the Si alloy after 72 hours at 600°C showed similar results to the same alloy held at 48 hours at the same oxidation temperature (Figure 5.30). Aluminum, manganese, and oxygen are the main elements present within the oxide layer. Silicon does not have a significant area that is predominantly rich, but there is a very small segments where silicon can be found. Copper and nickel share very similar regions where both elements appear to be rich, however it is only in small regions.

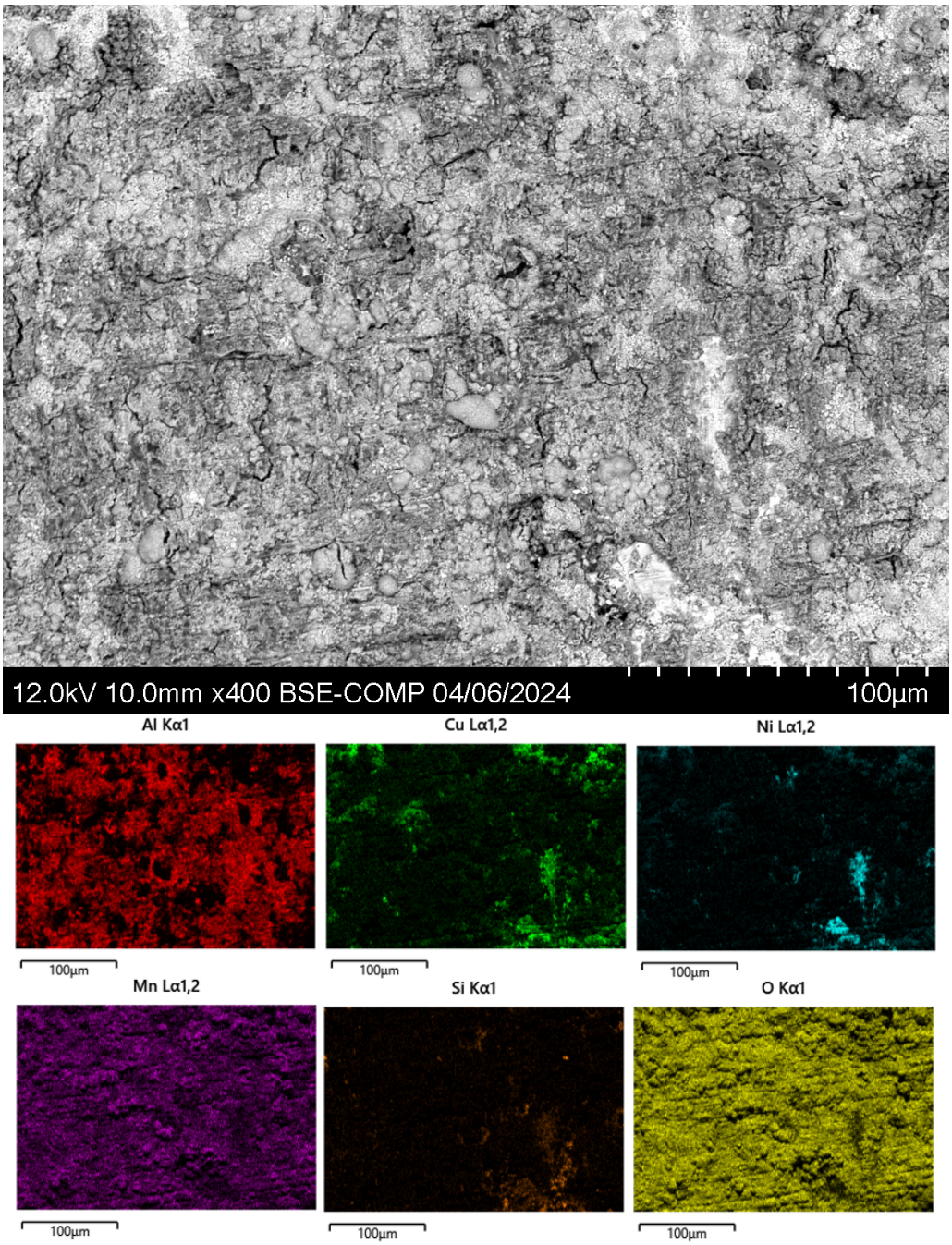

Figure 5.30 Oxide layer of Si alloy after 72 hour static oxidation at 600°C and energy dispersive spectroscopy elemental mapping

The microstructure post 72 hour oxidation at 600°C is comparable to the results of the Si alloys that were subjected to the previous oxidation studies mentioned. Manganese rich areas are shown with the black regions and the gray matrix is still primarily rich in aluminum, copper, and nickel. Silicon is dispersed throughout but seems to share the same regions where manganese is

rich. Nickel can be found within the white microconstituent and dispersed through the matrix. This can be seen in the Figure 5.31.

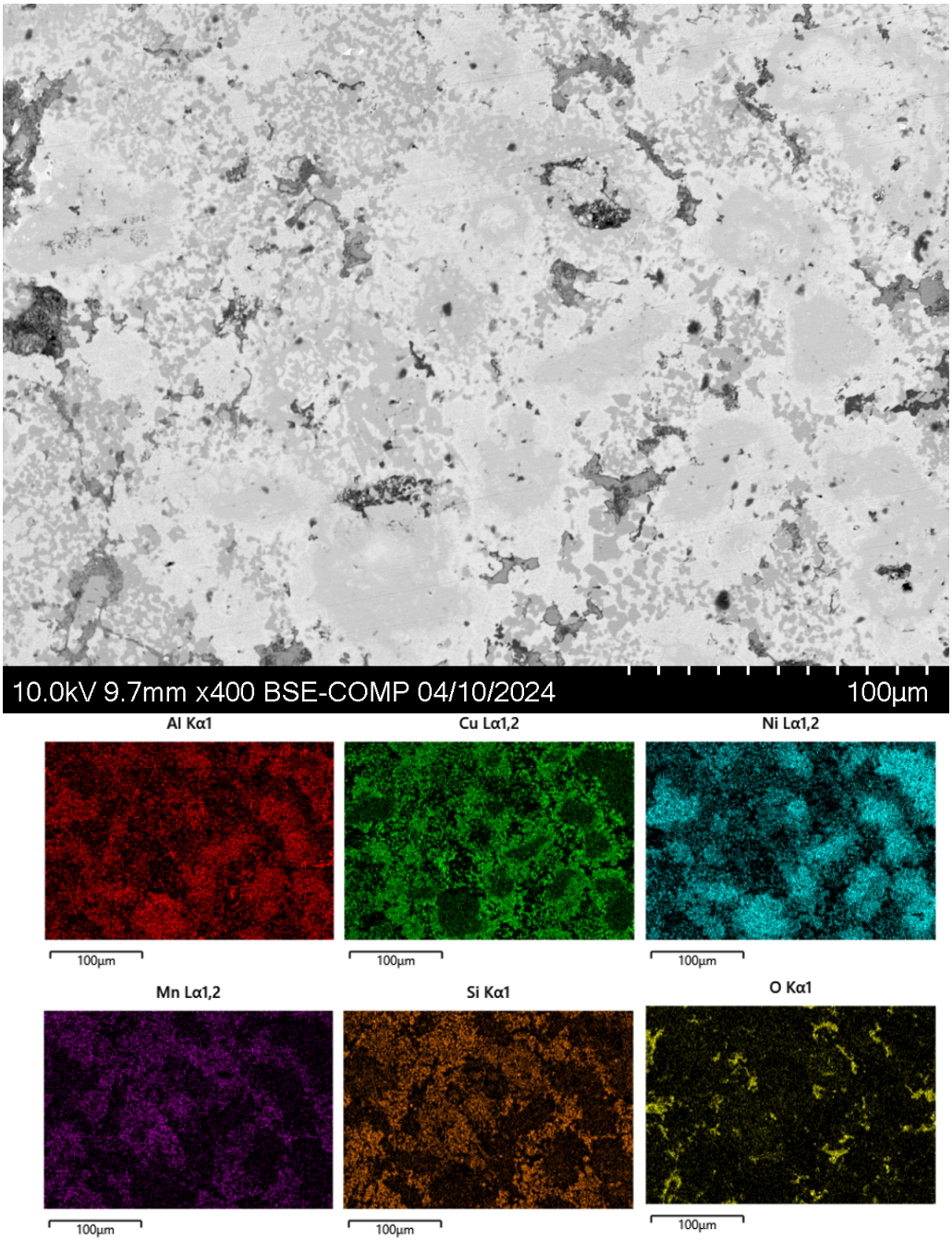

Figure 5.31 Microstructure of Si alloy after 72 hour static oxidation at 600°C and energy dispersive spectroscopy elemental mapping

The interface of the Si alloy after 72 hour oxidation at 600^{O}C can be seen in Figure 5.32. Based on the EDS data that was gathered, aluminum and oxygen appear to rich in the same regions located at the interface. The interface does not have a strong presence of copper and nickel.

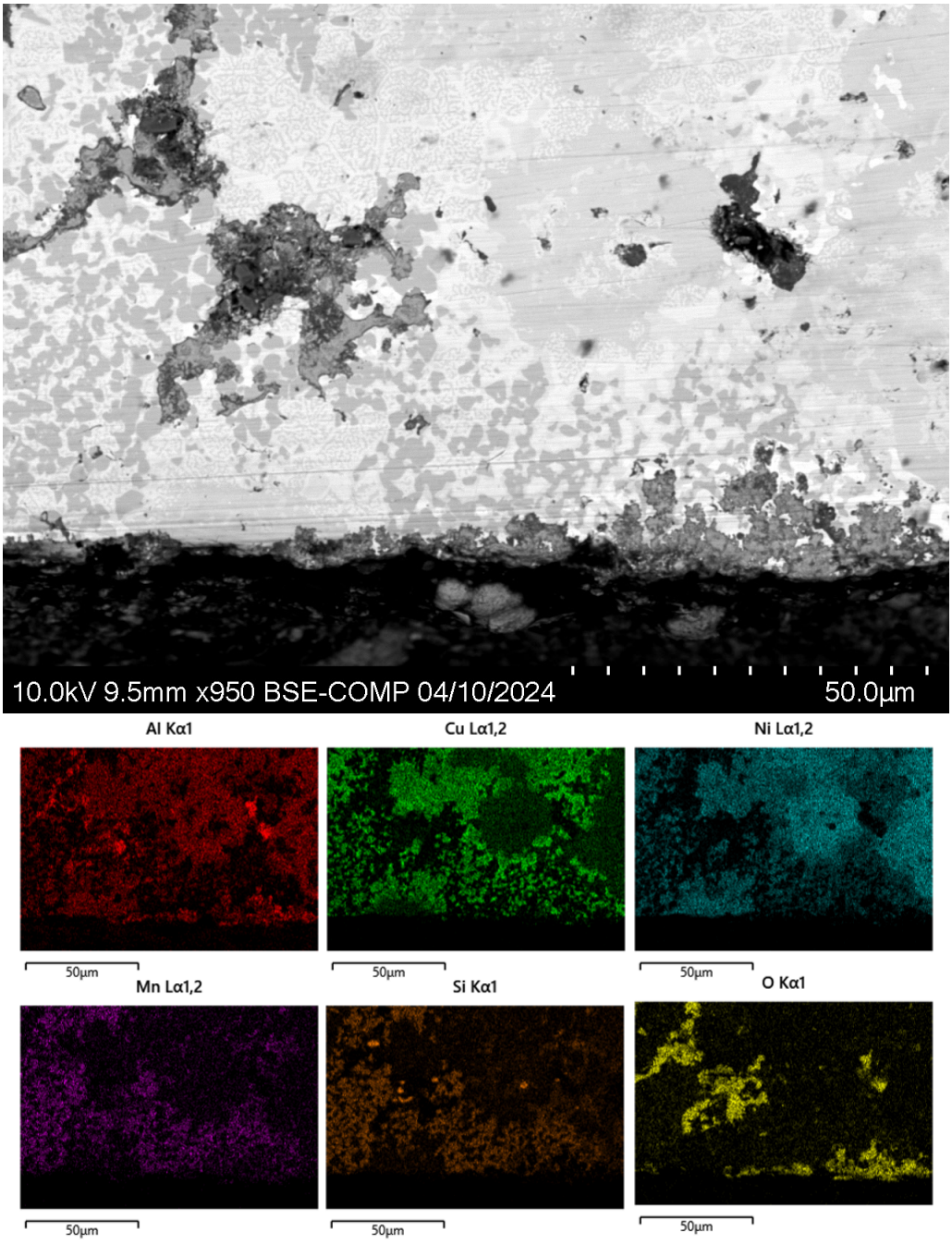

Figure 5.32 Oxide and bulk interface of Si Alloy after 72 hour static oxidation at 600^{o}C

and energy dispersive spectroscopy elemental mapping

Consistent with the previous XRD data that was collected, the oxide layers for the Non Si and Si alloy after a 72 hour duration of being exposed to 600°C contains aluminum and manganese oxides. The peaks relating to these oxides have been recognized as Al_2O_3 and Mn_2O_3 (Figure 5.33).

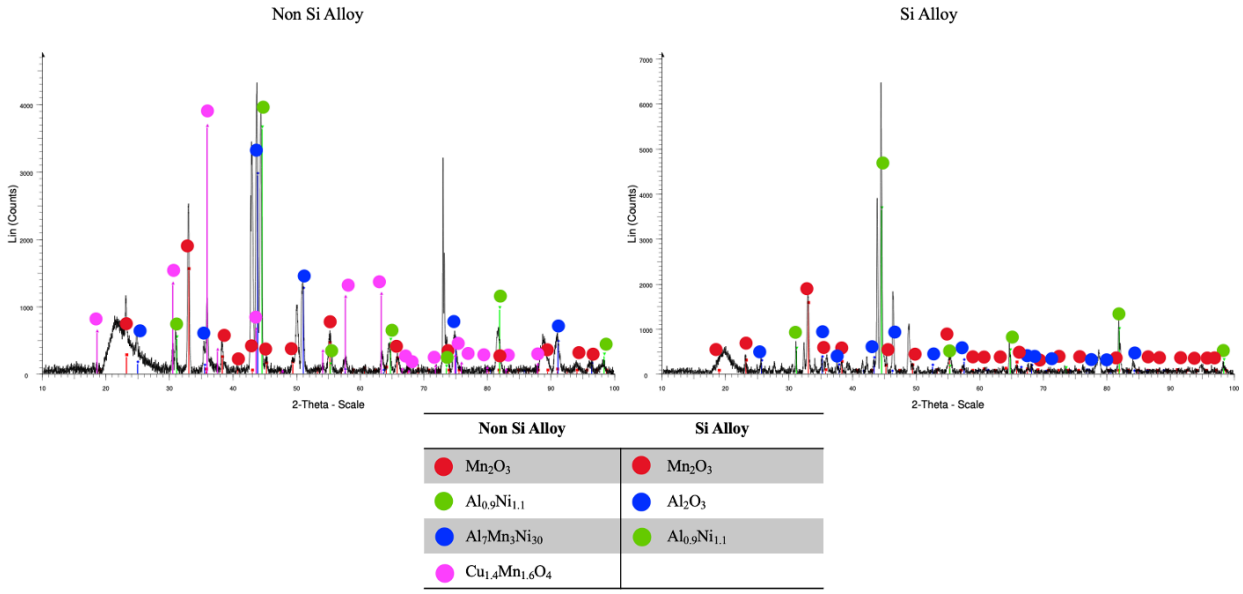

Figure 5.33 X-ray diffraction of oxide layer of Non Si and Si alloy after 72 hour static oxidation at 600°C

In Figure 5.34 the oxide layer of the Non Si alloy after being exposed to 1000°C for a 72 hour time duration is shown. Manganese and oxygen are dominate on the surface and the aluminum rich areas are present in between large areas of manganese oxides. As seen before, there are copper and nickel rich "twin-like" features present within the manganese oxides. The manganese oxides continue to grow in a faceted nature.

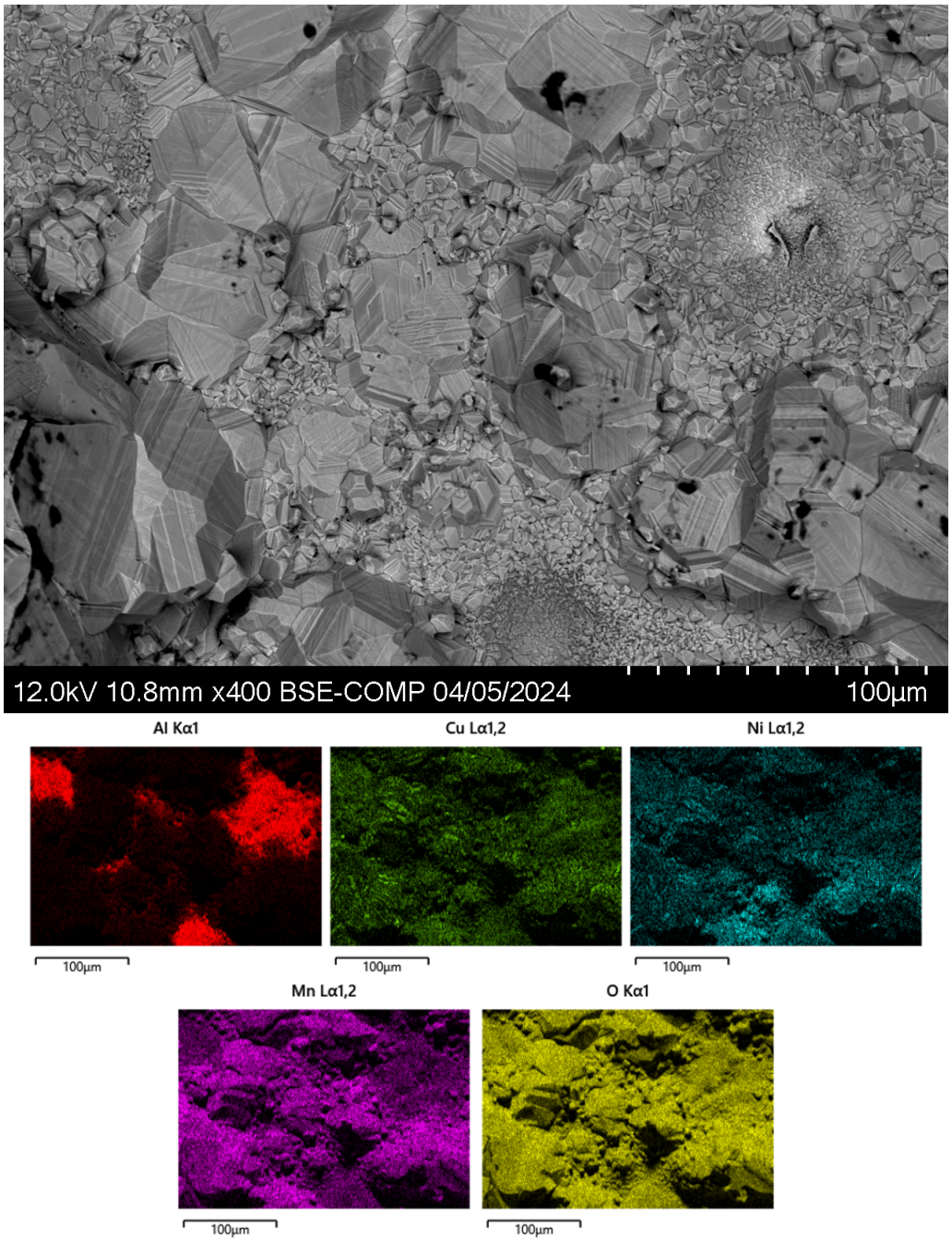

Figure 5.34 Oxide layer of Non Si alloy after 72 hour static oxidation at 1000°C and energy dispersive spectroscopy elemental mapping

The microstructure below in Figure 5.35 shows that aluminum oxides remain present within the bulk material, and this can be represented by the black regions. The aluminum oxides

reside within the interdentritic regions. The gray matrix remains consistent and there are copper and nickel rich regions.

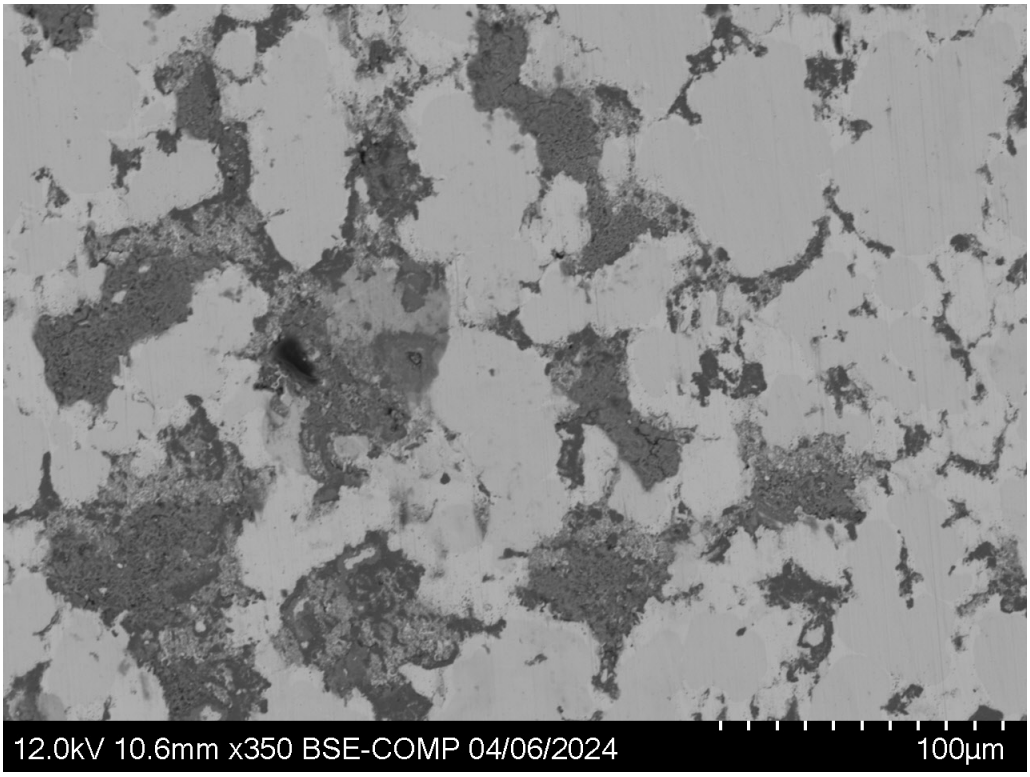

Figure 5.35 Microstructure of Non Si alloy after 72 hour static oxidation at 1000°C and energy dispersive spectroscopy elemental mapping

This SEM image of the oxide layer in the figure below shows the manganese oxide is located on the exterior and is easily visible on the surface. It is important to note the aluminum oxides present within the bulk, but also the thin layer that is seen right at the interface of the oxide layer and the bulk material. Copper and nickel are rich in the same regions, however they do not contribute the oxide and bulk interface.

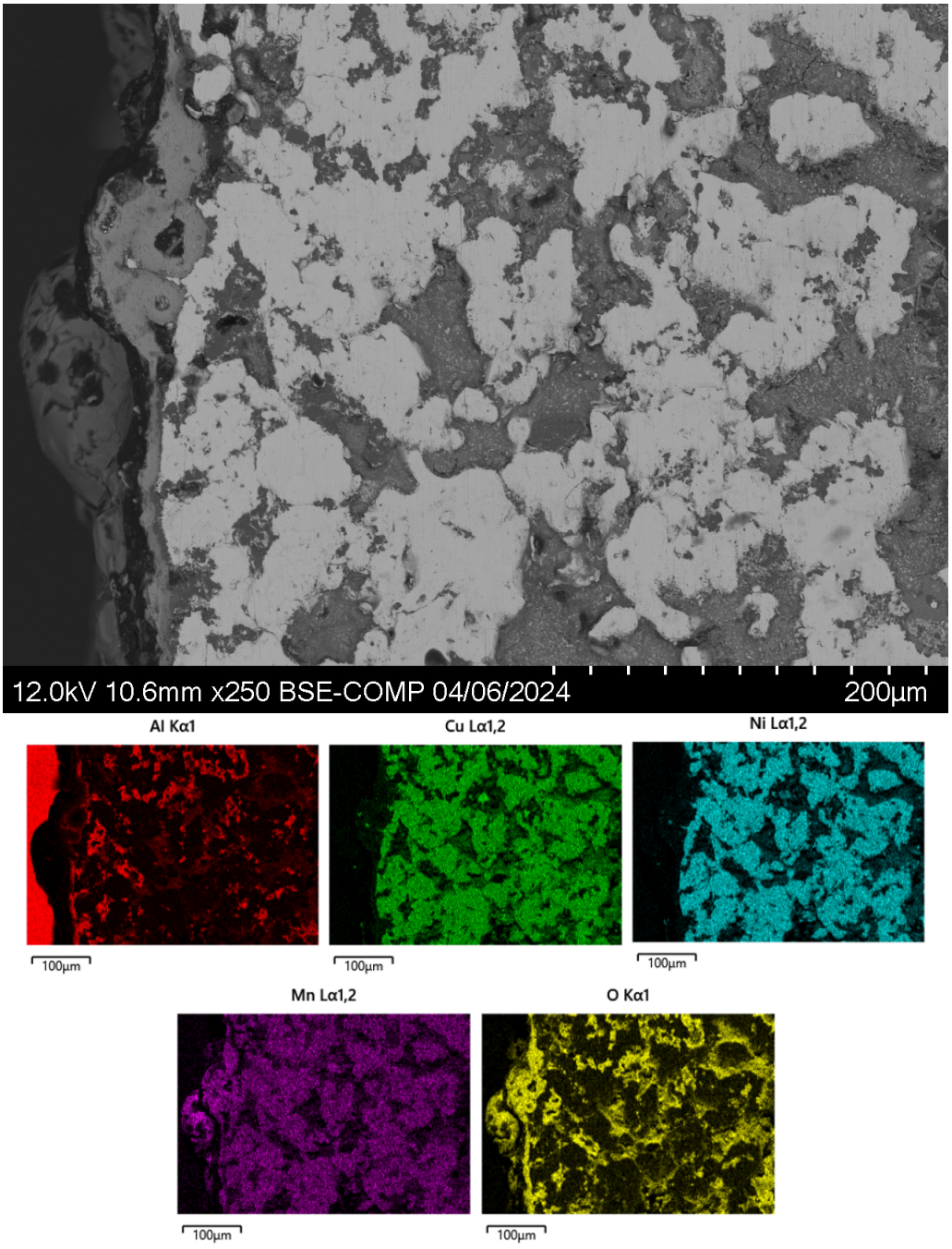

Figure 5.36 Oxide and bulk interface of Non Si Alloy after 72 hour static oxidation at 1000°C and energy dispersive spectroscopy elemental mapping

The oxide layer being displayed below represents the Si Alloy at 1000°C after 72 hours of oxidation. The oxidation layer that formed under these conditions is different in morphology compared to the previous oxidation experiments. According to the elemental mapping, aluminum and oxygen are rich all throughout the oxide layer.

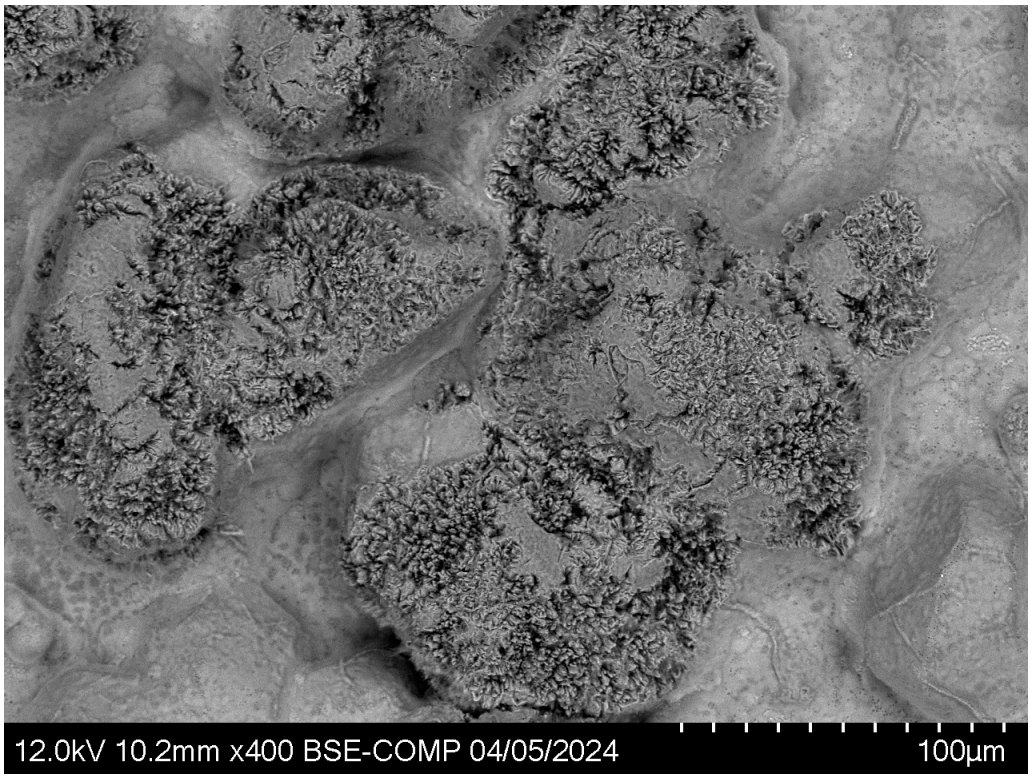

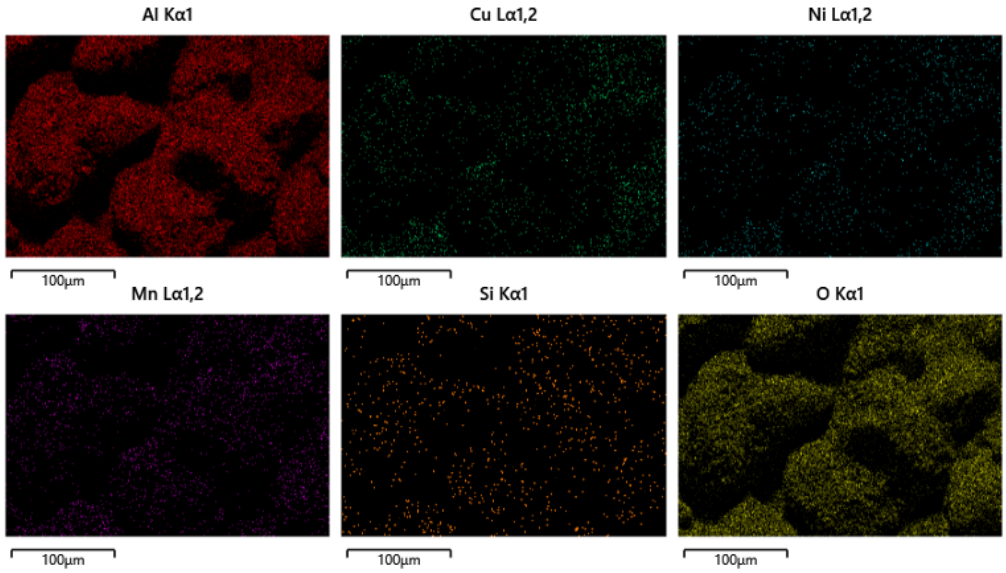

Figure 5.37 Oxide layer of Si alloy after 72 hour static oxidation at 1000°C and energy dispersive spectroscopy elemental mapping

Once being subjected to 1000°C oxidation for 72 hours, the Si alloy was heavily oxidized and can be viewed in Figure 5.38. The sample contained a great amount of scaling, would fragment when handled, and was nearly "powder-like."

Figure 5.38 Si alloy after 72 hour static oxidation at 1000°C

The average atomic percentage of each element in the oxide layer, bulk microstructure, and interface after 72 hour oxidation at 1000°C is documented in Table 5.3. The elemental compositions follow the same trend as discussed during the 48 hour oxidation results. The Non Si alloy shows a significant amount of manganese present within the oxide layer at both 600°C and 1000°C. The Si alloy at 600°C, has a higher elemental composition of aluminum and manganese compared to the other elements within the oxide layer. At 1000oC, the aluminum composition increases and the manganese composition decreases.

Table 5.3 Average elemental composition of oxide layer, bulk microstructure, and interface of Non Si and Si alloy after 72 oxidation at 600°C and 1000°C

72 Hour Oxidation at 600 C							
Non Si Alloy				Si Alloy			
	Oxide Layer	Bulk	Interface		Oxide Layer	Bulk	Interface
Element	Avg At%	Avg At%	Avg At%	Element	Avg At%	Avg At%	Avg At%
Al	8.43	18.17	14.9	Al	18.13	16	15.47
Cu	7.27	21.37	14.67	Cu	3.8	22.57	19.63
Ni	3.07	16.97	10.13	Ni	0.87	19.4	21.57
Mn	29.77	15.47	18.03	Mn	24.43	16.3	14.3
Si				Si	0.47	16.97	14.33
O	51.5	28.07	42.3	O	52.37	8.8	14.73
72 Hour Oxidation at 1000 C							
Non Si Alloy				Si Alloy			
	Oxide Layer	Bulk	Interface		Oxide Layer	Bulk	Interface
Element	Avg At%	Avg At%	Avg At%	Element	Avg At%	Avg At%	Avg At%
Al	5.67	25.8	28.97	Al	38.17		
Cu	3.5	30.63	15.23	Cu	0.63		
Ni	0.57	23.93	12.43	Ni	0.03		
Mn	39.3	19.6	12.7	Mn	1.1		
Si				Si	0.07		
O	50.97		27.56	O	60.03		

The XRD spectra obtained from the oxide layers after 72 hour oxidation for 1000°C is portrayed in Figure5.39. The oxides present include Mn_3O_4 and Al_2O_4.

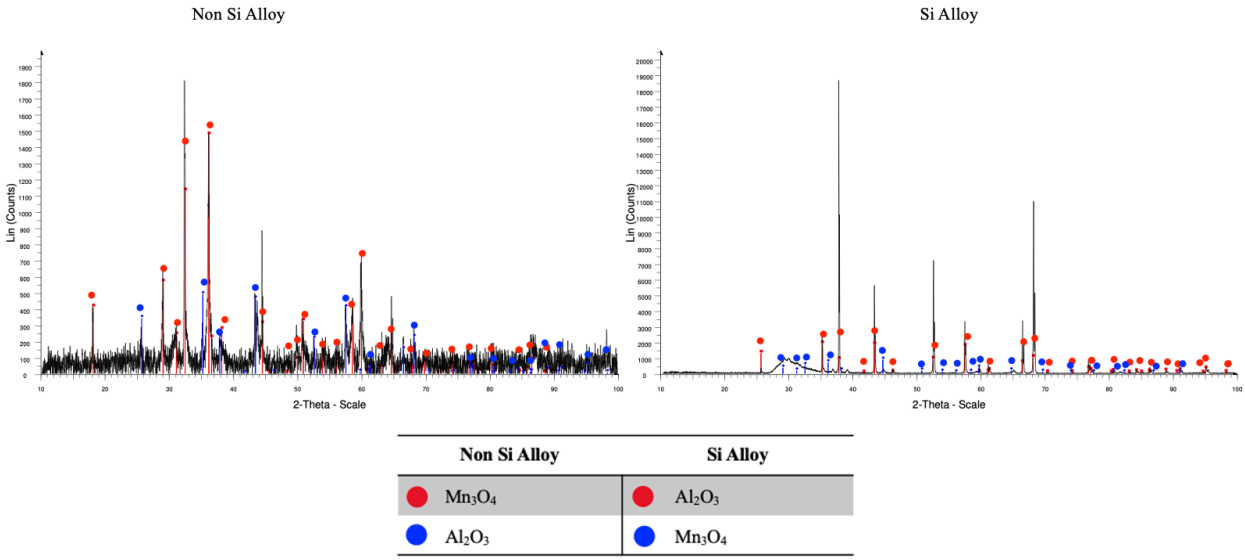

Figure 5.39 X-ray diffraction of oxide layer of Non Si and Si alloy after 72 hour static oxidation at 1000°C

Chapter 6: Cyclic Oxidation Results

6.1 Cyclic Oxidation for one week at 600°C for Non Si and Si Alloy

Figure 6.1 displays the oxide layer for the Non Si alloy after cyclic heating at 600°C. The oxide layer that formed is shown to be rich in manganese and oxygen. There are scattered regions that appear to be rich in aluminum as well. There are smaller regions that show a presence of copper and nickel as well based on the EDS results. Cracking is evident and is mainly located near oxide growth.

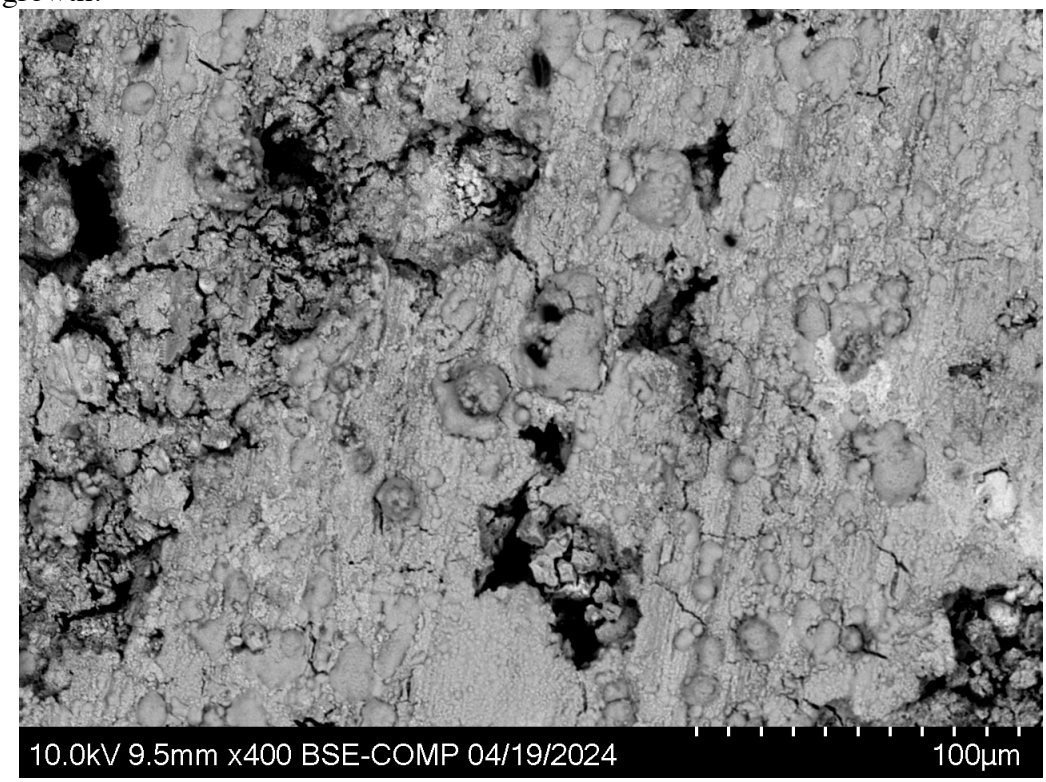

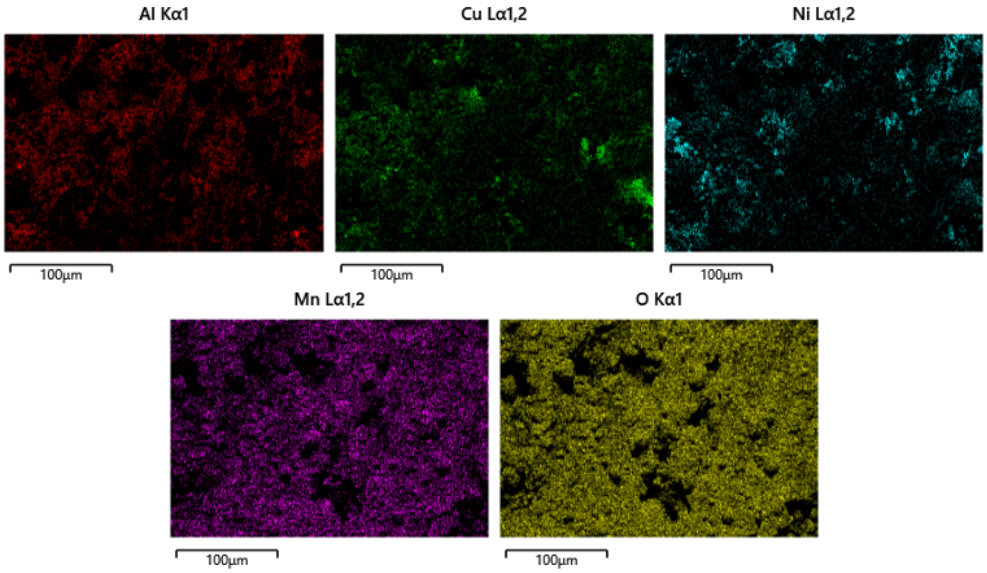

Figure 6.1 Oxide layer of Non Si alloy after cyclic oxidation for a week at 600°C and energy dispersive spectroscopy elemental mapping

The bulk microstructure for the Non Si alloy after cyclic heating at 600°C remains consistent with the previous microstructures. Manganese oxides are present within the bulk and can be recognized as the darker regions. The manganese oxides reside within the interdentritic regions. The nickel rich region is still present, and the matrix remains rich in copper, nickel, and aluminum. The thin copper rich regions appear in the microstructure after cyclic oxidation as well.

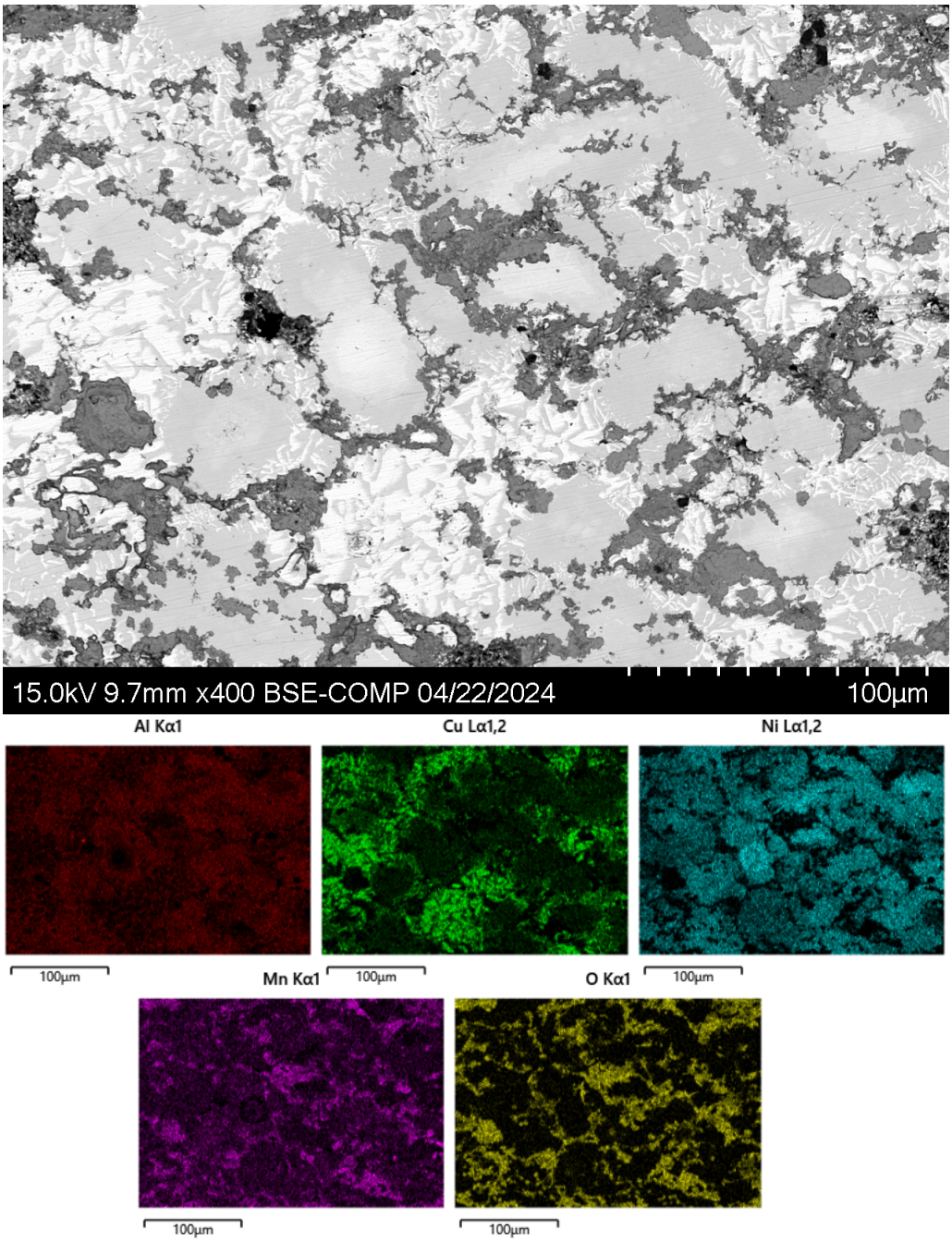

Figure 6.2 Microstructure of Non Si alloy after cyclic oxidation for a week at 600°C and energy dispersive spectroscopy elemental mapping

The interface after cyclic oxidation at 600°C can be seen in Figure 6.3. The dark regions at the interface are primarily manganese, aluminum, and oxygen and there is a clear distinction within the elemental maps.

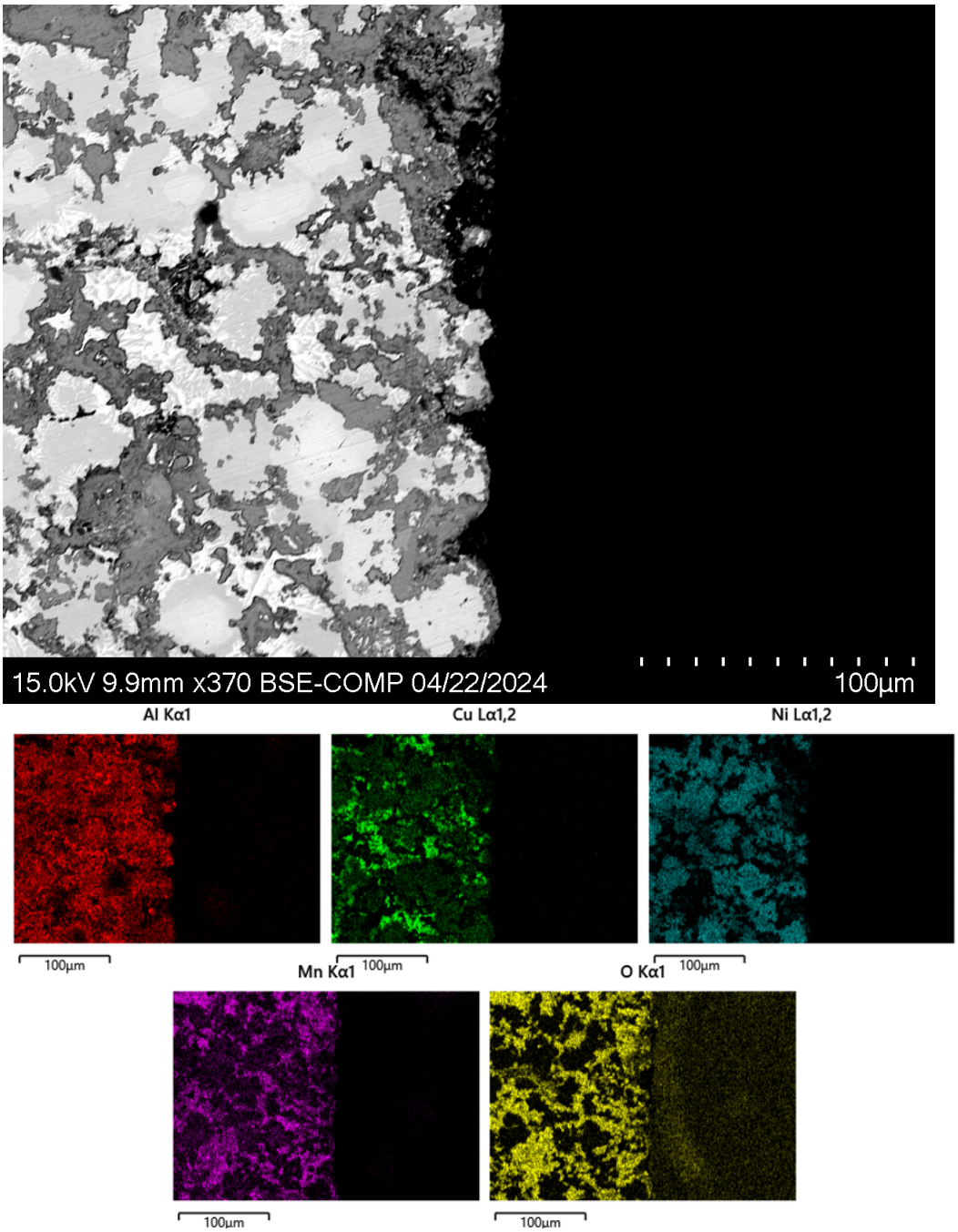

Figure 6.3 Oxide and bulk interface of Non Si Alloy after cyclic oxidation for a week at 600°C and energy dispersive spectroscopy elemental mapping

The Si alloy after cyclic heating at 600°C is shown in Figure 6.4. The oxide layer appears to be mainly aluminum rich, with manganese also scattered throughout the surface. There are small

distinct areas that are very rich in copper and nickel. Silicon does not have a major contribution the oxide layer.

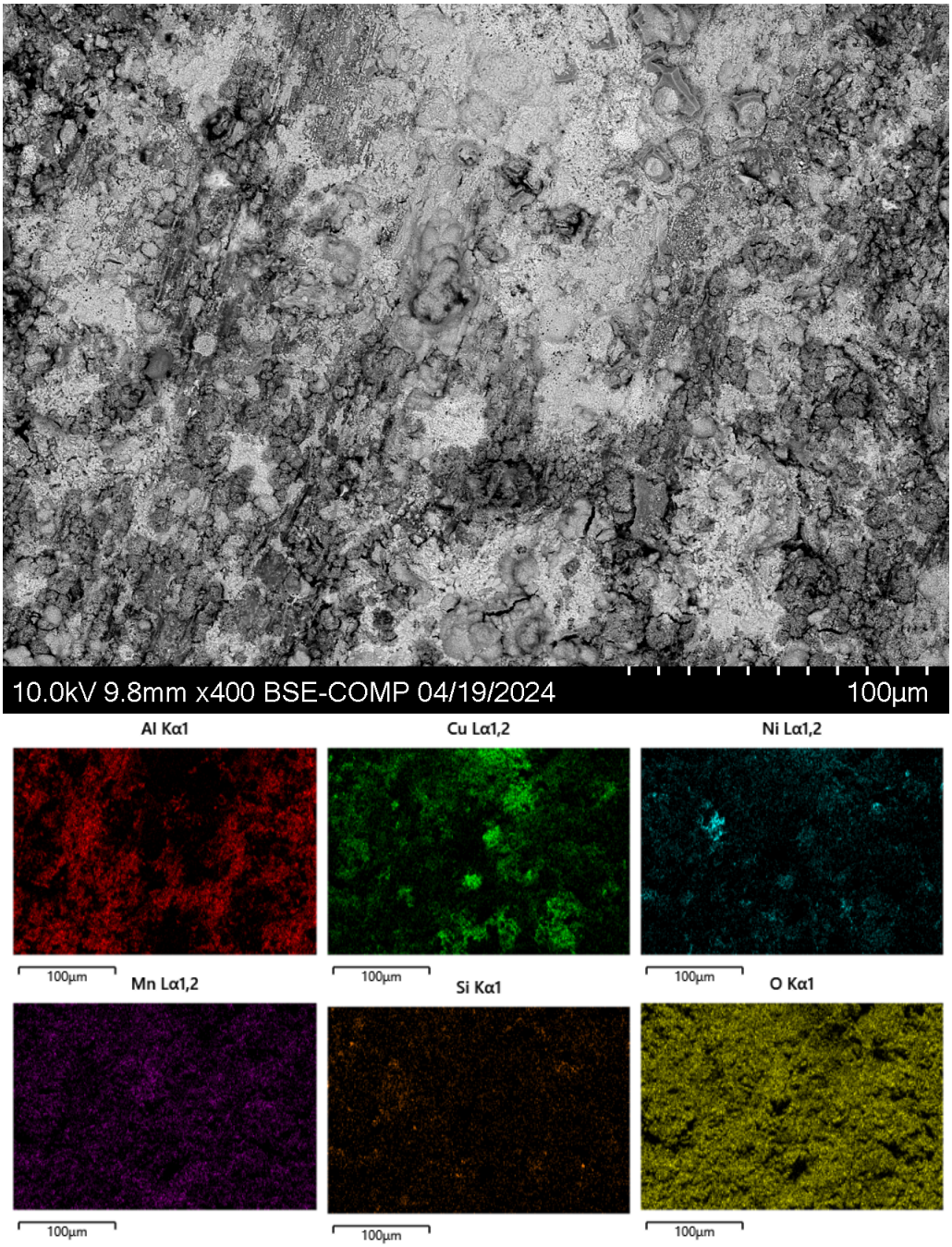

Figure 6.4 Oxide layer of Si alloy after cyclic oxidation for a week at 600°C and energy dispersive spectroscopy elemental mapping

The microstructure of the Si alloy after cyclic heating remains consistent with previous samples that were held at the same temperature but were exposed to static oxidation. Manganese and aluminum oxides are present within the bulk material and are found within the interdendritic regions. The matrix is mainly comprised of copper, aluminum, and nickel.

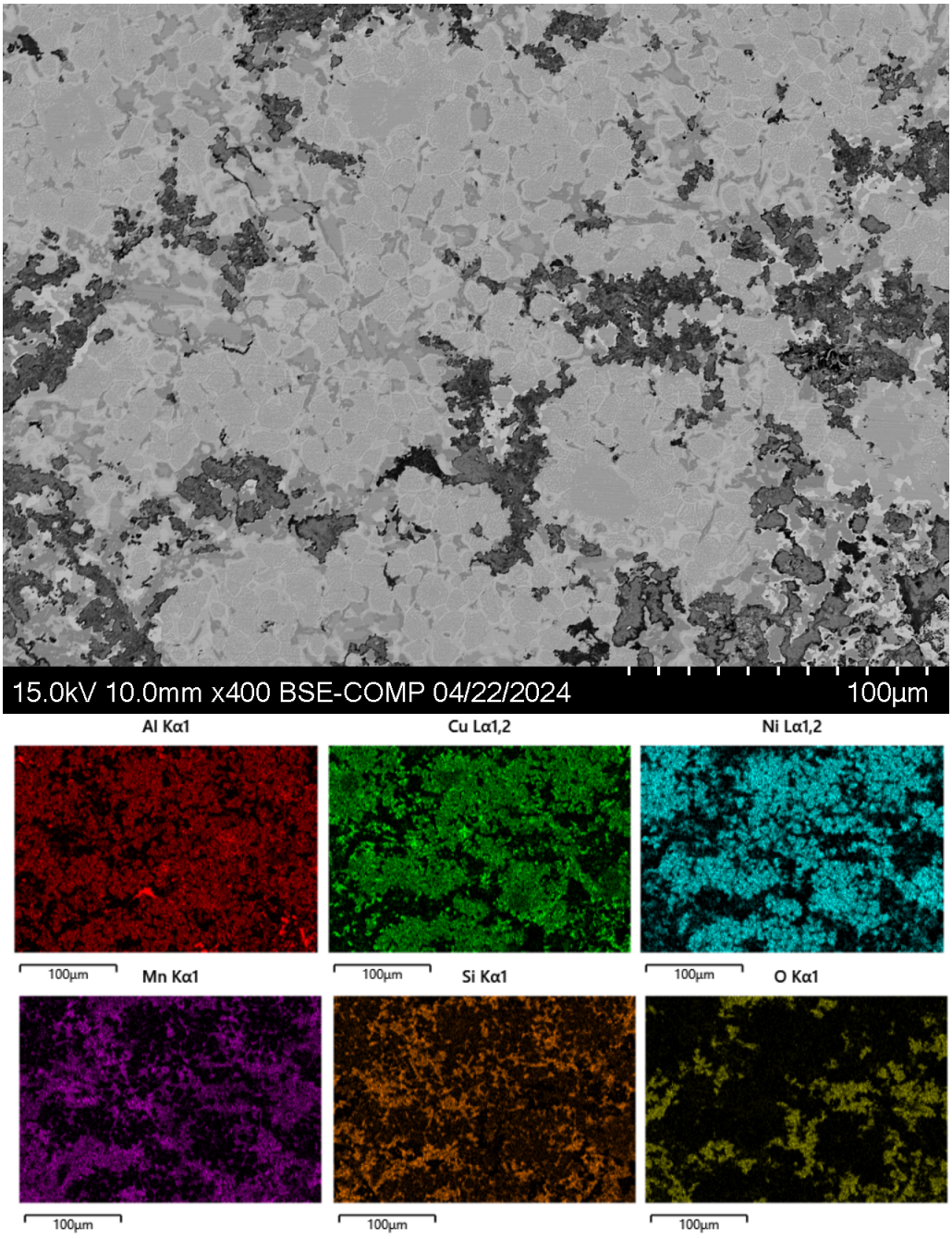

Figure 6.5 Microstructure of Si alloy after cyclic oxidation for a week at 600°C and energy dispersive spectroscopy elemental mapping

The interface between the Si alloy and the oxide layer that formed due to cyclic heating at 600°C can be viewed in Figure 6.6. The color mapping clearly shows a thin aluminum oxide layer present on the surface of the bulk material, with a larger manganese oxide located on the surface.

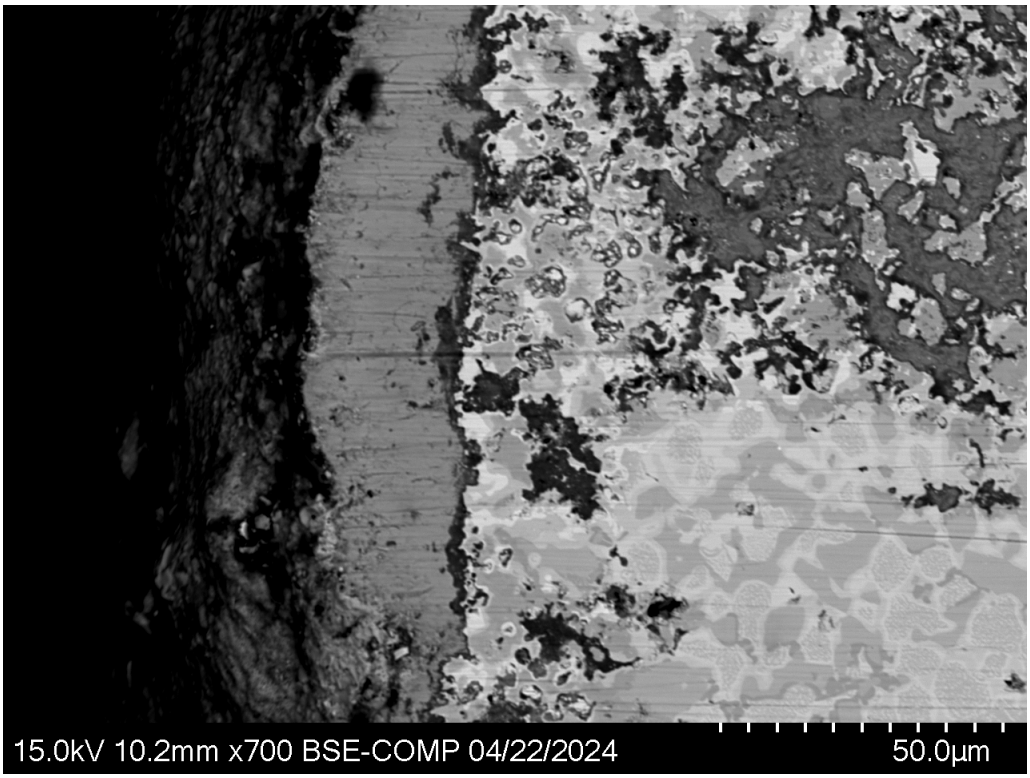

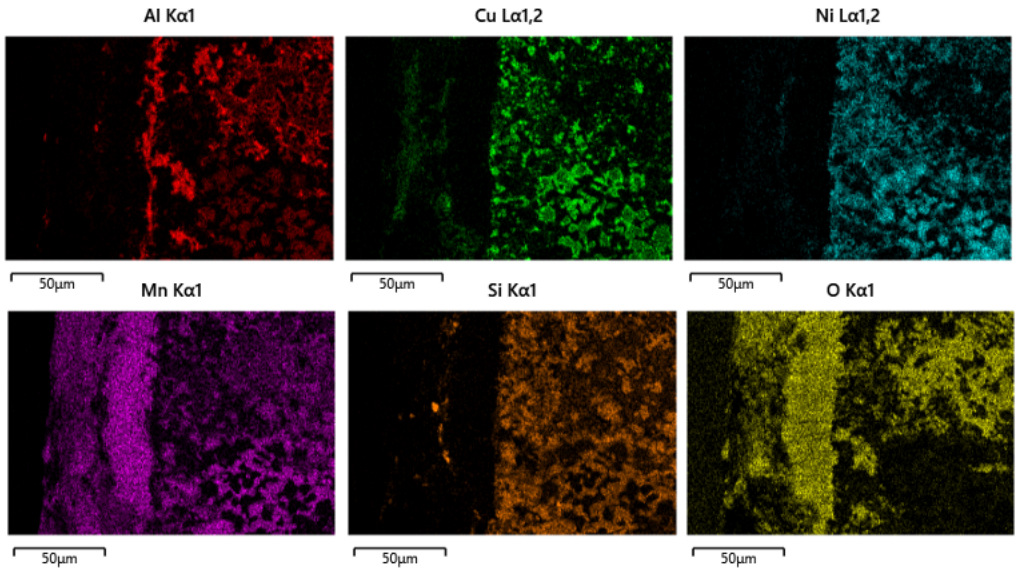

Figure 6.6 Oxide and bulk interface of Si Alloy after cyclic oxidation for a week at 600°C and energy dispersive spectroscopy elemental mapping

After cyclic oxidation held at 600°C, the oxide that continues to be identified based on the XRD data collected include Mn_2O_3.

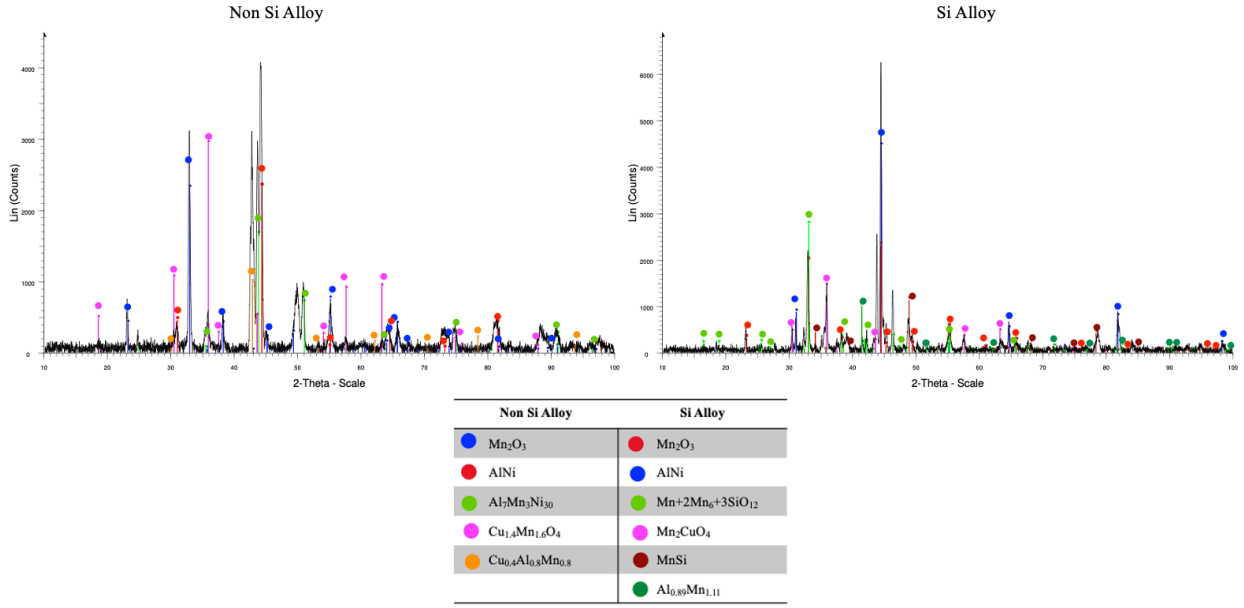

Figure 6.7 X-ray diffraction of oxide layer of Non Si and Si alloy after cyclic oxidation for a week at 600°C

6.2 Cyclic Oxidation for one week at 1000°C for Non Si and Si Alloy

After cyclic heating at 1000°C, the Non Si alloy's oxide layer is shown in the SEM image in Figure 6.8. In this image there is a distinction between the manganese and copper rich areas. The manganese rich areas are dark gray and the copper rich areas are lighter in color. Nickel appears to be dispersed throughout and aluminum is rich in similar areas as manganese.

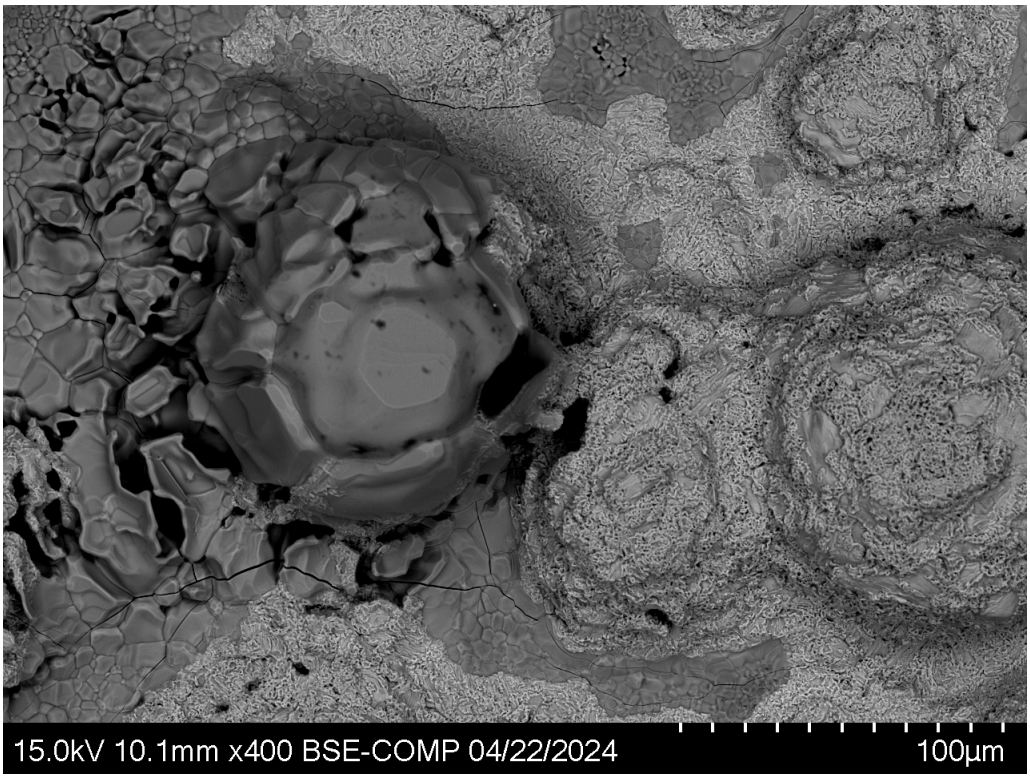

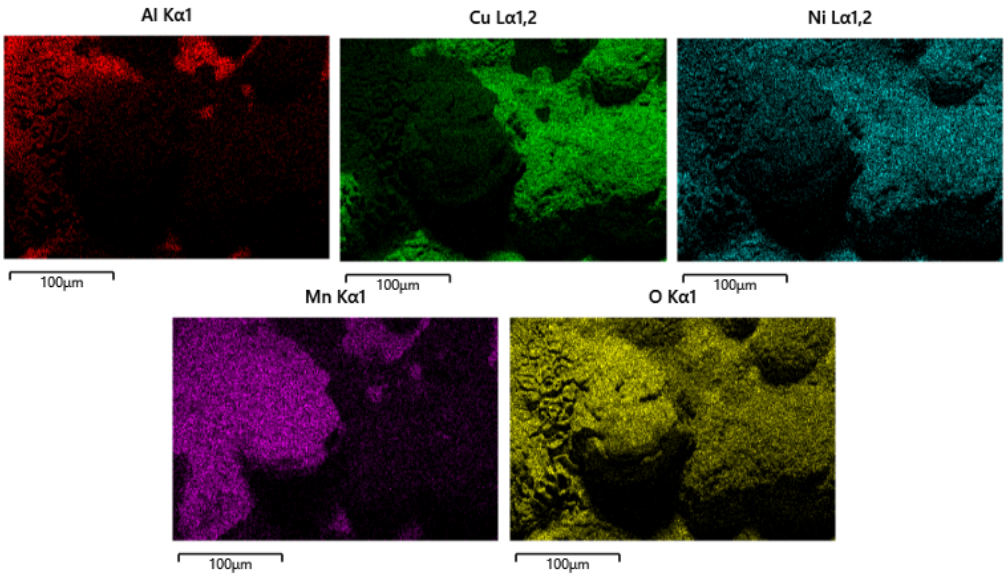

Figure 6.8 Oxide layer of Non Si alloy after cyclic oxidation for a week at 1000°C and energy dispersive spectroscopy elemental mapping

The bulk microstructure of the Non Si Alloy is extremely different that any of the previous microstructures shown (Figure 6.9). The gray areas are rich in aluminum while the light areas are rich in copper and nickel. Manganese appears to be scattered throughout.

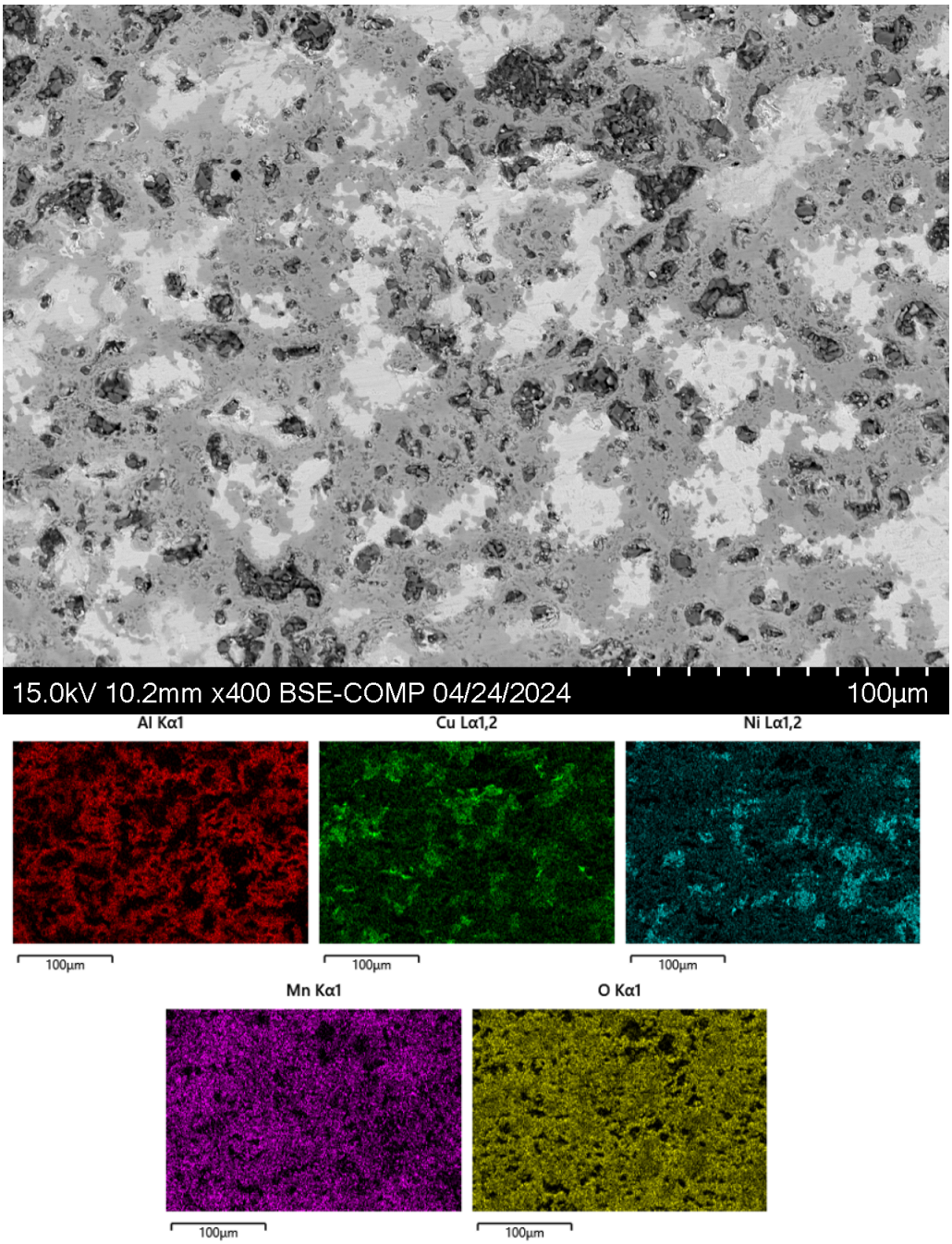

Figure 6.9 Microstructure of Non Si alloy after cyclic oxidation for a week at 1000°C and energy dispersive spectroscopy elemental mapping

At the interface of the Non Si alloy, after being subject to cyclic oxidation at 1000°C, aluminum is present as a thin layer. Within the interface the aluminum oxide gradually changes to the manganese oxide present on the exterior.

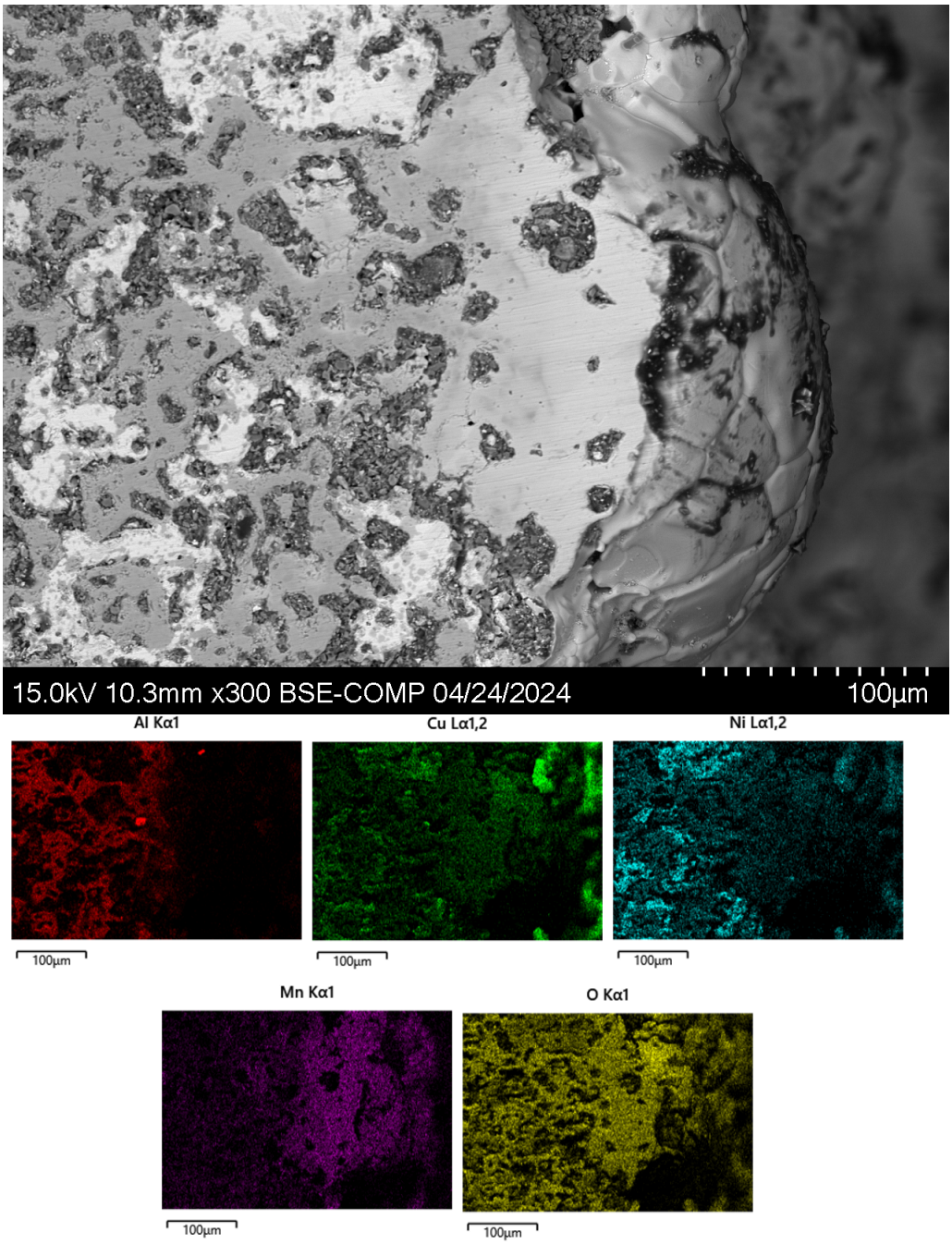

Figure 6.10 Oxide and bulk interface of Non Si Alloy after cyclic oxidation for a week at 1000°C and energy dispersive spectroscopy elemental mapping

The Si alloy was exposed to cyclic oxidation at 1000°C, and the oxide layer can be viewed in Figure 6.11 The dark areas are rich in aluminum and the lighter areas are rich in manganese.

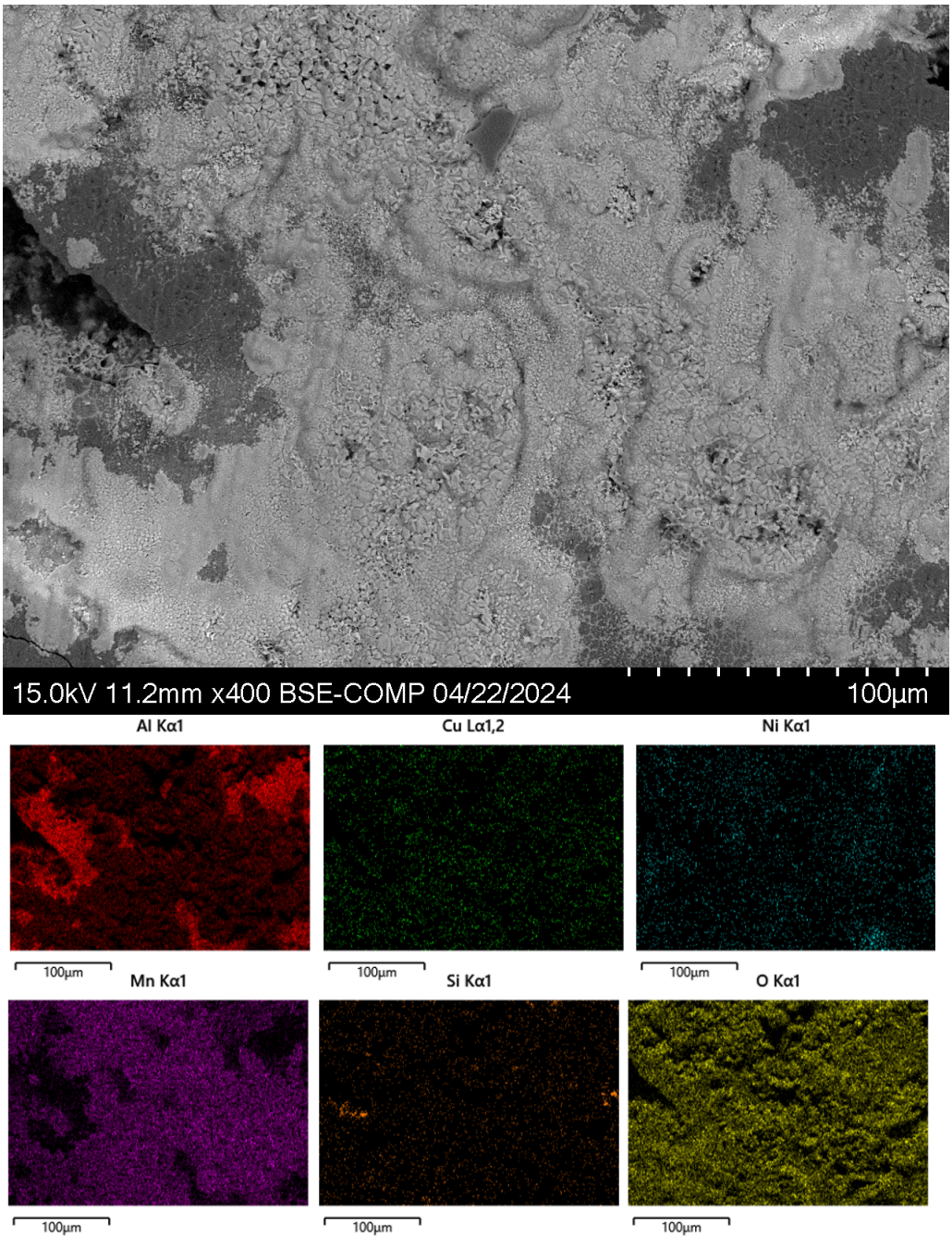

Figure 6.11 Oxide layer of Si alloy after cyclic oxidation for a week at 1000°C and energy dispersive spectroscopy elemental mapping

After cyclic oxidation at 1000°C, the Si alloy was extremely oxidized and fragmented once being held. This was documented in Figure 6.12.

Figure 6.12 Si Alloy after one week of cyclic oxidation at 1000°C

The average atomic percentage of the oxide layer, bulk microstructure, and the interface of the Non Si and Si alloy after being exposed to cyclic oxidation at 600oC and 1000oC are shown in Table 6.1. At 600°C, the Non Si alloy is rich in manganese within the oxide layer. As the temperature increases to 1000°C, the manganese compositions decreases and the copper content increases as well. The Si alloy at 600°C shows similar results to the previous samples at this temperature. Aluminum and manganese remain rich within the oxide layer. At 1000°C, the oxide layer of the Si alloy continues to be rich in aluminum and manganese.

Table 6.1 Average elemental composition of oxide layer, bulk microstructure, and interface of Non Si and Si alloy after cyclic oxidation at 600°C and 1000°C

Cyclic Oxidation at 600 C							
Non Si Alloy				Si Alloy			
	Oxide Layer	Bulk	Interface		Oxide Layer	Bulk	Interface
Element	Avg At%	Avg At%	Avg At%	Element	Avg At%	Avg At%	Avg At%
Al	6.77	17.70	14.10	Al	13.93	16.50	11.53
Cu	15.73	19.40	13.57	Cu	7.83	16.17	11.20
Ni	3.00	16.97	11.10	Ni	1.57	15.23	6.90
Mn	34.90	16.07	15.93	Mn	25.53	16.23	19.93
Si				Si	0.57	14.47	11.00
O	50.43	29.27	44.87	O	50.73	21.40	39.40
Cyclic Oxidation at 1000 C							
Non Si Alloy				Si Alloy			
	Oxide Layer	Bulk	Interface		Oxide Layer	Bulk	Interface
Element	Avg At%	Avg At%	Avg At%	Element	Avg At%	Avg At%	Avg At%
Al	2.50	14.73	13.47	Al	26.83		
Cu	25.63	10.50	13.60	Cu	0.97		
Ni	3.67	10.10	7.77	Ni	0.80		
Mn	20.47	10.67	11.37	Mn	14.80		
Si				Si	0.33		
O	47.67	54.03	53.80	O	54.33		

The oxide layers from both alloys continued to obtain a manganese and aluminum oxide. Based on the XRD spectra, the oxides that were identified were MnO and Al_2O_3 (Figure 6.13).

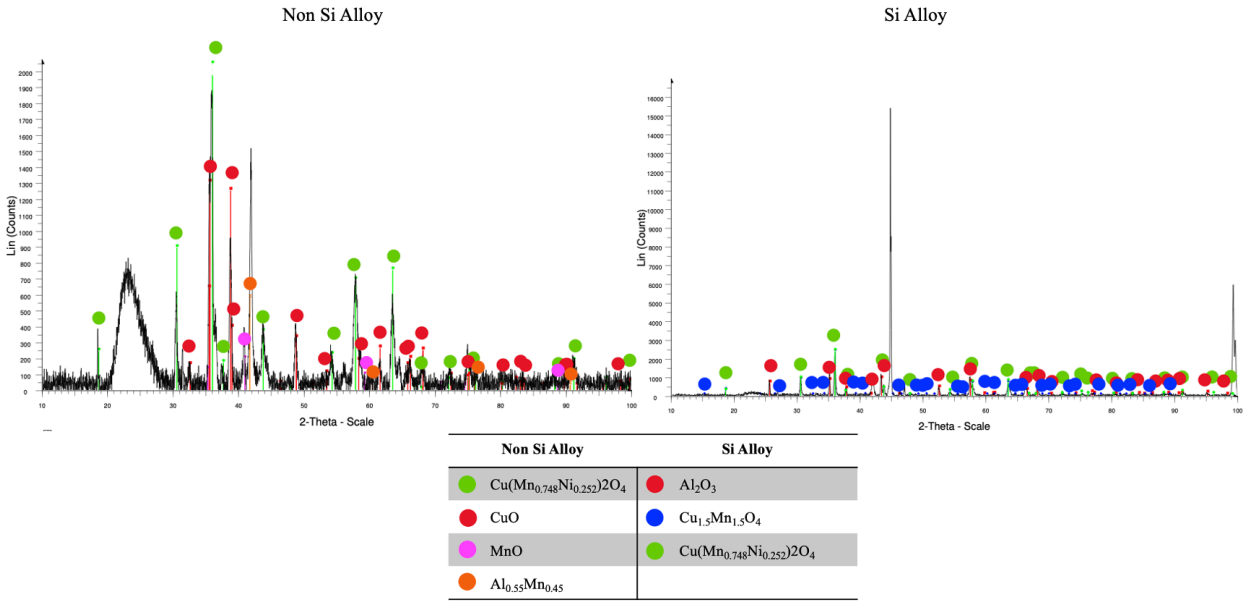

Figure 6.13 X-ray diffraction of oxide layer of Non Si and Si Alloy after cyclic oxidation for a week at 1000°C

Chapter 7: Oxidation Data

7.1 Static Oxidation Plots for Non Si and Si Alloy

After static oxidation was completed at 600°C and 1000°C at 24, 48, and 72 hours the mass gain per surface area vs temperature was plotted. This data can be shown in the graph in Figure 7.1. The green data points represent the Non Si Alloy, and the blue data points were selected to represent the Si Alloy. The shape and color of the data point can be seen in the legend in the figure and can be related to the exact oxidation conditions for each alloy. Based off this graph, the Non Si Alloy had a higher mass gain per surface area compared to the Si Alloy. Another observation is that increasing the temperature from 600°C to 1000°C the mass gain per surface area also increased for each alloy and for each time duration. The only sample that this statement is not true is for the Non Si Alloy that was held for 72 hours at 600°C and 1000°C. When the temperature was increased this resulted in a decreased in mass per surface area. Also, while the temperature stays constant, and the time of oxidation increases the mass gain per surface areas increases as well. This is not true again, for the Non Si Alloy at 1000°C at 72 hours. Even though the mass increased at this temperature for the samples that were held for 24 and 48 hours, the mass decreased once it was held for 72 hours.

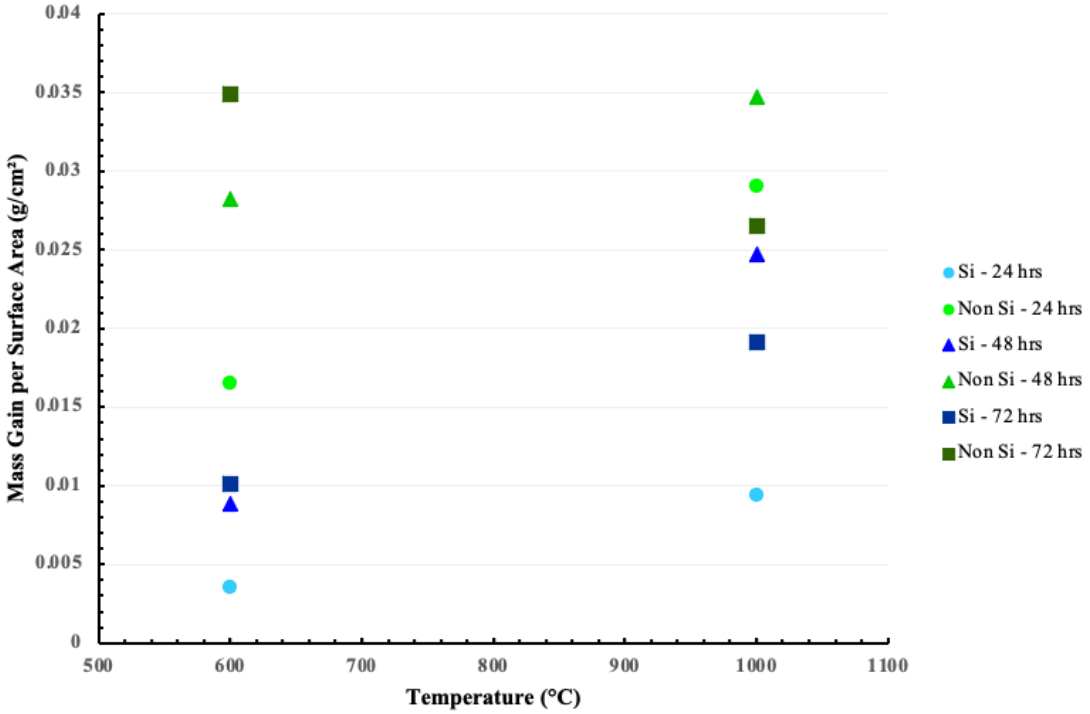

Figure 7.1 600°C and 1000°C static oxidation plot of mass gain per surface area versus temperature for Non Si and Si alloys at 24, 48, and 72 hour oxidation time

7.2 Cyclic Oxidation Curves for Non Si and Si Alloy

The mass gain per surface area was also recorded during cyclic oxidation experiments and the data can be found in Figure 7.2. The graph that is displayed is mass gain per surface area vs the number of cycles. Each cycle represents a 24 hour heating period, and there are 7 cycles to equal one full week of oxidation exposure. The green data points represent the Non Si Alloy and the blue data points represent the Si Alloy, and the legend on the side of the graph can indicate the exact oxidation temperature. All of the oxidation curves showed in an increasing trend. Comparing the Non Si Alloy at 600°C and the Non Si Alloy at 1000°C, shows the biggest difference. The sample that was held at 1000°C shows the greatest increase in mass per surface area from cycle 1 to cycle 2. The Si Alloy at 1000°C did have a greater increase in mass gain per surface area compared to the Si Alloy at 600°C, yet the difference was not as significant as the Non Si Alloy. Overall, the Non Si Alloy increased in mass more at both oxidation temperatures, than the Si Alloy.

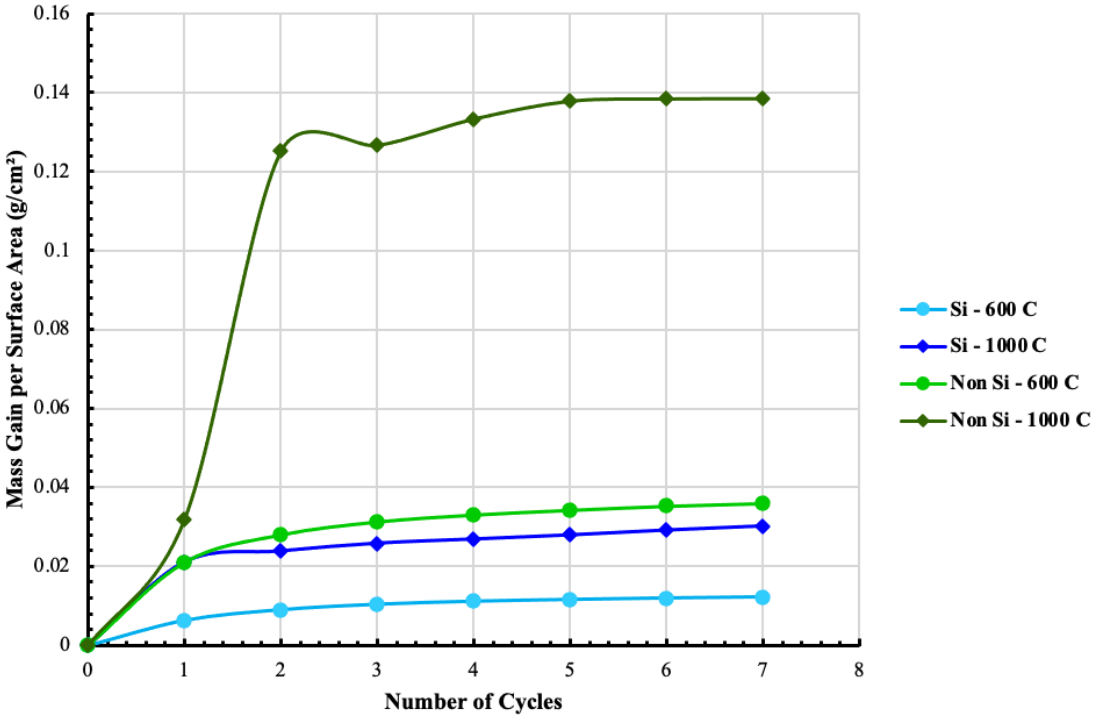

Figure 7.2 600°C and 1000°C cyclic oxidation curves for Non Si and Si alloy for 1 week oxidation time

Chapter 8: Conclusions

High entropy alloys composed of Al-Cu-Ni-Mn and Al-Cu-Ni-Mn-Si were characterized in both their as received condition and oxidized condition, and their oxidation behavior was studied throughout this investigation. In the as received condition three microconstituents were identified in both alloys. Within the Non Si alloy it was found that the white region was rich in nickel, the black region was rich in manganese, and the gray matrix was comprised of all the elements but has a stronger presence of copper, nickel, and aluminum. In the Si alloy, similar microconstituents were identified. The white region remained rich in nickel, the black region remained rich in manganese with silicon also present, and the gray matrix remained comparable. Both structures took on a dendritic form, and this can be due to casting being the processing method of both the alloys.

During static oxidation, it can be concluded that aluminum and manganese are the two elements primarily being oxidized and is present within the oxide layers. When aluminum oxides and forms a thin layer within the interface of the bulk material and the oxide layer, and eventually manganese oxides form over this layer. Within the bulk material, aluminum and manganese oxides that are present are located within interdentritic regions. Copper and nickel are more resistant to oxidation and remain rich in the microstructure. It can also be established that as oxidation time and temperature increases, the mass gain per surface area also increases. This trend was consistent throughout both the Non Si and Si alloys. The only outlier was the Non Si alloy that was held for 72 hours at 1000^{o}C. It can also be determined that the Si alloy cannot with stand oxidation at 1000^{o}C.

During cyclic oxidation, aluminum and manganese remained to be the two elements that showed to be oxidizing. Aluminum and manganese oxides were present within the oxide layer and were located within interdendritic regions in the bulk material. It was found that as oxidation time and temperature increases, the mass gain per surface area increases as well. Remaining consistent with the static oxidation results, the Si alloy was not capable of withstanding oxidation at 1000^{o}C.

Overall, the Non Si alloy showed favorable results when exposed to elevated temperature oxidation compared to the Si alloy. The addition of silicon did not assist in oxidation resistance, it actually promoted oxidation to occur. Based on the Ellingham diagram in Figure 1.5, it can be seen that aluminum, silicon, and manganese are located lower on the diagram than copper and nickel. Through elemental mapping, it was apparent that the oxides were rich in aluminum and manganese, and understanding the Ellingham diagram it proves as to why they oxidized. Also, with copper and nickel being located higher on the diagram, it shows that they have better resistance to oxidation. The microstructures after being exposed to oxidation had regions that were heavily rich in nickel and copper. This means that since nickel and copper were resistant to oxidation, the aluminum and manganese were diffusing away from the matrix and forming oxides, leaving the remaining areas as copper and nickel rich.

References

[1] Da Costa Garcia Filho, F., Ritchie, R. O., Meyers, M. A., & Neves Monteiro, S. (2022). Cantor- derived medium-entropy alloys: bridging the gap between traditional metallic and high-entropy alloys. Journal of Materials Research and Technology, 17, 1868-1895. https://doi.org/10.1016/j.jmrt.2022.01.118

[2] Ye, Y.F., Wang, Q., Lu, J., Liu, C.T., & Yang, Y. (2016). High-entropy alloy: challenges and prospects. Materials Today, 19(6), 349-362. https://doi.org/10.1016/j.mattod.2015.11.026

[3] Kerber, S. J., & Tverberg, J. (2000). STAINLESS STEEL. *Advanced Materials & Processes*, *158*(5), 33. https://link.gale.com/apps/doc/A67718760/AONE?u=anon~c65b8153&sid=googleScholar&xid=f464d0a4

[4] Cantor, B., Chang, I.T.H., Knight, P., & Vincent, A.J.B. (2004, July). Materials Science and Engineering: A. *Microstructural development in equiatomic multicomponent alloys*, *375-377*, 213-218. https://doi.org/10.1016/j.msea.2003.10.257

[5] Jien-Wei, Y. E. H. (2006). Recent progress in high entropy alloys. *Ann. Chim. Sci. Mat*, *31*(6), 633-648.

[6] Li, W., Xie, D., Li, D., Zhang, Y., Gao, Y., & Liaw, P. K. (2021, May). Mechanical behavior of high-entropy alloys. Progress in Materials Science, 118. https://doi.org/10.1016/j.pmatsci.2021.100777

[7] Yeh, J.-W. (2006, December). Recent Progress in High-Entropy Alloys. European Journal of Control, 31, 633-648. 10.3166/acsm.31.633-648

[8] Tokarewicz, M., & Grądzka-Dahlke, M. (2021). Review of recent research on AlCoCrFeNi high-entropy alloy. *Metals*, *11*(8), 1302.

[9] Miracle, D.B., & Senkov, O.N. (2016, October 21). A critical review of high entropy alloys and related concepts. Acta Materialia, Volume, 448-511. https://doi.org/10.1016/j.actamat.2016.08.081

[10] Baker, I., Cantor, B., & Yeh, J. W. (2023). High Entropy Alloys and Materials. *High Entropy Alloys & Materials*, *1*(1), 1-3.

[11] Li, Z., Zhao, S., Ritchie, R. O., & Meyers, M. A. (2019). Mechanical properties of high-entropy alloys with emphasis on face-centered cubic alloys. *Progress in Materials Science*, *102*, 296-345.

[12] Yeh, J. W., Chen, S. K., Lin, S. J., Gan, J. Y., Chin, T. S., Shun, T. T., ... & Chang, S. Y. (2004). Nanostructured high-entropy alloys with multiple principal elements: novel alloy design concepts and outcomes. *Advanced engineering materials*, *6*(5), 299-303.

[13] George, E. P., Raabe, D., & Ritchie, R. O. (2019). High-entropy alloys. *Nature reviews materials*, *4*(8), 515-534.

[14] Tsai, M.-H., & Yeh, J.-W. (2014, April 30). High-Entropy Alloys: A Critical Review. *Materials Research Letters*, *2*(3), 107-123. https://doi.org/10.1080/21663831.2014.912690

[15] Senkov, O.N., Wilks, G.B., Miracle, D.B., Chuang, C.P., & Liaw, P.K. (2010). Refractory high entropy alloys. *Intermetallics*, *18*(9), 1758-1765. https://doi.org/10.1016/j.intermet.2010.05.014

[16] Romero, Rebecca Alexandra, "Investigation of Refractory High Entropy Alloys for Extreme Environment Applications" (2022). Open Access Theses & Dissertations. 3540. http://scholarworks.utep.edu/open_etd/3540

[17] Jones, D. A. (1996). *Principles and prevention of corrosion*. Prentice Hall.

[18] Logani, R. C., & Smeltzer, W. W. (1971). Principles of metal oxidation. *Canadian metallurgical quarterly*, *10*(3), 149-163.

[19] Hasegawa, M. (2014). Ellingham diagram. In *Treatise on Process Metallurgy* (pp. 507-516). Elsevier.

[20] Martin, A., & Thuo, M. (2023). Beyond Hume-Rothery Rules. *Accounts of Materials Research*, *4*(10), 809-813.

[21] Varma, S.K., Sanchez, F., & Ramana, C.V. (2020, September 15). Microstructure in a Nb-Cr-V- W-Ta high entropy alloy during annealing. Journal of Materials Science and Technology, 53, 66-72. https://doi.org/10.1016/j.jmst.2020.03.028

[22] Varma, S.K., Sanchez, F., Mancayo, S., & Ramana, C.V. (2020, February 1). Static and cyclic oxidation of Nb-Cr-V-W-Ta high entropy alloy in air from 600 to 1400 C. Journal of Materials Science and Technology, 38, 189-196. https://doi.org/10.1016/j.jmst.2019.09.005

[23] Hitter, M. M. L., & Varma, S. K. (2023). Microstructural characterization, oxidation behavior, and properties of a new Al–Cu–Ni–Mn–Si non-BCC high entropy alloy at 600, 700, and 800° C. *Journal of Materials Research and Technology*, *23*, 680-686

Vita

Mckenna Mae Lin Hitter was born and raised in El Paso, Texas. After graduating as salutatorian from Eastlake High school in 2016, she pursued a Bachelor of Science degree in Metallurgical and Materials Science and Engineering at The University of Texas at El Paso. While attending UTEP, Mckenna was a member of Alpha Xi Delta, the American Foundry Society, Alpha Sigma Mu Honor Society, Tau Beta Pi Honor Society and the Society of Women in Engineering. She worked as a teaching assistant for Nanofunctional Physical Metallurgy and Mechanical Behavior of Materials and was involved with the Center for Advancement of Space Safety Mission Assurance Research. She was recognized as the Outstanding Undergraduate Honoree for the college of engineering and the metallurgical engineering department.

Upon graduating in 2020 she continued as a doctoral student and continued to assist in teaching courses. Mckenna had the opportunity to present her research multiple times at The Minerals, Metals, and Materials and Material Science and Technology national conferences. She earned a publication and was given the John R. Serrano Memorial Copper Endowed Research award. In her last year at UTEP, she was selected as Ms. Texas Western for the university and was selected as St. Pat for the College of Engineering. Mckenna was also able to complete two internships throughout her academic career, one with Northrop Grumman and the second being with the Air Force Research Laboratory.

After graduation, Mckenna hopes to pursue a career within the aerospace and defense industry. Eventually, she would love to become a professor and help students reach their goals like her mentors did for her.

Contact Information: mckennamae98@gmail.com